Texture of two vanishing subtraces in neutrino mass matrix and current experimental tests

A. Ismael,[1,2,*] E. I. Lashin,[1,2,†] and N. Chamoun[3,‡]

[1]*Department of Physics, Faculty of Science, Ain Shams University, Cairo 11566, Egypt*
[2]*Centre for Fundamental Physics, Zewail City of Science and Technology, 6 October City, Giza 12578, Egypt*
[3]*Physics Department, HIAST, P.O. Box 31983, Damascus, Syria*

(Received 23 August 2022; accepted 20 January 2023; published 21 February 2023)

We present a full phenomenological and analytical study for the neutrino mass matrix characterized by two vanishing 2×2 subtraces. We update one past result in light of the recent experimental data. Out of the fifteen possible textures, we find seven cases can accommodate the experimental data instead of eight as in the past study. We also introduce few symmetry realizations for viable and nonviable textures based on non-Abelian (A_4 or S_4) flavor symmetry within the type-II seesaw scenario.

DOI: 10.1103/PhysRevD.107.035017

I. INTRODUCTION

The fact that neutrinos are massive was the first firm sign of physics beyond standard model. Many flavor models for neutrino mass matrix were conceived, motivated by phenomenological data on neutrino oscillations, and the examination of specific textures became a traditional approach to the flavor structure in the lepton sector.

Zero textures were studied extensively [1–4], but other forms of textures were equally studied, such as zero minors [5,6], and partial $\mu - \tau$ symmetry textures [7]. The main motivation for such a phenomenological approach is simplicity and predictive power, especially when the texture, under study, has a small number of free parameters but, nonetheless, leads to simple relations and interesting predictions for observables. Most of the textures with only one constraint were found able to accommodate data, such as the one vanishing element (or minor or subtrace) textures [8–10]. Textures with more constraints are more restrictive and many fail to be viable [2,3,5,6,11–15]. One way to constrain the number of free parameters in the neutrino mass matrix is to work in the subspace of vanishing nonphysical phases, which has the additional benefit of simplifying the resulting formulas [16].

In [17], a particular texture of vanishing two subtraces was studied. Therein, analytical expressions for the measurable neutrino observables were derived, and numerical analysis was done to show that eight patterns, out of the 15 independent ones, can accommodate data. However, new bounds on experimental data have appeared since then, in particular the nonvanishing value of the smallest mixing angle [18], and the objective of this work is just to reexamine the texture of vanishing two subtraces in light of the new data. Moreover, we shall carry out a complete numerical analysis, where all the free parameters are scanned within their experimentally accepted ranges, in contrast to [17] where slices of the parameter space were chosen by picking up some admissible values for the mixing angles, some of which correspond to the now obsolete value 5^o for the smallest mixing angle, and scanning over the remaining few free parameters.[1] Seven patterns are found to accommodate data, with one of them allowing for two types of hierarchies, another one accepting normal hierarchy (NH) alone, and five textures accommodating only inverted hierarchy (IH) type.

Furthermore, we present in this work a strategy for justifying the textures viability/unviability by studying the correlations, by which we mean certain formulas involving the correlated observables under study, in the "unphysical" subspace of vanishing solar mass squared difference δm^2. Actually, even if experimental data preclude a vanishing

*ahmedEhusien@sci.asu.edu.eg
†slashin@zewailcity.edu.eg; elashin@ictp.it
‡nidal.chamoun@hiast.edu.sy

[1]The procedure in [17] consisted of fixing the solar mass squared difference, and θ_{13}, to their best-fit experimental measurements, then picking up the value of δ which, for given (θ_{12}, θ_{23}) chosen within their allowed experimental ranges, would make R_ν acceptable, noting the very sensitive dependence of R_ν on δ.

ratio of solar to atmospheric squared mass differences R_ν, however its value is of order 10^{-2}, small enough to approximate the full true correlations by those resulting from imposing a vanishing R_ν where the analytical expressions become easier to handle and would allow to test directly the viability. Actually, we shall distinguish between various correlations of different precision levels. The utmost precision level corresponds to the full numeric correlation, possibly written as an expansion showing an approximate truncation term, with no approximations to δm^2 at all. Then comes the intermediate precision level correlation which originates from equalling to zero the exact expression of δm^2, and it can be presented in a truncated form as well. The least precision level correlation, which we shall consider in our work, results when putting equal to zero an approximate truncated part of the δm^2 exact expression. We could see that the resulting correlations are in many cases very similar to the true non-approximate correlations, which are the ones depicted in the presented figures.

We motivate our study as follows: First, the two zero textures can be seen as two 1×1 vanishing subtraces. Therefore, the two vanishing 2×2 subtrace textures can be considered as a nontrivial generalization of the two zero textures. Second, like the two zero textures, the two vanishing trace conditions put four real constraints on the neutrino mass matrix, which leave only five free parameters. Third, our model is very predictive concerning the CP-violating phases. There exist strong restrictions on them at all σ levels with either hierarchy types for all cases. Fourth, one can look at the two vanishing subtraces texture, comprising 15 cases, as a special case of the broader class characterized by two antiequalities between elements, which would contain 105 cases. Actually, the authors of [11] have studied the class of 65 textures characterized by two equalities, with no condition on the nonphysical phases, so some of the studied textures, there, are equivalent physically to the case where some equalities are replaced by antiequalities. However, in our study, we shall study neutrino patterns whose equivalent matrices with vanishing nonphysical phases have the form of two vanishing subtraces, providing thus more constraints on the studied texture, and the study cannot be considered related to that of [11].

The simple results one obtains are suggestive of some nontrivial symmetries or other underlying dynamics. While Abelian symmetries are simple and were used abundantly within type-I and type-II seesaw scenarios (e.g., see Refs. [10,16] and references therein), non-Abelian discrete symmetries are considered a far richer and more interesting choice for the flavor sector. Model builders have tried to derive experimental values of quark/lepton masses and mixing angles by assuming non-Abelian discrete flavor symmetries of quarks and leptons. In particular, lepton mixing has been intensively discussed in the context of non-Abelian discrete flavor symmetries, as seen, e.g., in the reviews [19,20]. We present two examples of non-Abelian symmetries within the type-II seesaw scenario, the first one based on the alternating A_4 group (even permutations of four objects) leading to a texture where the two vanishing traces in question lie on the diagonal, then present a second example based on the symmetric group S_4 (permutations of four objects) where the two traces in question do not lie on the diagonal.

The plan of the paper is as follows. We present the notations in Sec. II, followed in Sec. III by the texture definition. In Sec. IV, we present the simple viability check strategy based on imposing a vanishing solar mass squared difference and studying the consequent correlations. In Sec. V, we present the numerical analysis of all seven (out of fifteen) viable patterns, where for each one we present the analytical results and the correlation plots. In Sec. VI, we present symmetry realizations for two cases, and end up with conclusions and summary in Sec. VII. In Appendix A, we present the analysis of the eight failing patterns, whereas in Appendix B we state the analytical formulas for the Majorana phases for the viable patterns. Appendix C is devoted to the group theory of A_4, whereas in Appendix D, we present the group theory basics for $(S_n, n = 1, \ldots, 4)$ useful to understand the corresponding realization.

II. NOTATIONS

In the "flavor" basis, where the charged lepton mass matrix is diagonal, and thus the observed neutrino mixing matrix comes solely from the neutrino sector, we have

$$V^\dagger M_\nu V^* = \begin{pmatrix} m_1 & 0 & 0 \\ 0 & m_2 & 0 \\ 0 & 0 & m_3 \end{pmatrix}, \tag{1}$$

with $(m_i, i = 1, 2, 3)$ real and positive neutrino masses. We adopt the parametrization where the third column of V is real, and work in the subspace of vanishing nonphysical phases. The lepton mixing matrix V contains three mixing angles and three CP-violating phases. It can be written as a product of the Dirac mixing matrix U (consisting of three mixing angles and a Dirac phase) and a diagonal matrix P (consisting of two Majorana phases). Thus, we have

$$P^{\mathrm{Maj}} = \mathrm{diag}(e^{i\rho}, e^{i\sigma}, 1),$$
$$U = R_{23}(\theta_{23}) R_{13}(\theta_{13}) \mathrm{diag}(1, e^{-i\delta}, 1) R_{12}(\theta_{12}), \tag{2}$$

TABLE I. The experimental bounds for the oscillation parameters at 1-2-3σ levels, taken from the global fit to neutrino oscillation data [22] [the numerical values of Δm^2 are different from those in the reference which uses the definition $\Delta m^2 = |m_3^2 - m_1^2|$ instead of Eq. (4)]. Normal and inverted hierarchies are respectively denoted by NH and IH.

Parameter	Hierarchy	Best fit	1σ	2σ	3σ
δm^2 (10^{-5} eV^2)	NH, IH	7.50	[7.30, 7.72]	[7.12, 7.93]	[6.94, 8.14]
Δm^2 (10^{-3} eV^2)	NH	2.51	[2.48, 2.53]	[2.45, 2.56]	[2.43, 2.59]
	IH	2.48	[2.45, 2.51]	[2.42, 2.54]	[2.40, 2.57]
θ_{12} (°)	NH, IH	34.30	[33.30, 35.30]	[32.30, 36.40]	[31.40, 37.40]
θ_{13} (°)	NH	8.53	[8.41, 8.66]	[8.27, 8.79]	[8.13, 8.92]
	IH	8.58	[8.44, 8.70]	[8.30, 8.83]	[8.17, 8.96]
θ_{23} (°)	NH	49.26	[48.47, 50.05]	[47.37, 50.71]	[41.20, 51.33]
	IH	49.46	[48.49, 50.06]	[47.35, 50.67]	[41.16, 51.25]
δ (°)	NH	194.00	[172.00, 218.00]	[152.00, 255.00]	[128.00, 359.00]
	IH	284.00	[256.00, 310.00]	[226.00, 332.00]	[200.00, 353.00]

$$V = UP^{\mathrm{Maj}} = \begin{pmatrix} c_{12}c_{13}e^{i\rho} & s_{12}c_{13}e^{i\sigma} & s_{13} \\ (-c_{12}s_{23}s_{13} - s_{12}c_{23}e^{-i\delta})e^{i\rho} & (-s_{12}s_{23}s_{13} + c_{12}c_{23}e^{-i\delta})e^{i\sigma} & s_{23}c_{13} \\ (-c_{12}c_{23}s_{13} + s_{12}s_{23}e^{-i\delta})e^{i\rho} & (-s_{12}c_{23}s_{13} - c_{12}s_{23}e^{-i\delta})e^{i\sigma} & c_{23}c_{13} \end{pmatrix}, \tag{3}$$

where $R_{ij}(\theta_{ij})$ is the rotation matrix through the mixing angle θ_{ij} in the (i, j) plane, (δ, ρ, σ) are three CP-violating phases, and we denote $(c_{12} \equiv \cos\theta_{12}\ldots)$.

The neutrino mass spectrum is divided into two categories: normal hierarchy (**NH**) where $m_1 < m_2 < m_3$, and inverted hierarchy (**IH**) where $m_3 < m_1 < m_2$. The solar and atmospheric neutrino mass-squared differences, and their ratio R_ν, are defined as follows:

$$\delta m^2 \equiv m_2^2 - m_1^2, \quad \Delta m^2 \equiv \left| m_3^2 - \frac{1}{2}(m_1^2 + m_2^2) \right|, \quad R_\nu \equiv \frac{\delta m^2}{\Delta m^2}, \tag{4}$$

with data indicating ($R_\nu \ll 1$). Two parameters which put bounds on the neutrino mass scales, by the nuclear experiments on beta-decay kinematics and neutrinoless double-beta decay, are the effective electron-neutrino mass:

$$\langle m \rangle_e = \sqrt{\sum_{i=1}^{3} (|V_{ei}|^2 m_i^2)}, \tag{5}$$

and the effective Majorana mass term $\langle m \rangle_{ee}$:

$$\langle m \rangle_{ee} = |m_1 V_{e1}^2 + m_2 V_{e2}^2 + m_3 V_{e3}^2| = |M_{\nu 11}|. \tag{6}$$

Cosmological observations put bounds on the "sum" parameter Σ:

$$\Sigma = \sum_{i=1}^{3} m_i. \tag{7}$$

The last measurable quantity we shall consider is the Jarlskog rephasing invariant [21], which measures CP violation in the neutrino oscillations defined by

$$J = s_{12}c_{12}s_{23}c_{23}s_{13}c_{13}^2 \sin\delta. \tag{8}$$

The allowed experimental ranges of the neutrino oscillation parameters at different σ error levels as well as the best fit values are listed in Table I [22].

For the nonoscillation parameters, we adopt the upper limits, which are obtained by the KATRIN and Gerda experiment for m_e and m_{ee} [23,24].[2] However, we adopt for Σ the results of Planck 2018 [26] from temperature information with low energy by using the simulator SIMLOW:

$$\begin{aligned} \Sigma &< 0.54 \text{ eV}, \\ m_{ee} &< 0.228 \text{ eV}, \\ m_e &< 1.1 \text{ eV}. \end{aligned} \tag{9}$$

[2]In [25], a more recent lower upper bound of 0.9 eV for m_e was reported. However, the results of Table V show that adopting this newer limit will not change the conclusions and viability of the patterns.

TABLE II. The fifteen possible textures of two traceless submatrices. In the last column, we stated the current viability with the accommodated hierarchy type, to be contrasted with that of [17] in that I_4 ceases now to be allowed.

Texture	Symbol[a] and viability in [17]	Independent constraints	Current viability
$(\mathbf{C}_{33}, \mathbf{C}_{13})$	D_1, ✓	$M_{ee}+M_{\mu\mu}=0, M_{e\mu}+M_{\mu\tau}=0$	**IH**
$(\mathbf{C}_{22}, \mathbf{C}_{33})$	D_2, ✓	$M_{ee}+M_{\mu\mu}=0, M_{ee}+M_{\tau\tau}=0$	**NH**, **IH**
$(\mathbf{C}_{11}, \mathbf{C}_{12})$	D_3, ✓	$M_{\mu\mu}+M_{\tau\tau}=0, M_{e\mu}+M_{\tau\tau}=0$	**IH**
$(\mathbf{C}_{13}, \mathbf{C}_{23})$	N_1, ✓	$M_{e\mu}+M_{\mu\tau}=0, M_{ee}+M_{\mu\tau}=0$	**NH**
$(\mathbf{C}_{13}, \mathbf{C}_{12})$	N_2, ✗	$M_{e\mu}+M_{\mu\tau}=0, M_{e\mu}+M_{\tau\tau}=0$	
$(\mathbf{C}_{33}, \mathbf{C}_{23})$	I_1, ✗	$M_{ee}+M_{\mu\mu}=0, M_{ee}+M_{\mu\tau}=0$	
$(\mathbf{C}_{33}, \mathbf{C}_{12})$	I_2, ✓	$M_{ee}+M_{\mu\mu}=0, M_{e\mu}+M_{\tau\tau}=0$	**IH**
$(\mathbf{C}_{13}, \mathbf{C}_{11})$	I_3, ✓	$M_{e\mu}+M_{\mu\tau}=0, M_{\mu\mu}+M_{\tau\tau}=0$	**IH**
$(\mathbf{C}_{11}, \mathbf{C}_{23})$	I_4, ✓	$M_{\mu\mu}+M_{\tau\tau}=0, M_{ee}+M_{\mu\tau}=0$	
$(\mathbf{C}_{22}, \mathbf{C}_{23})$	I_5, ✗	$M_{ee}+M_{\tau\tau}=0, M_{ee}+M_{\mu\tau}=0$	
$(\mathbf{C}_{33}, \mathbf{C}_{11})$	I_6, ✗	$M_{ee}+M_{\mu\mu}=0, M_{\mu\mu}+M_{\tau\tau}=0$	
$(\mathbf{C}_{22}, \mathbf{C}_{12})$	I_7, ✓	$M_{ee}+M_{\tau\tau}=0, M_{e\mu}+M_{\tau\tau}=0$	**IH**
$(\mathbf{C}_{22}, \mathbf{C}_{11})$	I_8, ✗	$M_{ee}+M_{\tau\tau}=0, M_{\mu\mu}+M_{\tau\tau}=0$	
$(\mathbf{C}_{22}, \mathbf{C}_{13})$	No symbol, ✗	$M_{ee}+M_{\tau\tau}=0, M_{e\mu}+M_{\mu\tau}=0$	
$(\mathbf{C}_{23}, \mathbf{C}_{12})$	No symbol, ✗	$M_{ee}+M_{\mu\tau}=0, M_{e\mu}+M_{\tau\tau}=0$	

[a]The symbols (D, N, I) corresponded, respectively, in [17] to ["degenerate" ($m_1 \sim m_2 \sim m_3$), normal, inverted] ordering type, for some candidate benchmark points taken in each pattern with "testable" θ_x tuned to accommodate allowed values of (R_ν, θ_z, θ_y), whereas no such θ_x was possible in the last two patterns.

Actually, for the parameter Σ, we did not opt to take neither the most constraining cosmological bound ($\Sigma < 0.09$ eV) [27] using data from supernovae Ia luminosity distances with baryon acoustic oscillation observations and determinations of the growth rate parameter, nor the strict constraint of Planck 2018 combining baryon acoustic oscillation data in ΛCDM cosmology, which amounts to ($\Sigma < 0.12$ eV) [26], nor the bound ($\Sigma < 0.2$ eV) stated in PDG Live[3] originating from fits assuming various cosmological considerations, for the following reasons. First, since this constraint, as we shall see, proves to be quite severe ruling out many viable patterns, then by relaxing this "cosmological" constraint, we give more weight to colliders' data in testing our particle physics model. Second, we note that, even cosmology wise, this bound assumes some cosmological assumptions which are not anonymous. For example, in [28] it was argued that adopting the assumption of decaying neutrino into invisible dark radiation, on timescales of the age of the Universe, will alleviate the Σ bound and push it higher up to ($\Sigma < 0.9$ eV). Having said this though, we shall comment on the effect of adopting the severe bounds, coming from cosmology, where at least some patterns remain viable.

For simplification and clarity purposes regarding the analytical formulas, we henceforth denote, in line with the notations of the past study [17], the mixing angles as follows:

$$\theta_{12} \equiv \theta_x, \qquad \theta_{23} \equiv \theta_y, \qquad \theta_{13} \equiv \theta_z. \tag{10}$$

However, we shall keep the standard nomenclature in the tables and figures for rapid consultation purposes.

III. TEXTURES WITH TWO TRACELESS SUBMATRICES

The matrix M_ν is a 3×3 complex symmetric matrix. Thus, it has six independent 2×2 submatrices. When they are taken into pairs, we obtain 15 possibilities. Each location at the (i, j) entry of the 3×3 symmetric neutrino mass matrix M_ν determines, by deleting the ith line and jth column, a 2×2 submatrix, denoted by $\boldsymbol{C}_{ij}$. We are considering the texture characterized by two traceless such submatrices, which are shown in Table II.

The two vanishing-trace conditions are written as

$$\begin{aligned} M_{\nu\,ab}+M_{\nu\,cd}&=0,\\ M_{\nu\,ij}+M_{\nu\,kl}&=0, \end{aligned} \tag{11}$$

where $(ab)\neq(cd)$ and $(ij)\neq(kl)$. We write Eq. (11) in the terms of the V matrix elements as

$$\begin{aligned} \sum_{m=1}^{3}(U_{am}U_{bm}+U_{cm}U_{dm})\lambda_m&=0,\\ \sum_{m=1}^{3}(U_{im}U_{jm}+U_{km}U_{lm})\lambda_m&=0, \end{aligned} \tag{12}$$

where

[3]https://pdglive.lbl.gov/DataBlock.action?node=S066MNS.

$$\lambda_1 = m_1 e^{2i\rho}, \qquad \lambda_2 = m_2 e^{2i\sigma}, \qquad \lambda_3 = m_3. \tag{13}$$

By writing Eq. (12) in a matrix form, we obtain

$$\begin{pmatrix} A_1 & A_2 \\ B_1 & B_2 \end{pmatrix} \begin{pmatrix} \frac{\lambda_1}{\lambda_3} \\ \frac{\lambda_2}{\lambda_3} \end{pmatrix} = -\begin{pmatrix} A_3 \\ B_3 \end{pmatrix}, \tag{14}$$

where

$$\begin{aligned} A_m &= U_{am}U_{bm} + U_{cm}U_{dm}, \\ B_m &= U_{im}U_{jm} + U_{km}U_{lm}, \quad m = 1, 2, 3. \end{aligned} \tag{15}$$

By solving Eq. (12), we obtain

$$\begin{aligned} \frac{\lambda_1}{\lambda_3} &= \frac{A_3B_2 - A_2B_3}{B_1A_2 - A_1B_2}, \\ \frac{\lambda_2}{\lambda_3} &= \frac{A_1B_3 - A_3B_1}{B_1A_2 - A_1B_2}. \end{aligned} \tag{16}$$

Therefore, we get the mass ratios and the Majorana phases in terms of the mixing angles and the Dirac phase

$$\begin{aligned} m_{13} &\equiv \frac{m_1}{m_3} = \left|\frac{A_3B_2 - A_2B_3}{B_1A_2 - A_1B_2}\right|, \\ m_{23} &\equiv \frac{m_2}{m_3} = \left|\frac{A_1B_3 - A_3B_1}{B_1A_2 - A_1B_2}\right|, \end{aligned} \tag{17}$$

and

$$\begin{aligned} \rho &= \frac{1}{2}\arg\left(\frac{A_3B_2 - A_2B_3}{B_1A_2 - A_1B_2}\right), \\ \sigma &= \frac{1}{2}\arg\left(\frac{A_1B_3 - A_3B_1}{B_1A_2 - A_1B_2}\right). \end{aligned} \tag{18}$$

The neutrino masses are written as

$$m_3 = \sqrt{\frac{\delta m^2}{m_{23}^2 - m_{13}^2}}, \quad m_1 = m_3 \times m_{13}, \quad m_2 = m_3 \times m_{23}. \tag{19}$$

As we see, we have five input parameters corresponding to $(\theta_x, \theta_y, \theta_z, \delta, \delta m^2)$, which together with four real constraints in Eq. (12) allow us to determine the 9 degrees of freedom in M_ν.

IV. R_ν ROOTS AS A SIMPLE STRATEGY FOR VIABILITY CHECKING

In [17], one noted the sensitivity of R_ν to δ, in that imposing the "small" allowed values of R_ν singled out two corresponding δ's symmetric with respect to π. To see this, we note that the expression of the U's involving $e^{i\delta}$ [cf. Eq. (2)] means that doing the transformation

$$\delta \to 2\pi - \delta \tag{20}$$

would correspond to complex conjugating A and B, and so the ratios (m_{13}, m_{23}), and consequently R_ν, remain invariant as we have from Eq. (17):

$$R_\nu = \frac{m_{23}^2 - m_{13}^2}{|1 - \frac{1}{2}(m_{13}^2 + m_{23}^2)|} \approx 10^{-2}. \tag{21}$$

Also, since $R_\nu \ll 1$ is a very restrictive constraint on the allowed points, one can approximate the allowed parameter space with that corresponding to vanishing R_ν, i.e. to a zero for the $(m_2^2 - m_1^2)$ expression. This means that any allowed point $(\theta_x, \theta_y, \theta_z, \delta, \delta m)$ would lie in the vicinity of the point $(\theta_x, \theta_y, \theta_z, \delta, \delta m = 0)$. In our textures, R_ν, being a function of A and B and thus of U, is a function of the angles $(\theta_x, \theta_y, \theta_z$ and $\delta)$, so a root of R_ν, or equivalently of $(m_{23}^2 - m_{13}^2)$, would impose functional relations between these angles corresponding to correlations quite approaching the real ones. We shall see that the zeros of $(m_{23}^2 - m_{13}^2)$ play a decisive role in determining the correlation between the mixing and Dirac phase angles, and that would reflect on all other correlations depending on these angles, like those of ρ and σ.

In fact, imposing, in the textures under discussion, a zero for $(m_{23}^2 - m_{13}^2)$ leads to determining δ as a function of the angles $(\theta_x, \theta_y, \theta_z)$. Taking into consideration that the range of variability for the allowed θ_z is quite tight, we can fix it to its best fit value $\theta_z \approx 8.5^o$, and obtain δ as a function of (θ_x, θ_y). Drawing two curves obtained by fixing (θ_x) to its extreme values, one gets the approximative correlation region between δ and θ_y delimited by the former two curves. Exchanging the roles of θ_x and θ_y leads to the correlation (δ, θ_x).

We illustrate this in Fig. 1 where in the left (right) part, for one pattern to be studied later, we take the minimum

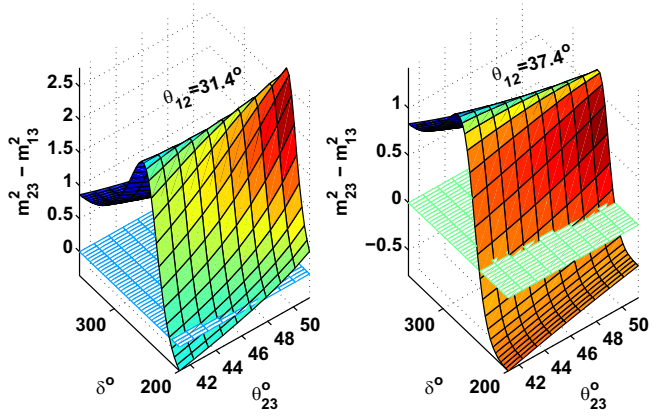

FIG. 1. Intersection of the zero surface $(m_1 = m_2)$ with that of $(m_{23}^2 - m_{13}^2)$ (as a 2-dim surface in δ, θ_y after fixing θ_x) gives an approximate correlation (θ_y, δ), in the texture (C_{22}, C_{12}), whose delimiting curves correspond to extreme values for θ_x.

TABLE III. Various precision-level correlations.

Observable expression using	$\delta m^2 \neq 0$ (physical world)	$\delta m^2 = 0$ (nonphysical world)
Complete formula	Full	Exact
Expansion up to a certain order in s_z	Truncated full	Approximate/truncated exact

(maximum) allowed value of $\theta_x = \theta_{12} = 31.4^o(37.4^o)$. Then, the surface of $(m_{23}^2 - m_{13}^2)$ as an expression in $(\delta, \theta_y = \theta_{23})$ intersects with the surface $(m_{23}^2 - m_{13}^2 = 0)$ in a curve representing the correlation (δ, θ_y) for the considered (θ_z, θ_x). Thus, the extreme corresponding "intersection" curves of $(\delta, \theta_y = \theta_{23})$ delimit the corresponding correlation region.

Another remark applies here in that if the zeros of $(m_{23}^2 - m_{13}^2)$ imply $(m_{13} = 1)$, then the corresponding pattern is failing and cannot accommodate data. This comes because one cannot here get the good order of magnitude for $|m_3^2 - \frac{1}{2}(m_1^2 + m_2^2)| \equiv \Delta m^2 \approx 10^{-3}$, since, up to order $10^{-5} \approx (m_2^2 - m_1^2)$, we have $m_3 = m_1$ leading to $\Delta m^2 = \frac{1}{2}(m_2^2 - m_1^2) = O(10^{-5})$ which cannot be amended to 10^{-3}. We shall see that two patterns are failing due to this remark. In general, one can plug any expression resulting from imposing zeros of $(m_{23}^2 - m_{13}^2)$ into the expression of m_{13} to deduce the hierarchy type.

In practice, we should distinguish between various kinds of correlations at successive levels of precision. First, there are the "full" correlations, where no approximation was used, and all experimental constraints were taken into consideration in the numerical scanning. One can take successive terms up to a certain order in the expansion of these full correlations in powers of s_z to get "truncated full" correlations. Second come the approaching correlations resulting from equating the exact expression of the squared mass difference $(m_{23}^2 - m_{13}^2)$ to zero, which we would call "exact" correlations. These correlations, formulas involving the observables, can in their turn be expanded to some order in powers of s_z to get "truncated exact" correlations. Third, the squared mass difference expression may form a complicated analytical expression of $(\theta_x, \theta_y, \theta_z, \delta)$, so one might resort to expanding this expression in increasing powers of s_z, and get "approximate" correlations resulting from putting equal to zero the expansion, up to a fixed order in s_z, of the $(m_{23}^2 - m_{13}^2)$ expression. We illustrate these different correlations in Table III, where the first column corresponds to the "physical world" with $(\delta m^2 \neq 0)$, whereas the second column corresponds to the "nonphysical world" where $(\delta m^2 = 0)$ leading to exact or approximate correlations. Concretely, for the measurable quantity m_{13}, suppose we have the following mathematical expressions [where, to fix the ideas, we assume the expansion is done up to $\mathcal{O}(s_z)$]:

$$\begin{aligned} m_{13} = f = f_0 + \mathcal{O}(s_z), \quad & m_{23}^2 - m_{13}^2 = g = g_0 + \mathcal{O}(s_z), \\ (g = 0 \Rightarrow m_{13} = h = h_0 + \mathcal{O}(s_z)), \quad & (g_0 = 0 \Rightarrow m_{13} = k = k_0 + \mathcal{O}(s_z)), \end{aligned} \tag{22}$$

then we have $(k_0 = h_0)$ and the following meanings:

$$\begin{aligned} \text{full means}: m_{13} = f, \quad & \text{truncated full means}: m_{13} = f_0, \\ \text{exact means}: m_{13} = h, \quad & \text{truncated exact means}: m_{13} = h_0 = k_0, \\ \text{approximate means}: m_{13} = k. & \end{aligned} \tag{23}$$

We checked that the exact correlations are very near the full ones in all patterns, whereas the approximate correlations may represent a non-negligible deviation unless one expands up to sufficiently high order in s_z.

V. NUMERICAL RESULTS

In this section, we introduce the numerical and analytical results for all seven viable two-vanishing-subtraces cases, and present the corresponding correlations graphs (we shall justify the nonviability of the remaining eight cases in Appendix A. For each texture, we give the analytical expression for the coefficients A and B of Eq. (15), and the leading expansion of the parameter R_ν. Because of cumbersomeness, we do not present the expressions of the other observables $(m_{13}, m_{23}, \rho, \sigma, m_{ee}, m_e)$, some of which appear in [6], but rather make use of the roots of the δm^2 expression to find approximate formulas allowing to interpret their correlations. However, for completeness, we put in Appendix B the leading orders of the

Majorana phases (ρ, σ), whose detailed study helps in justifying their relatively tight extents, even though, as said above, we shall use the R_ν-roots strategy in order to interpret, when possible, the general feature of the CP violation phases' narrow ranges.

As mentioned before, the free parameter space is fifth dimensional corresponding, say, to the three mixing angles (θ_x, θ_y, θ_z), the Dirac phase δ, and the solar neutrino mass difference δm^2. We throw N points of order $(10^7$–$10^{10})$ in the five-dimensional parameter space $(\theta_x, \theta_y, \theta_z, \delta, \delta m^2)$, and check first the type of the mass hierarchy through Eqs. (17) and (19). Second, we test the experimental bounds of Δm^2 besides those of Eq. (9) in order to determine the experimentally allowed regions. We notice from Table I that the experimental bounds of the neutrino oscillation parameters are different, except for θ_x and δm^2, in the two hierarchy cases, and so we have to repeat the sampling for each hierarchy case. The various predictions for the ranges of the neutrino physical parameters $(\theta_x, \theta_y, \theta_z, \delta, \rho, \sigma, m_1, m_2, m_3, m_{ee}, m_e, J)$ at all σ error levels with either hierarchy type are introduced in Table V.

We find that out of the 15 possible textures, only seven can accommodate the experimental data. Only the texture $(\mathbf{C}_{22}, \mathbf{C}_{33})$ is viable for both normal and inverted hierarchies, whereas the texture $(\mathbf{C}_{13}, \mathbf{C}_{23})$ can accommodate the data only for normal hierarchy, and the textures $(\mathbf{C}_{33}, \mathbf{C}_{13})$, $(\mathbf{C}_{22}, \mathbf{C}_{33})$, $(\mathbf{C}_{11}, \mathbf{C}_{12})$, $(\mathbf{C}_{33}, \mathbf{C}_{12})$, $(\mathbf{C}_{11}, \mathbf{C}_{13})$, $(\mathbf{C}_{22}, \mathbf{C}_{12})$ are viable for inverted hierarchy only. All cases can accommodate data at all three σ levels except the textures $(\mathbf{C}_{22}, \mathbf{C}_{33})$ in normal ordering and $(\mathbf{C}_{11}, \mathbf{C}_{12})$, which is of inverted type, accommodating data only at the 3σ level, and the textures, of inverted type, $(\mathbf{C}_{33}, \mathbf{C}_{12})$ and $(\mathbf{C}_{22}, \mathbf{C}_{12})$ which fail at the 1σ level.

We also find that neither m_1 for normal hierarchy nor m_3 for inverted hierarchy does approach a vanishing value, so there are no signatures for the singular textures. From Table V, we see that the allowed ranges for θ_y are strongly restricted for the texture $(\mathbf{C}_{22}, \mathbf{C}_{33})$ in normal ordering and in the texture $(\mathbf{C}_{11}, \mathbf{C}_{12})$, which is of inverted ordering, at the 3-σ level. There exist acute restrictions on the allowed ranges of the CP-violating phases (δ, ρ, σ) at all σ levels with either hierarchy type for all textures. We note from Eq. (8) that the J parameter depends strongly on δ ($J \propto \sin\delta$) because of the tight allowed experimental ranges of the mixing angles, which makes J variations, due to these angles' changes, tiny compared with those resulting from δ changes. The allowed values of the J parameter at the 1-σ level for the texture $(\mathbf{C}_{13}, \mathbf{C}_{23})$, which is of normal ordering, are negative. Therefore, the corresponding Dirac phase δ lies in the third or fourth quarters. Table V also reveals that $m_{ee} < 0.04$ eV for the textures $(\mathbf{C}_{13}, \mathbf{C}_{23})$, $(\mathbf{C}_{33}, \mathbf{C}_{12})$, $(\mathbf{C}_{13}, \mathbf{C}_{11})$ and $(\mathbf{C}_{22}, \mathbf{C}_{12})$. However, it has a bit higher upper bound $m_{ee} < 0.17$ for the remaining cases.

If we adopt the tightest bound of the sum parameter ($\Sigma < 0.09$ eV), or the strict Planck 2018 bound ($\Sigma < 0.12$ eV), we find that only the texture $(\mathbf{C}_{22}, \mathbf{C}_{33})$ in normal ordering can accommodate the data, in line with the conclusions of [27] that this low bound highly compromises the viability of the inverted mass ordering. Five patterns remain viable [$(\mathbf{C}_{22}, \mathbf{C}_{33})$ with $(\mathbf{C}_{13}, \mathbf{C}_{23})$ in normal ordering, and $(\mathbf{C}_{22}, \mathbf{C}_{12})$ with $(\mathbf{C}_{33}, \mathbf{C}_{12})$ and with $(\mathbf{C}_{11}, \mathbf{C}_{13})$ in inverted ordering] if we assume the constraint $\Sigma < 0.2$ eV as Table IV shows. However, as said earlier, we shall take the relaxed Planck 2018 bound $\Sigma < 0.54$ eV as we believe that by relaxing cosmological bounds, laboratory data are made to carry more weight than nonanonymously agreed upon cosmological data.

We introduce 15 correlation plots for each viable texture, in any allowed hierarchy type, generated from the accepted points of the neutrino physical parameters at the 3-σ level. The red (blue) plots represent the normal (inverted) ordering. The first and second rows represent the correlations between the mixing angles and the CP-violating phases. The third row introduces the correlations amidst the CP-violating phases, whereas the fourth one represents the correlations between the Dirac phase δ and each of J, m_{ee}

TABLE IV. The parameter Σ predictions, evaluated in eV, in the viable patterns adopting a relaxed Planck 2018 constraint ($\Sigma < 0.54$ eV). The second (third) line shows the corresponding viability adopting a strictest (more constrained) bound from [27] (PDG Live).

Texture	$(\mathbf{C}_{22}, \mathbf{C}_{33})$	$(\mathbf{C}_{22}, \mathbf{C}_{12})$	$(\mathbf{C}_{11}, \mathbf{C}_{12})$	$(\mathbf{C}_{33}, \mathbf{C}_{12})$	$(\mathbf{C}_{33}, \mathbf{C}_{13})$	$(\mathbf{C}_{11}, \mathbf{C}_{13})$	$(\mathbf{C}_{13}, \mathbf{C}_{23})$
Ordering	**N & I**	**I**	**I**	**I**	**I**	**I**	**N**
Predictions	**N**: $\Sigma \in$ [0.089, 0.211] **I**: $\Sigma \in$ [0.467, 0.539]	$0.192 \leq \Sigma \leq 0.205$	$0.532 \leq \Sigma \leq 0.540$	$0.125 \leq \Sigma \leq 0.136$	$0.291 \leq \Sigma \leq 0.330$	$0.151 \leq \Sigma \leq 0.163$	$0.163 \leq \Sigma \leq 0.213$
$\Sigma < 0.09$	✓ ✗	✗	✗	✗	✗	✗	✗
$\Sigma < 0.2$	✓ ✗	✓	✗	✓	✗	✓	✓

and m_2 parameters, respectively. The last row shows the degree of mass hierarchy plus the (m_{ee}, m_2) correlation.

In order to interpret the numerical results, we write down, for each pattern of the fifteen possible ones, the complete analytical expression of $(\delta m^2 = m_{23}^2 - m_{12}^2)$, possibly written as an expansion in s_z when the exact expression turns out to be too complicated, and analyze its zeros analytically and numerically. By assuming these zeros, we can justify the viability/nonviability of the pattern and its ordering hierarchy type, say by examining respectively the resulting (R_ν, m_{13}). Moreover, whenever the texture is viable, by assuming the zeros of the complete (leading order of the) δm^2 expression we get exact (approximate) correlation spectrum properties which would provide some explanations for the distinguishing features in the corresponding full correlation plots presented at the 3-σ level, such as those involving (ρ, σ).

Finally, we reconstruct M_ν with either allowed hierarchy type for each viable texture from the one representative point at the 3-σ level in the five-dimensional parameter space. The point is chosen to be as close as possible to the best fit values for mixing and Dirac phase angles.

A. Texture $(\mathbf{C_{22}}, \mathbf{C_{33}}) \equiv (M_{ee} + M_{\tau\tau} = 0, M_{ee} + M_{\mu\mu} = 0)$

A and B are given by

$$\begin{aligned} A_1 &= c_x^2 c_z^2 + (-c_x c_y s_z + s_x s_y e^{-i\delta})^2, \\ A_2 &= s_x^2 c_z^2 + (-s_x c_y s_z - c_x s_y e^{-i\delta})^2, \\ A_3 &= s_z^2 + c_y^2 c_z^2 \\ B_1 &= c_x^2 c_z^2 + (-c_x s_y s_z - s_x c_y e^{-i\delta})^2, \\ B_2 &= s_x^2 c_z^2 + (-s_x s_y s_z + c_x c_y e^{-i\delta})^2, \\ B_3 &= s_z^2 + s_y^2 c_z^2. \end{aligned} \tag{24}$$

We have the following truncated expression for R_ν:

$$R_\nu = \frac{2t_{2y}}{s_{2x} c_\delta} s_z + \mathcal{O}(s_z^2). \tag{25}$$

From Table V, we see that $(\mathbf{C_{22}}, \mathbf{C_{33}})$ texture is not viable at the 1-2-σ levels for normal ordering. We find that the mixing angles (θ_x, θ_z) extend over their allowed experimental ranges with either hierarchy type. However, there exists a strong restriction on θ_y in the case of normal ordering to lie in the interval $[44.87°, 45.13°]$. For normal ordering, there exists a mild forbidden gap $[252.5°, 288.4°]$ for δ, whereas the phases ρ and σ are restricted to the interval $[74°, 106°]$. For inverted ordering, we find a tight forbidden gap for δ and ρ around 270° and 90° respectively at the 3-σ level. The phases δ, ρ, and σ are tightly restricted at all σ levels; they are bound to the intervals $[267.36°, 272.53°]$, $[87.42°, 92.68°]$, and $[87.11°, 92.66°]$ respectively at the 3-σ-level. Table V also shows that neither m_1 for normal hierarchy nor m_3 for inverted hierarchy does reach zero at all error levels. Thus, the singular mass matrix is not predicted for this texture at all σ levels.

For normal ordering plots (Fig. 2), we see a tight forbidden gap for θ_y around 45° together with a mild forbidden region for the phase δ. We find a strong linear correlation between ρ and σ. One also notes the sinusoidal relations for (ρ, δ) and (σ, δ) correlations. We also find a moderate mass hierarchy where $0.32 \leq m_{13} \leq 0.79$ besides a quasidegeneracy characterized by $1.01 \leq \frac{m_2}{m_1} \leq 1.13$.

For inverted ordering plots (Fig. 3), we find narrow disallowed regions for ρ and δ around 90° and 270° respectively. We also see a narrow forbidden gap for θ_y around 45° as in normal ordering. We notice a quasidegeneracy characterized by $m_1 \approx m_2 \approx m_3$.

In order to justify these observations, we compute the mass-squared-difference full and approximate expressions, and we use the abbreviation "Num" ("Den") for "Numerator" ("Denominator"):

$$\begin{aligned} m_{23}^2 - m_{13}^2 &= \frac{\mathrm{Num}(m_{23}^2 - m_{13}^2)}{\mathrm{Den}(m_{23}^2 - m_{13}^2)}: \\ \mathrm{Num}(m_{23}^2 - m_{13}^2) &= 4c_z^2 c_{2y}\left(\frac{1}{2} s_{2y} s_{2x}(c_z^2 - 2) s_z c_\delta + c_{2y} c_{2x} s_z^2\right), \\ \mathrm{Den}(m_{23}^2 - m_{13}^2) &= -s_{2x}^2 s_{2y}^2 (1 + c_z^2) s_z^2 c_\delta^2 \\ &\quad + s_{2x} s_{2y} c_{2y} c_{2x} (2 + c_z^2) s_z c_\delta \\ &\quad - \frac{1}{4} s_{2x}^2 s_{2y}^2 c_z^4 s_z^2 - c_{2y}^2 c_{2x}^2, \end{aligned} \tag{26}$$

$$m_{23}^2 - m_{13}^2 = \frac{2t_{2y} t_{2x} c_\delta s_z}{c_{2x}} + \mathcal{O}(s_z^2). \tag{27}$$

Few remarks are in order here. First, we see from Eq. (27) that we should have $t_{2y} c_\delta > 0$ in order to meet the constraint $m_2 > m_1$, and thus we should have

$$\theta_y < \frac{\pi}{4} \Rightarrow \delta > \frac{3\pi}{2}, \qquad \theta_y > \frac{\pi}{4} \Rightarrow \delta < \frac{3\pi}{2}, \tag{28}$$

which is observed in the correlations between δ and θ_y in both **NH** and **IH**. Second, from Eq. (25), we see that both $\theta_y = \frac{\pi}{4}$ and $\delta = \frac{3\pi}{2}$ are separately forbidden, as each will give a too high value for R_ν unable to be brought back to the small experimental order of magnitude 10^{-2}. This explains why we observe a narrow gap around $(\theta_y = \frac{\pi}{4})$ and around $(\delta = \frac{3\pi}{2})$ in the relevant correlations for both **NH** and **IH**.

Third, and as was stated before, studying the zeros of $(m_{23}^2 - m_{13}^2)$ would put us near the allowed points in the parameter space. From Eq. (26), we see that this corresponds to two regimes.

(i) $c_{2y} \approx 0 \Rightarrow \theta_y \approx \frac{\pi}{4} \Rightarrow$ **NH**:
In this regime, we get

TABLE V. The various predictions for the ranges of the neutrino physical parameters for the 7 viable textures at all σ levels.

Pattern $(C_{22}, C_{33}) \equiv (M_{\nu 11} + M_{\nu 33} = 0, M_{\nu 11} + M_{\nu 22} = 0)$												
Quantity	$\theta_{12}^{\circ} \equiv \theta_x^o$	$\theta_{23}^{\circ} \equiv \theta_y^o$	$\theta_{13}^{\circ} \equiv \theta_z^o$	δ°	ρ°	σ°	m_1 (10^{-1} eV)	m_2 (10^{-1} eV)	m_3 (10^{-1} eV)	m_{ee} (10^{-1} eV)	m_e (10^{-1} eV)	J (10^{-1})
Normal hierarchy												
1σ	✗	✗	✗	✗	✗	✗	✗	✗	✗	✗	✗	✗
2σ	✗	✗	✗	✗	✗	✗	✗	✗	✗	✗	✗	✗
3σ	31.40–37.40	44.87–45.13	8.13–8.92	128.07–252.50 ∪ 288.40–358.93	74.61–105.36	74.64–105.34	0.17–0.65	0.19–0.65	0.53–0.82	0.16–0.62	0.19–0.65	−0.35–0.28
Inverted hierarchy												
1σ	33.30–35.30	48.49–50.06	8.44–8.70	268.68–269.25	90.69–91.08	87.72–88.57	1.64–1.71	1.64–1.71	1.56–1.64	1.56–1.64	1.64–1.71	−0.34– − 0.32
2σ	32.30–36.39	47.35–50.66	8.30–8.83	268.35–269.53	90.46–91.26	87.29–89.09	1.60–1.76	1.60–1.76	1.52–1.68	1.52–1.68	1.60–1.75	−0.35– − 0.31
3σ	31.40–37.39	41.19–44.97 ∪ 45.03–51.24	8.17–8.96	267.36–269.80 ∪ 270.20–272.53	87.42–89.78 ∪ 90.22–92.68	87.11–92.66	1.57–1.82	1.58–1.82	1.49–1.75	1.50–1.74	1.57–1.82	−0.36– − 0.30
Pattern $(C_{22}, C_{12}) \equiv (M_{\nu 11} + M_{\nu 33} = 0, M_{\nu 12} + M_{\nu 33} = 0)$												
Quantity	$\theta_{12}^{\circ} \equiv \theta_x^o$	$\theta_{23}^{\circ} \equiv \theta_y^o$	$\theta_{13}^{\circ} \equiv \theta_z^o$	δ°	ρ°	σ°	m_1 (10^{-1} eV)	m_2 (10^{-1} eV)	m_3 (10^{-1} eV)	m_{ee} (10^{-1} eV)	m_e (10^{-1} eV)	J (10^{-1})
Inverted hierarchy												
1σ	✗	✗	✗	✗	✗	✗	✗	✗	✗	✗	✗	✗
2σ	34.40–36.40	47.35–50.66	8.30–8.83	226.00–236.25	102.59–106.02	32.23–39.70	0.71–0.74	0.71–0.74	0.51–0.54	0.30–0.33	0.70–0.73	−0.29– − 0.23
3σ	31.40–37.39	41.16–51.25	8.17–8.96	200.00–244.53	95.33–107.77	14.34–46.26	0.70–0.74	0.70–0.75	0.50–0.55	0.30–0.37	0.70–0.74	−0.32– − 0.10
Pattern $(C_{11}, C_{12}) \equiv (M_{\nu 22} + M_{\nu 33} = 0, M_{\nu 21} + M_{\nu 33} = 0)$												
Quantity	$\theta_{12}^{\circ} \equiv \theta_x^o$	$\theta_{23}^{\circ} \equiv \theta_y^o$	$\theta_{13}^{\circ} \equiv \theta_z^o$	δ°	ρ°	σ°	m_1 (10^{-1} eV)	m_2 (10^{-1} eV)	m_3 (10^{-1} eV)	m_{ee} (10^{-1} eV)	m_e (10^{-1} eV)	J (10^{-1})
Inverted hierarchy												
1σ	✗	✗	✗	✗	✗	✗	✗	✗	✗	✗	✗	✗
2σ	✗	✗	✗	✗	✗	✗	✗	✗	✗	✗	✗	✗
3σ	31.40–37.39	51.16–51.25	8.17–8.96	262.79–268.92	5.71–9.54	168.06–173.00	1.79–1.82	1.80–1.82	1.73–1.75	1.73–1.75	1.79–1.82	−0.35– − 0.30
Pattern $(C_{33}, C_{12}) \equiv M_{\nu 11} + M_{\nu 22} = 0, M_{\nu 12} + M_{\nu 33} = 0)$												
Quantity	$\theta_{12}^{\circ} \equiv \theta_x^o$	$\theta_{23}^{\circ} \equiv \theta_y^o$	$\theta_{13}^{\circ} \equiv \theta_z^o$	δ°	ρ°	σ°	m_1 (10^{-1} eV)	m_2 (10^{-1} eV)	m_3 (10^{-1} eV)	m_{ee} (10^{-1} eV)	m_e (10^{-1} eV)	J (10^{-1})
Inverted hierarchy												
1σ	✗	✗	✗	✗	✗	✗	✗	✗	✗	✗	✗	✗
2σ	32.30–36.39	47.35–50.67	8.30–8.83	231.94–248.79	100.59–105.16	38.47–51.29	0.52–0.54	0.53–0.55	0.20–0.22	0.30–0.33	0.52–0.54	−0.33– − 0.25
3σ	31.40–37.39	41.16–51.25	8.17–8.96	226.89–254.21	99.40–106.17	34.65–57.53	0.52–0.55	0.53–0.56	0.19–0.23	0.30–0.37	0.52–0.55	−0.35– − 0.22

(Table continued)

TABLE V. *(Continued)*

Pattern $(C_{33}, C_{13}) \equiv (M_{\nu 11} + M_{\nu 22} = 0, M_{\nu 12} + M_{\nu 23} = 0)$												
Quantity	$\theta_{12}^{\circ} \equiv \theta_x^o$	$\theta_{23}^{\circ} \equiv \theta_y^o$	$\theta_{13}^{\circ} \equiv \theta_z^o$	δ°	ρ°	σ°	m_1 $(10^{-1}$ eV$)$	m_2 $(10^{-1}$ eV$)$	m_3 $(10^{-1}$ eV$)$	m_{ee} $(10^{-1}$ eV$)$	m_e $(10^{-1}$ eV$)$	J (10^{-1})
Inverted hierarchy												
Pattern $(C_{33}, C_{13}) \equiv (M_{\nu 11} + M_{\nu 22} = 0, M_{\nu 12} + M_{\nu 23} = 0)$												
Quantity	$\theta_{12}^{\circ} \equiv \theta_x^o$	$\theta_{23}^{\circ} \equiv \theta_y^o$	$\theta_{13}^{\circ} \equiv \theta_z^o$	δ°	ρ°	σ°	m_1 $(10^{-1}$ eV$)$	m_2 $(10^{-1}$ eV$)$	m_3 $(10^{-1}$ eV$)$	m_{ee} $(10^{-1}$ eV$)$	m_e $(10^{-1}$ eV$)$	J (10^{-1})
Inverted hierarchy												
1σ	33.30–35.30	48.49–50.06	8.44–8.70	264.35–265.70	93.91–94.53	80.10–81.43	1.06–1.10	1.07–1.10	0.94–0.98	0.99–1.03	1.06–1.10	−0.34– − 0.32
2σ	32.30–36.39	47.35–50.67	8.30–8.83	263.62–266.47	93.59–94.83	79.40–82.26	1.05–1.12	1.05–1.12	0.93–1.00	0.97–1.05	1.05–1.12	−0.35– − 0.31
3σ	31.40–37.39	41.17–51.24	8.17–8.96	262.85–267.59	92.56–95.16	78.67–84.28	1.00–1.13	1.01–1.14	0.88–1.02	0.95–1.07	1.00–1.13	−0.36– − 0.30
Pattern $(C_{13}, C_{11}) \equiv M_{\nu 12} + M_{\nu 23} = 0, M_{\nu 22} + M_{\nu 33} = 0)$												
Quantity	$\theta_{12}^{\circ} \equiv \theta_x^o$	$\theta_{23}^{\circ} \equiv \theta_y^o$	$\theta_{13}^{\circ} \equiv \theta_z^o$	δ°	ρ°	σ°	m_1 $(10^{-1}$ eV$)$	m_2 $(10^{-1}$ eV$)$	m_3 $(10^{-1}$ eV$)$	m_{ee} $(10^{-1}$ eV$)$	m_e $(10^{-1}$ eV$)$	J (10^{-1})
Inverted hierarchy												
1σ	33.39–35.30	48.49–50.06	8.44–8.70	301.96–309.99	165.23–167.75	46.81–52.37	0.59–0.60	0.60–0.61	0.33–0.34	0.33–0.34	0.59–0.60	−0.29– − 0.25
2σ	32.30–36.39	47.35–50.67	8.30–8.83	297.60–315.86	163.81–169.35	43.84–56.57	0.59–0.60	0.59–0.61	0.33–0.34	0.32–0.34	0.58–0.60	−0.31– − 0.22
3σ	31.40–37.39	41.17–51.24	8.17–8.96	292.68–321.16	162.53–170.80	39.98–60.41	0.58–0.62	0.59–0.63	0.32–0.37	0.32–0.36	0.58–0.62	−0.33– − 0.19
Pattern $(C_{13}, C_{23}) \equiv (M_{\nu 12} + M_{\nu 23} = 0, M_{\nu 11} + M_{\nu 23} = 0)$												
Quantity	$\theta_{12}^{\circ} \equiv \theta_x^o$	$\theta_{23}^{\circ} \equiv \theta_y^o$	$\theta_{13}^{\circ} \equiv \theta_z^o$	δ°	ρ°	σ°	m_1 $(10^{-1}$ eV$)$	m_2 $(10^{-1}$ eV$)$	m_3 $(10^{-1}$ eV$)$	m_{ee} $(10^{-1}$ eV$)$	m_e $(10^{-1}$ eV$)$	J (10^{-1})
Normal hierarchy												
1σ	33.30–34.78	48.87–50.05	8.41–8.66	202.90–217.99	96.82–101.58	16.20–26.78	0.57–0.61	0.58–0.62	0.76–0.79	0.23–0.24	0.58–0.62	−0.21– − 0.13
2σ	32.30–36.39	47.37–50.71	8.27–8.79	152.02–232.55	81.53–106.09	0.02–36.72 ∪ 160.00–179.95	0.55–0.63	0.56–0.64	0.74–0.81	0.23–0.24	0.56–0.64	−0.28–0.16
3σ	31.40–37.39	41.20–51.32	8.13–8.92	128.01–242.79	73.50–108.48	0.07–44.68 ∪ 142.50–179.93	0.47–0.65	0.47–0.66	0.68–0.83	0.21–0.24	0.47–0.66	−0.31–0.28

$$m_{13}^2 = m_{23}^2 = \frac{(c_z^2-2)^2}{c_z^4+4(1+c_z^2)c_\delta^2} \approx \frac{1}{1+8c_\delta^2} < 1, \tag{29}$$

$$\rho \approx \sigma = \frac{1}{2}\tan^{-1}\left(\frac{s_{2\delta}}{1+2c_\delta^2}\right)+\frac{\pi}{2}+\mathcal{O}(s_z), \tag{30}$$

$$m_{ee} = \frac{m_3}{\sqrt{1+8c_\delta^2}}+\mathcal{O}(s_z^2). \tag{31}$$

From Eq. (29), this regime corresponds to **NH**. In this regime, δ can take any of this texture's allowed values, except the narrow band around $3\pi/2$. The correlations, resulting from Eq. (30), of ρ and σ with respect to δ are observed in the corresponding **NH** plots. Likewise, Eq. (31) justifies the shape of the correlation (m_{ee},δ) observed in this **NH** regime.

(ii) $(\frac{1}{2}s_{2y}s_{2x}(c_z^2-2)s_z c_\delta + c_{2y}c_{2x}s_z^2 \approx 0)\dagger \Rightarrow$ **IH**:
Here we have

$$m_{13}^2 = m_{23}^2 = 1+\frac{s_z^2}{s_y^2 c_y^2 c_z^4} > 1, \tag{32}$$

so this regime corresponds to **IH**. In this regime, we find, by putting $(c_z \approx 1)$ in the approximative regime-defining constraint (†), the following:

$$c_\delta \approx \frac{2s_z}{t_{2y}t_{2x}} \ll 1, \tag{33}$$

and so from the allowed values of $\delta \in [200^o, 353^o]$ (see Table I in the **IH** case) we see that δ should be around the value $3\pi/2$ without hitting it, whereas no restrictions over θ_y apart from disallowing the value $\pi/4$. This is what we observe in the relevant **IH** correlation plots.

Now, with $\delta \approx 3\pi/2$ one finds

$$\rho \approx \sigma = \frac{\pi}{2}+\mathcal{O}(s_z), \tag{34}$$

which we observe in the full, i.e. nonapproximate, numerical results. Thus, we could interpret the very tight ranges of the *CP* violation phases with $(\delta \sim 3\pi/2, \rho \sim \pi/2 \sim \sigma)$. Finally, with Eq. (32), we find a quasidegenerate spectrum $(m_{13} \approx m_{23} \approx 1)$ and that m_{ee} matches this common mass scale, which we observe in the plots.

Finally, we reconstruct the neutrino mass matrix for a representative point. For normal ordering, the representative point is taken as the following:

$$\begin{aligned}(\theta_{12},\theta_{23},\theta_{13}) &= (34.0696°, 45.1044°, 8.4838°),\\ (\delta,\rho,\sigma) &= (195.8781°, 95.4176°, 95.3851°),\\ (m_1,m_2,m_3) &= (0.0180\text{ eV}, 0.0199\text{ eV}, 0.0530\text{ eV}),\\ (m_{ee},m_e) &= (0.0171\text{ eV}, 0.0200\text{ eV}),\end{aligned} \tag{35}$$

the corresponding neutrino mass matrix (in eV) is

$$M_\nu = \begin{pmatrix} -0.0167-0.0034i & 0.0080+0.0003i & 0.0067+0.0004i \\ 0.0080+0.0003i & 0.0167+0.0034i & 0.0348-0.0035i \\ 0.0067+0.0004i & 0.0348-0.0035i & 0.0167+0.0034i \end{pmatrix}. \tag{36}$$

For inverted ordering, the representative point is taken as the following:

$$\begin{aligned}(\theta_{12},\theta_{23},\theta_{13}) &= (34.3118°, 49.2414°, 8.4204°),\\ (\delta,\rho,\sigma) &= (269.0126°, 90.8634°, 88.2051°),\\ (m_1,m_2,m_3) &= (0.1733\text{ eV}, 0.1735\text{ eV}, 0.1659\text{ eV}),\\ (m_{ee},m_e) &= (0.1660\text{ eV}, 0.1732\text{ eV}).\end{aligned} \tag{37}$$

The corresponding neutrino mass matrix (in eV) is

$$M_\nu = \begin{pmatrix} -0.1660-0.0001i & 0.0324-0.0001i & 0.0377+0.0001i \\ 0.0324-0.0001i & 0.1660+0.0001i & -0.0074-0.0001i \\ 0.0377+0.0001i & -0.0074-0.0001i & 0.1660+0.0001i \end{pmatrix}. \tag{38}$$

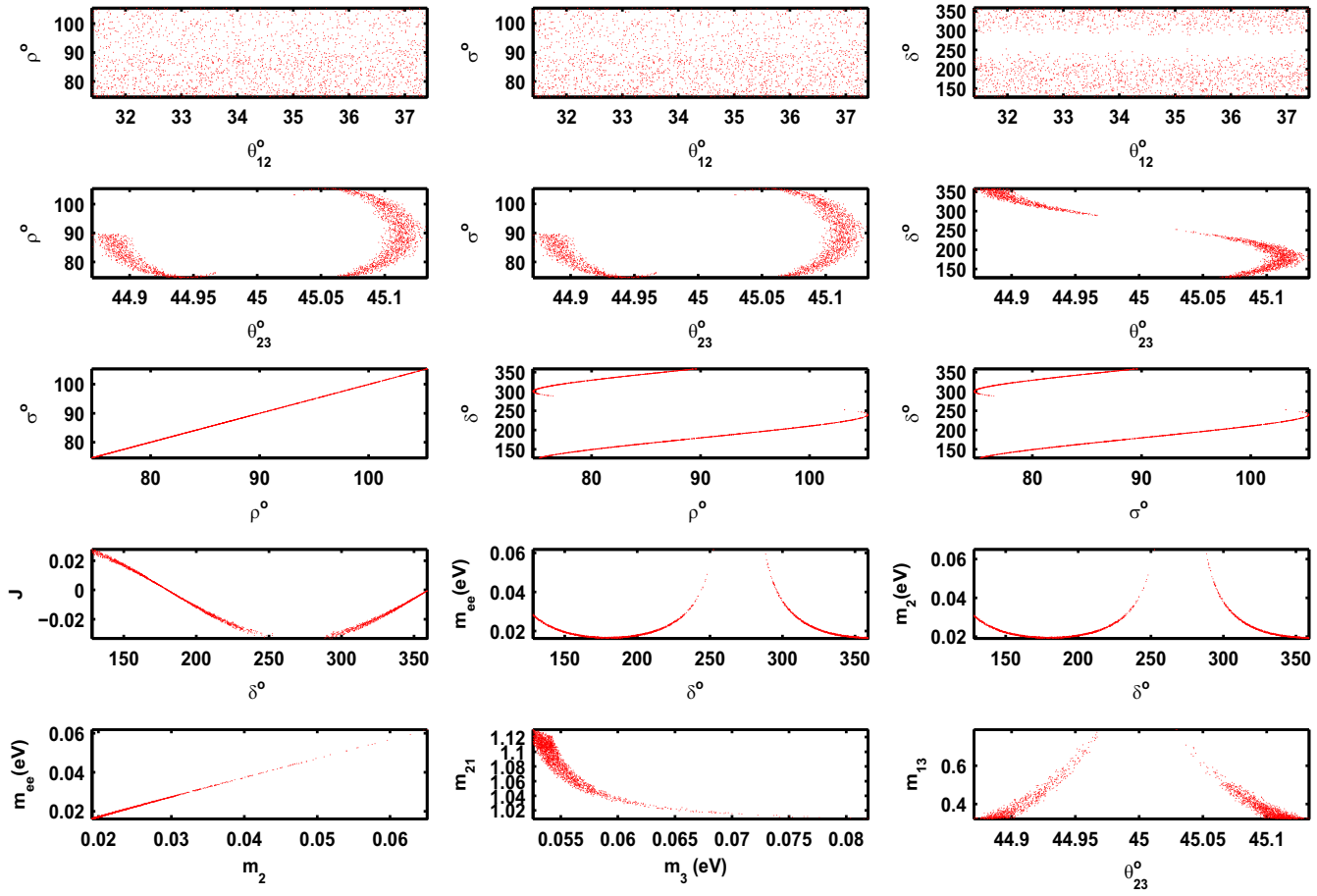

FIG. 2. The correlation plots for $(\mathbf{C}_{22}, \mathbf{C}_{33}) \equiv (M_{ee} + M_{\tau\tau} = 0, M_{ee} + M_{\mu\mu} = 0)$ texture, in the normal ordering hierarchy. The first and second rows represent the correlations between the mixing angles $(\theta_{12}, \theta_{23})$ and the CP-violating phases. The third row introduces the correlations amidst the CP-violating phases, whereas the fourth one represents the correlations between the Dirac phase δ and each of J, m_{ee} and m_2 parameters, respectively. The last row shows the degree of mass hierarchy plus the (m_{ee}, m_2) correlation.

B. Texture $(\mathbf{C}_{22},\mathbf{C}_{12}) \equiv (M_{ee} + M_{\tau\tau} = 0, M_{e\mu} + M_{\tau\tau} = 0)$

A and B are given by

$$
\begin{aligned}
A_1 &= c_x^2 c_z^2 + (-c_x c_y s_z + s_x s_y e^{-i\delta})^2,\\
A_2 &= s_x^2 c_z^2 + (-s_x c_y s_z - c_x s_y e^{-i\delta})^2,\\
A_3 &= s_z^2 + c_y^2 c_z^2,\\
B_1 &= c_x c_z(-c_x s_y s_z - s_x c_y e^{-i\delta}) + (-c_x c_y s_z + s_x s_y e^{-i\delta})^2,\\
B_2 &= s_x c_z(-s_x s_y s_z + c_x c_y e^{-i\delta}) + (-s_x c_y s_z - c_x s_y e^{-i\delta})^2,\\
B_3 &= s_y c_z s_z + c_y^2 c_z^2.
\end{aligned} \tag{39}
$$

Then R_ν is given by

$$
R_\nu = \frac{2c_y^4(c_{2x} + 2c_y c_x s_x c_\delta)}{|R_2|\mathrm{sgn}(R_1)} + \mathcal{O}(s_z), \tag{40}
$$

where

$$
\begin{aligned}
R_1 = {} & 4c_x^2 s_x^2 c_y^2 s_y^2 c_\delta^2 + 2c_y c_x s_x s_y^2(2 - c_y^2)c_{2x} c_\delta\\
& + c_x^2 s_x^2 c_y^6 + c_{2x}^2 c_y^4 - 2c_{2x}^2 c_y^2 + c_{2x}^2,
\end{aligned} \tag{41}
$$

$$
\begin{aligned}
R_2 = {} & 8c_x^2 s_x^2 c_y^2 s_y^2 c_\delta^2 + 2c_y c_x s_x c_{2x}(4 + c_y^4 - 6c_y^2)c_\delta\\
& + (-6c_x^2 s_x^2 + 1)c_y^4 - 4c_{2x}^2 c_y^2 + 2c_{2x}^2.
\end{aligned} \tag{42}
$$

Table V shows that $(\mathbf{C}_{22}, \mathbf{C}_{12})$ texture cannot accommodate the experimental data in the case of normal ordering, whereas it is viable at the 2-3-σ levels for inverted ordering. The allowed experimental ranges of the mixing angles $(\theta_x, \theta_y, \theta_z)$ are covered at all σ levels. We find wide disallowed regions for δ such as $[236.26°, 322°]$ at the 2-σ level and $[244.54°, 353°]$ at the 3-σ level. The phases $\rho(\sigma)$ are bounded to the intervals $[102.59°, 106.02°]([32.23°, 39.70°])$ at the 2-σ level and $[95.33°, 107.77°]([14.34°, 46.26°])$ at the 3-σ level. One also notes that m_3 does not approach a vanishing value, thus the singular mass matrix is not predicted.

From Fig. 4, we see that θ_x increases when CP-violating phases tend to increase. We also see a strong linear relation

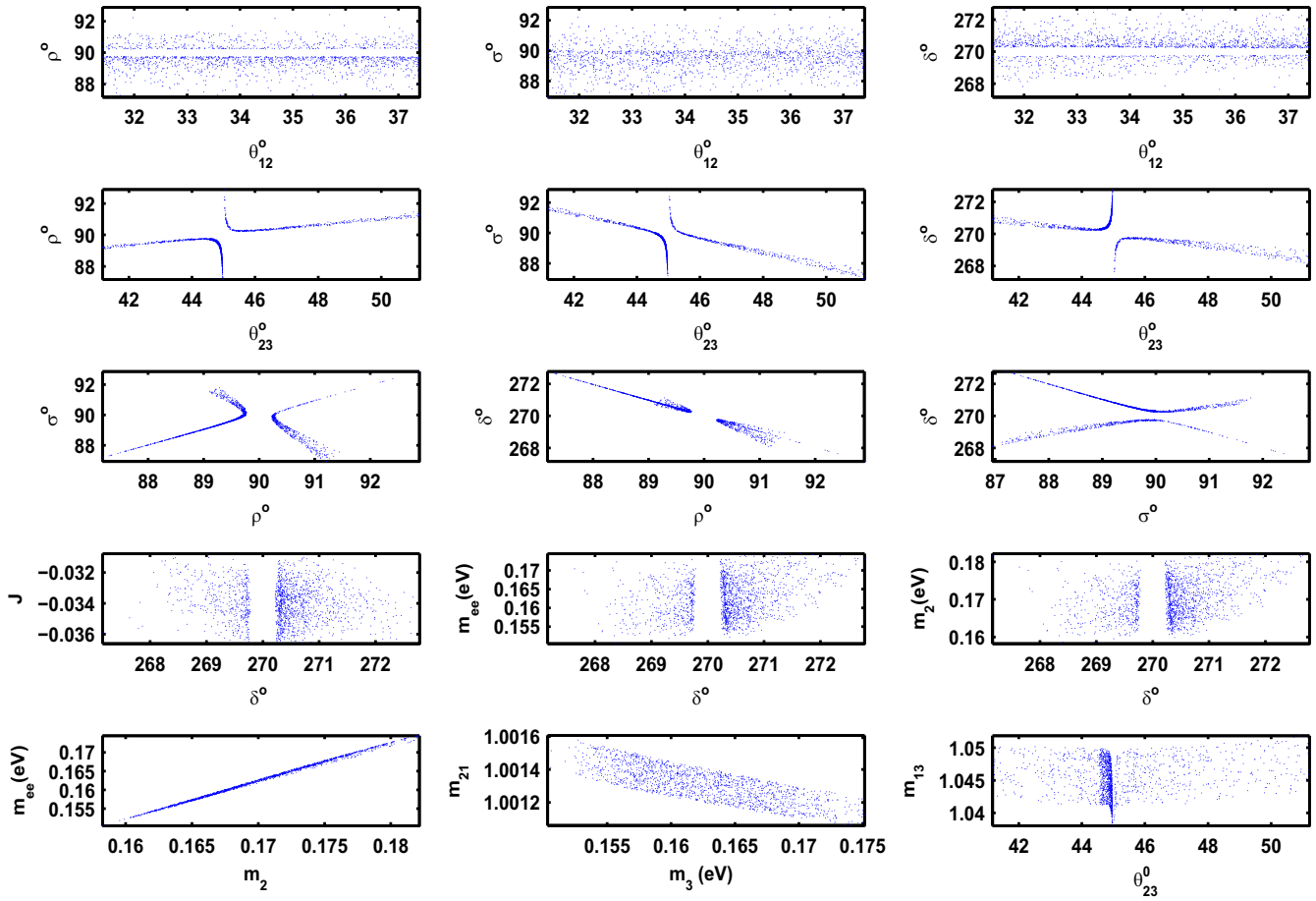

FIG. 3. The correlation plots for $(\mathbf{C}_{22}, \mathbf{C}_{33}) \equiv (M_{ee} + M_{\tau\tau} = 0, M_{ee} + M_{\mu\mu} = 0)$ texture, in the inverted ordering hierarchy. The first and second rows represent the correlations between the mixing angles $(\theta_{12}, \theta_{23})$ and the CP-violating phases. The third row introduces the correlations amidst the CP-violating phases, whereas the fourth one represents the correlations between the Dirac phase δ and each of J, m_{ee} and m_2 parameters, respectively. The last row shows the degree of mass hierarchy plus the (m_{ee}, m_2) correlation.

for (σ,δ) correlation as well as quasilinear relations for (ρ,δ) and (ρ,σ) correlations. We notice that one finds a quasidegeneracy characterized by $1.35 \leq m_{13} \leq 1.39$ and $m_1 \approx m_2$.

In order to explain the correlation plots, one compute the mass-squared-difference full and approximate expressions:

$$m_{23}^2 - m_{13}^2 = \frac{\mathrm{Num}(m_{23}^2 - m_{13}^2)}{\mathrm{Den}(m_{23}^2 - m_{13}^2)}:$$

$$\begin{aligned}\mathrm{Num}(m_{23}^2 - m_{13}^2) = {} & s_{2x}c_y c_\delta[c_z^3(c_z^2-2)c_y^4 + 2(2c_z^2-3)c_z(s_z c_z c_y - s_z^2)c_y^2 + s_z^2(-5c_z s_z^2 + 2s_y s_z)] \\ & - c_{2x}[(7c_y^4 - 2c_y^2 - 1)c_z^4 + 2s_z s_y(4c_y^2 + c_y^4 - 1)c_z^3 + (2 - 6c_y^4)c_z^2 - 2s_z s_y(-1 + 3c_y^2)c_z + c_{2y}] \end{aligned} \quad (43)$$

$$m_{23}^2 - m_{13}^2 = \frac{c_y^4(c_{2x} + 2c_y s_x c_x c_\delta)}{4s_x^2 c_x^2 s_y^2 c_y^2 c_\delta^2 + 2c_y s_y^2 s_x c_x c_{2x}(1 + s_y^2)c_\delta + c_y^6 c_x^2 s_x^2 + c_{2x}^2 c_y^4 - c_{2x}^2 c_{2y}} + \mathcal{O}(s_z). \quad (44)$$

We checked that the zeros of $\mathrm{Num}(m_{23}^2 - m_{13}^2)$ give exact correlations in excellent agreement with the full correlations, which are calculated based on numerical exact calculations taking all constraints into consideration. However, the zeros of the leading term of the mass-squared difference, i.e. of $(c_{2x} + 2c_y s_x c_x c_\delta)$, would lead to approximate correlations which agree mediocrely with the full and one needs higher orders inclusion in order to have a better

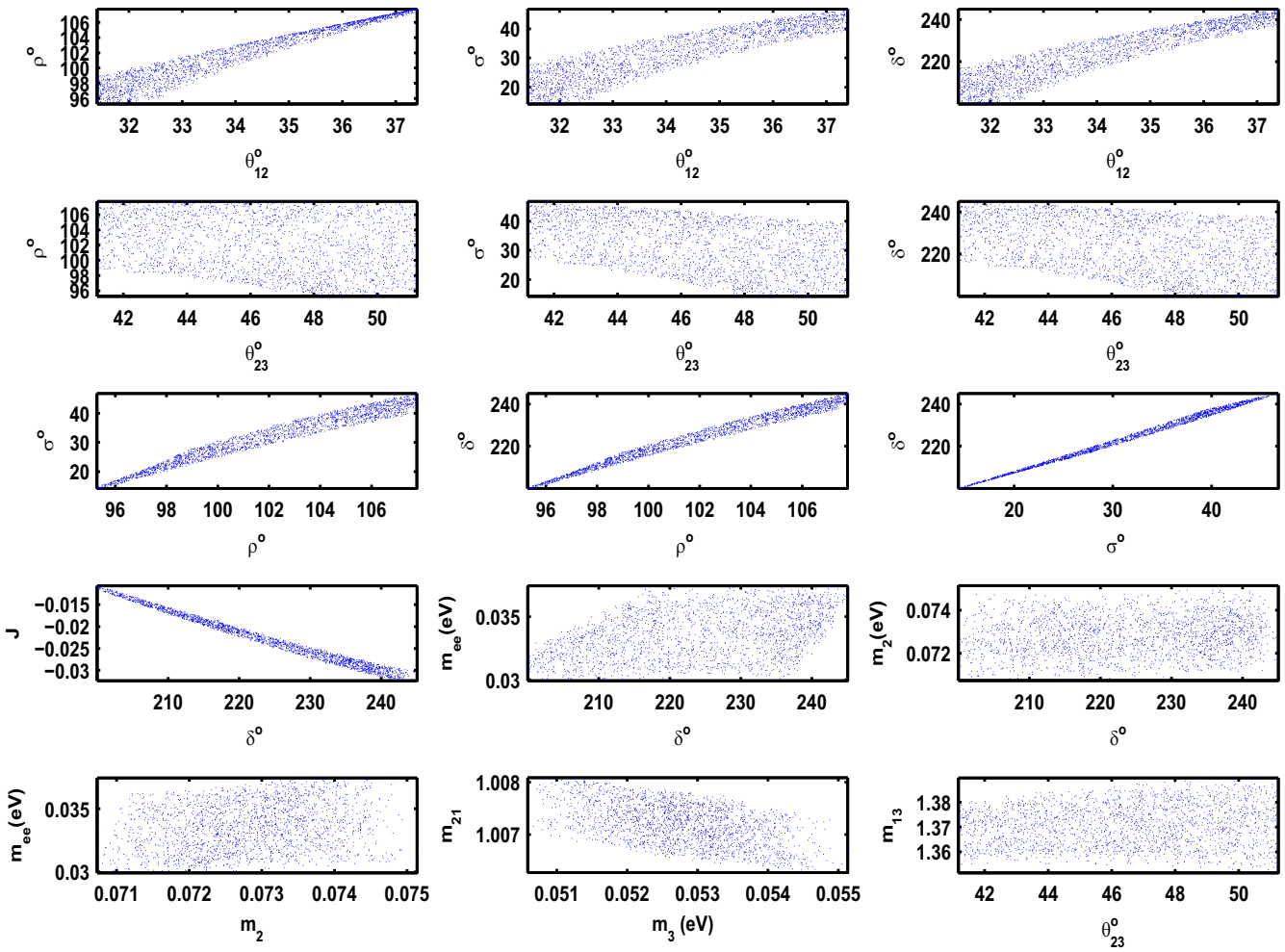

FIG. 4. The correlation plots for $(\mathbf{C}_{22}, \mathbf{C}_{12}) \equiv (M_{ee} + M_{\tau\tau} = 0, M_{e\mu} + M_{\tau\tau} = 0)$ texture in the case of inverted hierarchy. The first and second rows represent the correlations between the mixing angles $(\theta_{12}, \theta_{23})$ and the CP-violating phases. The third and fourth rows show the correlations amidst the CP-violating phases and the correlations between the Dirac phase δ and each of J, m_{ee} and m_2 parameters, respectively. The last row shows the degree of mass hierarchy plus the (m_{ee}, m_2) correlation.

agreement. As an illustrative example, we find that the full range for m_{13}, spanned by the allowed points considering all experimental constraints, is [1.35, 1.39]. Now, if we impose a zero for the $(m_{23}^2 - m_{13}^2)$ expression $[(c_{2x} + 2c_y s_x c_x c_\delta)$ expression], in terms of $(\theta_x, \theta_y, \theta_z, \delta)$, then one gets δ, say, in terms of θ_x, θ_y, θ_z, and so m_{13} is expressed in terms of these mixing angles which, when scanned over their allowable ranges, give the exact (approximate) range for m_{13} found to be [1.342, 1.376] ([1.35, 1.75]). This corresponds to a good (mediocre) approximation, indicating we have an **IH**. Moreover, plugging the zeros of $(m_{23}^2 - m_{13}^2)$ in the expression of m_{13} leads to

$$m_{13} = \sqrt{2 + t_y^2}\left(1 - \frac{2 s_y s_z}{c_y^2(1 + c_y^2)}\right) + \mathcal{O}(s_z^2). \quad (45)$$

We can now calculate the truncated exact range, corresponding to scanning the leading term in Eq. (45), and we would have found [1.03, 1.32], indicating again a **IH**, albeit the agreement of this correlation with the full range is again mediocre.

Moreover, one can fix $\theta_z \approx 8.5^o$, and for any given θ_x we draw the surface of $(m_{23}^2 - m_{13}^2)$ varying θ_y and δ over their experimentally allowed regions, then the intersection of this surface with the $(m_{23}^2 - m_{13}^2 = 0)$ determines an exact correlation between θ_y and δ. We checked that juxtaposing such curves, upon varying θ_x, generates approximately well the full correlation (θ_y, δ). In the left (right) part of Fig. 1, we take the minimum (maximum) allowed value of $\theta_x = \theta_{12} = 31.4^o(37.4^o)$, and find that the corresponding intersection curves of $(\delta, \theta_y = \theta_{23})$ delimit the corresponding correlation region.

Finally, fixing $\theta_x \approx 35^o$, we find from Table V that we can take the representative points $\rho \simeq 90^0, \sigma \simeq 30^0$, and so, with $m_1 \sim m_2 \sim 0.07$ eV in $m_{ee} \approx |m_1 \cos^2(35^o)e^{i\pi} + \sin^2(35^o)e^{i\pi/3} + m_3 \sin^2(\theta_z)|$ we get a partial cancellation of the contributions of (m_1, m_2) and we get $m_{ee} \sim 0.04$ eV.

Reconstructing the neutrino mass matrix for inverted ordering, the representative point is taken as follows:

$$\begin{aligned}(\theta_{12}, \theta_{23}, \theta_{13}) &= (34.3208°, 49.2183°, 8.5319°),\\ (\delta, \rho, \sigma) &= (222.6055°, 101.8830°, 30.2439°),\\ (m_1, m_2, m_3) &= (0.0724 \text{ eV}, 0.0729 \text{ eV}, 0.0527 \text{ eV}),\\ (m_{ee}, m_e) &= (0.0319 \text{ eV}, 0.0721 \text{ eV}),\end{aligned} \tag{46}$$

and the corresponding neutrino mass matrix (in eV) is

$$M_\nu = \begin{pmatrix} -0.0319 + 0.0003i & -0.0319 + 0.0003i & 0.0564 - 0.0004i \\ -0.0319 + 0.0003i & 0.0531 - 0.0003i & 0.0068 + 0.0003i \\ 0.0564 - 0.0004i & 0.0068 + 0.0003i & 0.0319 - 0.0003i \end{pmatrix}. \tag{47}$$

C. Texture $(\mathbf{C_{11}}, \mathbf{C_{12}}) \equiv (M_{\mu\mu} + M_{\tau\tau} = 0, M_{e\mu} + M_{\tau\tau} = 0)$

A and B are given by

$$\begin{aligned}A_1 &= c_x^2 s_z^2 + s_x^2 e^{-2i\delta},\\ A_2 &= s_x^2 s_z^2 + c_x^2 e^{-2i\delta},\\ A_3 &= c_z^2,\\ B_1 &= c_x c_z(-c_x s_y s_z - s_x c_y e^{-i\delta}) + (-c_x c_y s_z + s_x s_y e^{-i\delta})^2,\\ B_2 &= s_x c_z(-s_x s_y s_z + c_x c_y e^{-i\delta}) + (-s_x c_y s_z - c_x s_y e^{-i\delta})^2,\\ B_3 &= s_y c_z s_z + c_y^2 c_z^2.\end{aligned} \tag{48}$$

The R_ν approximate expression will be

$$R_\nu = \frac{2(s_{2x} c_y c_\delta c_{2y} - c_{2x} c_{2y}^2)}{|c_{2y}^2(1 - 2s_x^2 c_x^2) - s_{2x} c_{2x} c_y c_{2y} c_\delta|} + \mathcal{O}(s_z). \tag{49}$$

From Table V, we find that ($\mathbf{C}_{11}$, $\mathbf{C}_{12}$) texture can accommodate the experimental data only at the 3-σ level for inverted ordering. We find that the allowed experimental ranges for the mixing angles (θ_x, θ_z) extend over their allowed experimental ranges. However, the allowed range for θ_y is strongly restricted to the interval $[51.16°, 51.25°]$. We also notice that the phases δ, ρ and σ are bounded to the intervals $[262.79°, 268.92°]$, $[5.71°, 9.54°]$ and $[168.06°, 173.00°]$, respectively. Table V also reveals that m_3 does not reach a vanishing value. Therefore, the singular mass matrix is not expected for this texture.

From Fig. 5, we see that θ_x increases when the CP-violating phases tend to increase. We also find a quasilinear correlation between σ and δ. There exists a quasidegeneracy characterized by $m_1 \approx m_2 \approx m_3$.

In order to explain the correlation plots, one computes the mass-squared-difference full and approximate expressions:

$$\begin{aligned}m_{23}^2 - m_{13}^2 &= \frac{\text{Num}(m_{23}^2 - m_{13}^2)}{\text{Den}(m_{23}^2 - m_{13}^2)}:\\ \text{Num}(m_{23}^2 - m_{13}^2) &= -c_z^3\{s_{2x} c_y[c_z^2(6c_y^2 - 5)\\ &\quad + c_y s_{2y} s_{2z} + 4s_y^2]c_\delta\\ &\quad - c_{2y} c_{2x}(c_z c_{2y} + 2s_z s_y)\},\end{aligned} \tag{50}$$

$$\begin{aligned}m_{23}^2 - m_{13}^2 &= \frac{s_{2x} c_y c_{2y} c_\delta - c_{2y}^2 c_{2x}}{c_y^2 s_x^2 c_x^2}\\ &\quad + \frac{-2s_y s_z}{c_y^3 c_x^3 s_x^4}[2s_x^2 c_x c_y c_{2y} c_{2x} c_\delta^2\\ &\quad - s_x c_\delta(c_x^4(-5s_{2y}^2 + 4) + 5s_{2y}^2 c_x^2 + c_{2y})\\ &\quad - c_x c_y(4c_y^2 - 3)c_{2y} s_x^2 c_{2x}] + \mathcal{O}(s_z^2).\end{aligned} \tag{51}$$

The zeros of $\text{Num}(m_{23}^2 - m_{13}^2)$ give exact correlations in excellent agreement with the full correlations, and all correlations can be determined from these zeros. However, the zeros of the zeroth order leading term of the mass-squared difference would lead to (zeroth-order) approximate correlations which do not agree well with the full ones, and one has to go, say, up to the next-to-leading term in order to get (first-order) approximate correlations with a better agreement. Actually, even the zeroth-order leading term of the $(m_{23}^2 - m_{13}^2)$ expression can give useful interconnections. For example, from the constraint $m_2 > m_1$, we need to have $c_{2y} c_\delta > 0$, whence, considering the experimental constraints on (θ_y, δ), we have the following observed relations:

$$\delta > 270^o \Rightarrow \theta_y < 45^o, \qquad \delta < 270^o \Rightarrow \theta_y > 45^o. \tag{52}$$

Also, we have the (zeroth-order) approximate correlation:

$$c_\delta = \frac{c_{2y} c_{2x}}{s_{2x} c_y}, \tag{53}$$

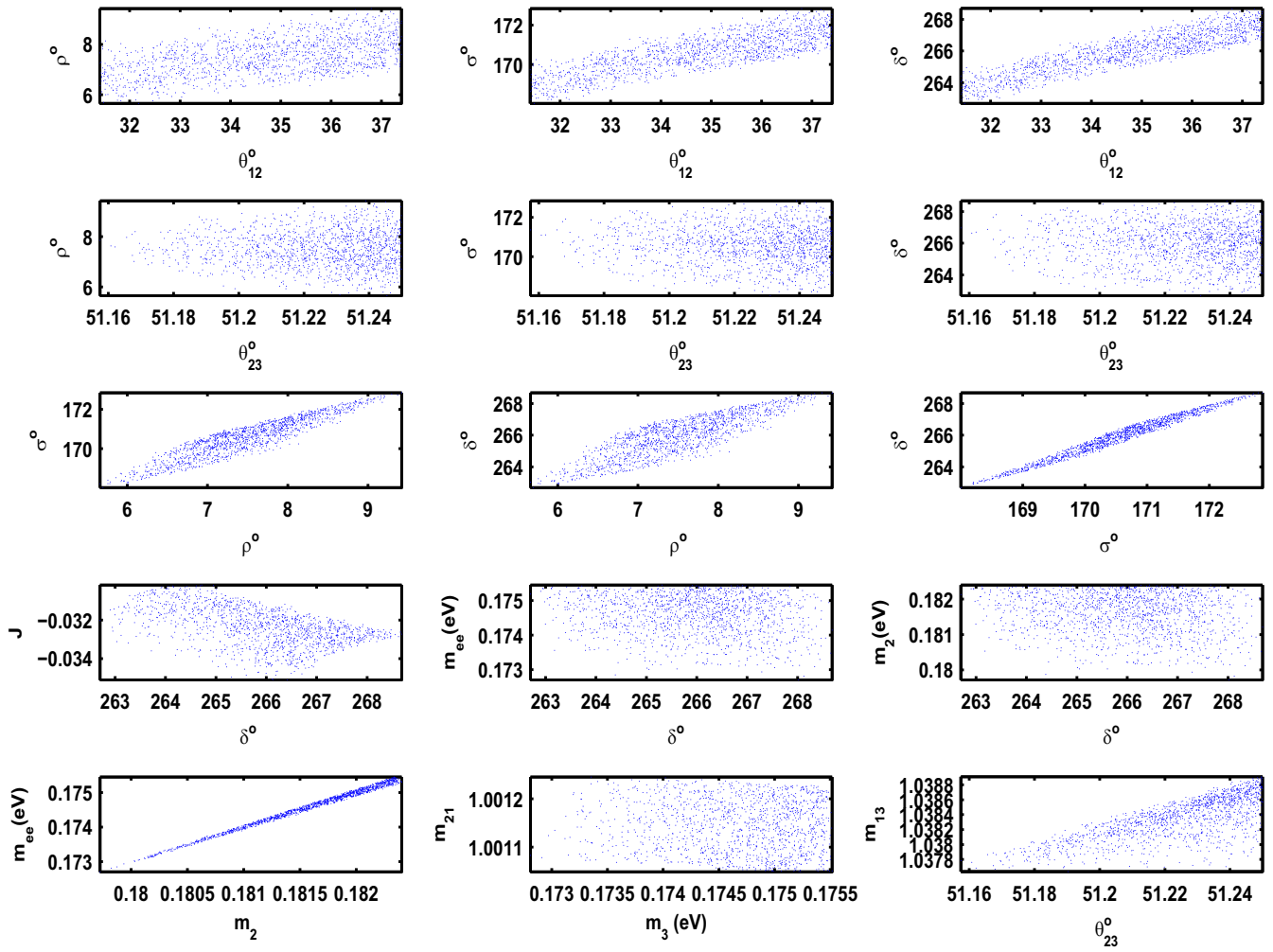

FIG. 5. The correlation plots for $(\mathbf{C}_{11}, \mathbf{C}_{12}) \equiv (M_{\mu\mu} + M_{\tau\tau} = 0, M_{e\mu} + M_{\tau\tau} = 0)$ texture in the case of inverted hierarchy. The first and second rows represent the correlations between the mixing angles $(\theta_{12}, \theta_{23})$ and the CP-violating phases. The third and fourth rows show the correlations amidst the CP-violating phases and the correlations between the Dirac phase δ and each of J, m_{ee} and m_2 parameters, respectively. The last row shows the degree of mass hierarchy plus the (m_{ee}, m_2) correlation.

giving an approximate range ($\delta \in [260^o, 275^o]$). Plugging the zeros of $(m_{23}^2 - m_{13}^2)$ in the expression of m_{13} leads to an exact correlation whose truncated approximation is given by

$$m_{13} = m_{23} = \sqrt{1 + \frac{c_{2y}^2}{c_y^2}} + \mathcal{O}(s_z) \geq 1. \tag{54}$$

This truncated correlation leads $m_{13} \gtrapprox 1$, so the ordering is of **IH** type. Taking θ_y in its allowed range, we see that the spectrum is quasidegenerate ($m_1 \sim m_2 \sim m_3$) and $\Sigma \approx 3m_3$.

From Table V, we find that in this texture we have $(\sigma \sim 170^o, \rho \sim 7^o)$, so in the expression of $m_{ee} = |m_1 c_x^2 e^{2i\rho} + m_2 s_x^2 e^{2i\sigma}|$, where we put $c_z \sim 1$ and neglect the contribution of m_3 as it is proportional to s_z^2, we have $m_{ee} \approx m_2$. Similarly, we can show that $m_e \sim m_2$.

Finally, we find that the bounds on $\Sigma \sim 3m_3$ and $m_{ee} \sim m_3$ in Eq. (9) are the severe ones by which, using $m_3^2 = \frac{\delta m^2}{m_{23}^2 - m_{13}^2}$, most of the θ_y range is excluded, and only a narrow neighborhood around the value $\theta_y \approx 51.2^o$ is allowed with $m_{13} \approx 1.04$ [cf. Eq. (54)].

For inverted ordering, the representative point is taken as follows:

$$\begin{aligned}(\theta_{12}, \theta_{23}, \theta_{13}) &= (34.3178°, 51.2346°, 8.5674°),\\ (\delta, \rho, \sigma) &= (265.0845°, 6.7720°, 169.8108°),\\ (m_1, m_2, m_3) &= (0.1811\text{ eV}, 0.1814\text{ eV}, 0.1745\text{ eV}),\\ (m_{ee}, m_e) &= (0.1744\text{ eV}, 0.1811\text{ eV}).\end{aligned} \tag{55}$$

The corresponding neutrino mass matrix (in eV) is

$$M_\nu = \begin{pmatrix} 0.1742 + 0.0087i & 0.0305 - 0.0002i & -0.0379 - 0.0019i \\ 0.0305 - 0.0002i & 0.0305 - 0.0002i & 0.1719 + 0.0002i \\ -0.0379 - 0.0019i & 0.1719 + 0.0002i & -0.0305 + 0.0002i \end{pmatrix}. \tag{56}$$

D. Texture $(\mathbf{C_{33}},\mathbf{C_{12}}) \equiv (M_{ee} + M_{\mu\mu} = 0, M_{e\mu} + M_{\tau\tau} = 0)$

A and B are given by

$$\begin{aligned} A_1 &= c_x^2 c_z^2 + (-c_x s_y s_z - s_x c_y e^{-i\delta})^2, \\ A_2 &= s_x^2 c_z^2 + (-s_x s_y s_z + c_x c_y e^{-i\delta})^2, \qquad A_3 = s_z^2 + s_y^2 c_z^2, \\ B_1 &= c_x c_z(-c_x s_y s_z - s_x c_y e^{-i\delta}) + (-c_x c_y s_z + s_x s_y e^{-i\delta})^2, \\ B_2 &= s_x c_z(-s_x s_y s_z + c_x c_y e^{-i\delta}) + (-s_x c_y s_z - c_x s_y e^{-i\delta})^2, \\ B_3 &= s_y c_z s_z + c_y^2 c_z^2. \end{aligned} \tag{57}$$

Therefore, R_ν takes a form

$$\begin{aligned} R_\nu &= \frac{2c_{2x}s_y^2(1-3c_y^2)(1+t_{2x}c_y c_\delta)}{|R_2|\mathrm{sgn}(R_1)} + \mathcal{O}(s_z): \\ R_1 &= -4c_x^2 c_y^4 s_x^2 c_\delta^2 - s_{2x}s_y^2 c_y(1+c_y^2)c_{2x}c_\delta \\ &\quad + s_y^4(-1 + c_x^2(4-c_y^2)s_x^2) + \mathcal{O}(s_z), \\ R_2 &= -8c_x^2 c_y^2 s_y^2 s_x^2 c_\delta^2 - s_{2x}c_y s_y^2(1+3c_y^2)c_{2x}c_\delta \\ &\quad + (3 - 10c_x^2 s_x^2)c_y^4 - 4c_x^2 s_x^2 c_y^2 - 1 + 6c_x^2 s_x^2. \end{aligned} \tag{58}$$

Table V shows that $(\mathbf{C}_{33}, \mathbf{C}_{12})$ texture is not viable at all σ error levels for normal ordering, whereas it can accommodate the experimental data for inverted ordering at 2-3-σ levels. The allowed experimental ranges of the mixing angles $(\theta_x, \theta_y, \theta_z)$ are covered at all allowed σ levels. The Dirac phase δ is bounded to the interval $[231.94°, 248.79°]$ at the 2-σ, and the range tends to be wider at the 3-σ level being $[226.89°, 254.21°]$. There exist acute restrictions on the phases $\rho(\sigma)$ at the 2-3-σ levels. They belong to the intervals $[100.59°, 105.16°]([38.47°, 51.29°])$ at the 2-σ level and $[99.40°, 106.17°]([34.65°, 57.53°])$ at the 3-σ level. Table V also reveals that m_3 does not reach zero, so the singular mass matrix is not predicted.

From Fig. 6, we see that θ_x increases when the CP-violating phases tend to increase. We also see a quasilinear relation for (θ_x, ρ) correlation. Figure 6 also shows a moderate mass hierarchy characterized by $2.34 \leq m_{13} \leq 2.67$ together with a quasidegeneracy characterized by $m_1 \approx m_2$.

In order to explain the correlation plots, one computes the mass-squared-difference full and approximate expressions:

$$\begin{aligned} m_{23}^2 - m_{13}^2 &= \frac{\mathrm{Num}(m_{23}^2 - m_{13}^2)}{\mathrm{Den}(m_{23}^2 - m_{13}^2)}: \\ \mathrm{Num}(m_{23}^2 - m_{13}^2) &= s_{2x}c_y c_\delta[3 - c_y^2(-2+c_y^2)c_z^2 + 2s_z s_y(-2+c_y^2)c_z^4 + (-2+12c_y^2+6c_y^4)c_z^3 \\ &\quad + 2s_z s_y(3+c_y^2)c_z^2 - c_{2y}c_z - 2s_y s_z] - c_{2x}[(4 + c_y^4 - 8c_y^2)c_z^4 + 2c_y^2 s_z s_y \\ &\quad (-4+3c_y^2)c_z^2 + (2c_y^4 - 4 + 6c_y^2)c_z^2 + 2c_y^2 s_z s_y c_z - c_{2y}] \end{aligned} \tag{59}$$

$$\mathrm{Num}(m_{23}^2 - m_{13}^2) = s_y^2(1-3c_y^2)(s_{2x}c_y c_\delta + c_{2x}) + \mathcal{O}(s_z). \tag{60}$$

The zeros of $\mathrm{Num}(m_{23}^2 - m_{13}^2)$ give exact correlations in excellent agreement with the full correlations (e.g., the exact interval for m_{13} is [2.33, 2.64] to be compared with the mentioned full interval [2.34, 2.67]). Also, the zeros of the leading term of the mass-squared difference numerator [i.e. the zeros of $(s_{2x}c_y c_\delta + c_{2x})$] lead to approximate correlations which are good, but less, when compared to the full ones.

Plugging the zeros of $(m_{23}^2 - m_{13}^2)$ in the expression of m_{13} leads to an exact correlation whose truncated approximation is given by

$$m_{13} = \sqrt{1 + \frac{1}{c_y^2}}\left(1 + \frac{2s_z}{s_y c_y^2}\right) + \mathcal{O}(s_z^2). \tag{61}$$

Scanning over the allowed values of θ_y and θ_z, we find that this truncated correlation leads to $(1 < m_{13} \in [2.12, 2.44])$, so the ordering is of **IH** type. As to m_{ee} we find a value around $[0.054 \times |\cos^2(35^o)e^{2i103\pi/180} + \sin^2(35^o)e^{2i47\pi/180}| \approx 0.0339$ eV].

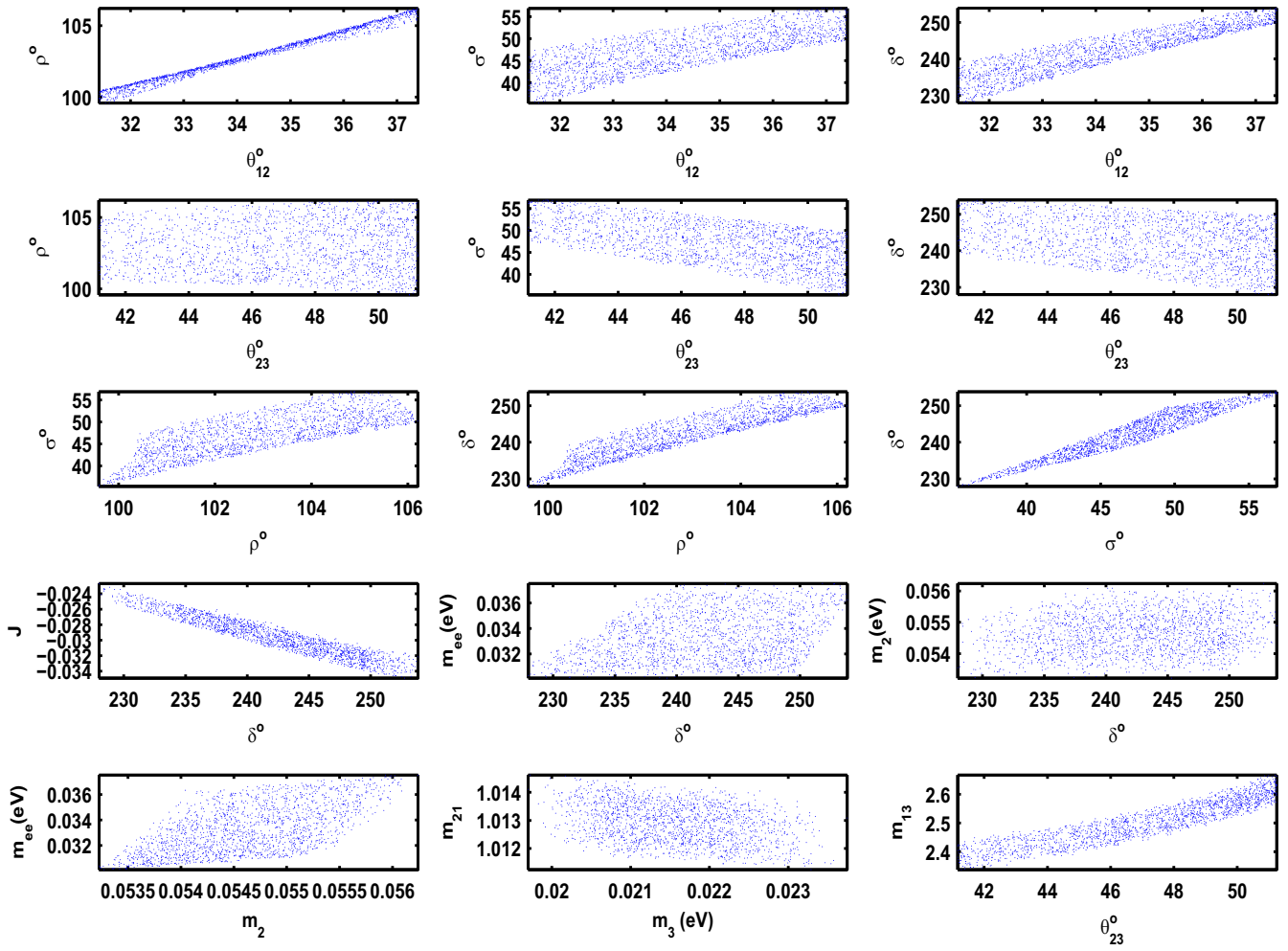

FIG. 6. The correlation plots for $(\mathbf{C}_{33}, \mathbf{C}_{12}) \equiv (M_{ee} + M_{\mu\mu} = 0, M_{e\mu} + M_{\tau\tau} = 0)$ texture in the case of inverted hierarchy. The first and second rows represent the correlations between the mixing angles $(\theta_{12}, \theta_{23})$ and the CP-violating phases. The third and fourth rows show the correlations amidst the CP-violating phases and the correlations between the Dirac phase δ and each of J, m_{ee} and m_2 parameters, respectively. The last row shows the degree of mass hierarchy plus the (m_{ee}, m_2) correlation.

A corresponding benchmark point is taken as

$$\begin{aligned}(\theta_{12}, \theta_{23}, \theta_{13}) &= (34.2034°, 49.4333°, 8.5030°),\\ (\delta, \rho, \sigma) &= (240.4593°, 102.7186°, 44.6611°),\\ (m_1, m_2, m_3) &= (0.0531\ \text{eV}, 0.0539\ \text{eV}, 0.0208\ \text{eV}),\\ (m_{ee}, m_e) &= (0.0315\ \text{eV}, 0.0528\ \text{eV}),\end{aligned} \tag{62}$$

with the reconstructed neutrino mass matrix (in eV) given as

$$M_\nu = \begin{pmatrix} -0.0314 + 0.0014i & -0.0212 + 0.0012i & 0.0367 - 0.0017i \\ -0.0212 + 0.0012i & 0.0314 - 0.0014i & -0.0076 + 0.0013i \\ 0.0367 - 0.0017i & -0.0076 + 0.0013i & 0.0212 - 0.0012i \end{pmatrix}. \tag{63}$$

E. Texture $(\mathbf{C_{33}},\mathbf{C_{13}}) \equiv (M_{ee}+M_{\mu\mu}=0, M_{e\mu}+M_{\mu\tau}=0)$

A and B are given by

$$
\begin{aligned}
A_1 &= c_x^2 c_z^2 + (-c_x s_y s_z - s_x c_y e^{-i\delta})^2,\\
A_2 &= s_x^2 c_z^2 + (-s_x s_y s_z + c_x c_y e^{-i\delta})^2, \qquad A_3 = s_z^2 + s_y^2 c_z^2,\\
B_1 &= c_x c_z(-c_x s_y s_z - s_x c_y e^{-i\delta})\\
&\quad + (-c_x s_y s_z - s_x c_y e^{-i\delta})(-c_x c_y s_z + s_x s_y e^{-i\delta}),\\
B_2 &= s_x c_z(-s_x s_y s_z + c_x c_y e^{-i\delta})\\
&\quad + (-s_x s_y s_z + c_x c_y e^{-i\delta})(-s_x c_y s_z - c_x s_y e^{-i\delta}),\\
B_3 &= s_z s_y c_z + s_y c_z^2 c_y. \qquad (64)
\end{aligned}
$$

The leading order truncated approximation for R_ν is given by

$$
\begin{aligned}
R_\nu &= \frac{-2s_y^3}{|s_{2x}c_{2y}c_\delta - c_{2x}s_y(1+c_y^2)|\mathrm{sgn}(R_1)} + \mathcal{O}(s_z):\\
R_1 &= -2c_y^4 s_{2x}^2 c_\delta^2 + c_y s_{2y} s_{2x}(1+c_y^2)c_{2x}c_\delta\\
&\quad - 2c_y^2 s_y^2(-c_y^2 s_x^2 c_x^2 - 3s_x^2 c_x^2 + 1). \qquad (65)
\end{aligned}
$$

We see from Table V that $(\mathbf{C}_{33},\ \mathbf{C}_{13})$ texture can accommodate the experimental data in the case of inverted hierarchy at all σ levels. However, the texture is not viable for normal hierarchy. We find that the mixing angles $(\theta_x, \theta_y, \theta_z)$ extend over their allowed experimental ranges at all σ levels. The Dirac phase δ is tightly restricted at all σ levels, and is bound to be in the range $[262.85°, 267.59°]$ at the 3-σ level. We notice that the Majorana phases $\rho(\sigma)$ are strongly restricted at all statistical levels to lie in the intervals $[92.56°, 95.16°]([78.67°, 84.28°])$ at the 3-σ level. Table V also reveals that m_3 does not reach a vanishing at all σ levels. Therefore, the singular texture is not expected with either hierarchy type at all σ levels.

We see from Fig. 7 that the mixing angle θ_y increases when the phases δ and σ tend to decrease. However, we notice that θ_y increases when ρ tends to increase. We also see that θ_x increases when the CP-violating phases tend to increase. We find the quasidegeneracy characterized by $m_1 \approx m_2$ and $1.11 \leq m_{13} \leq 1.14$.

In order to explain the correlation plots, one computes the mass-squared-difference full and approximate expressions:

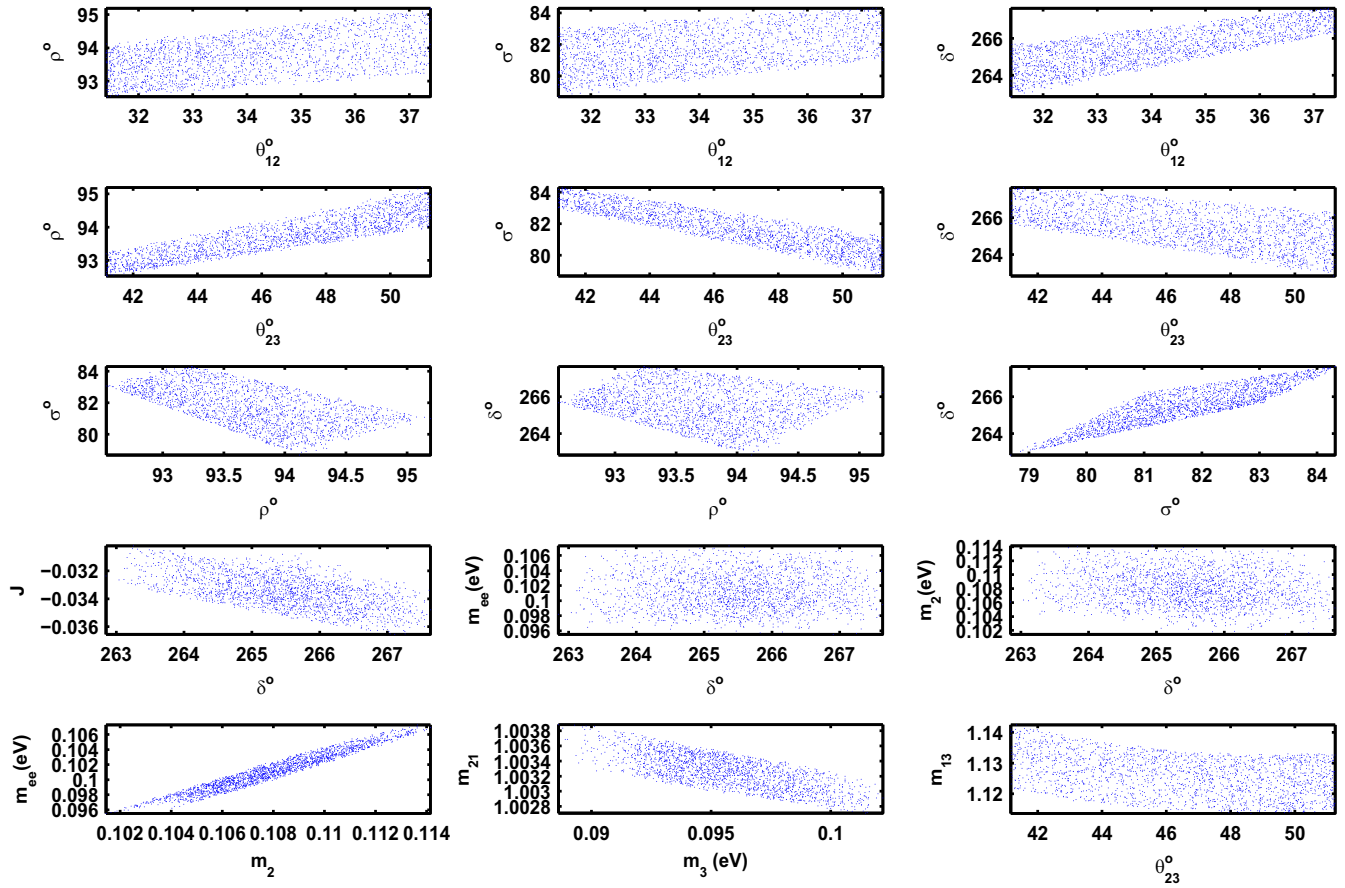

FIG. 7. The correlation plots for $(\mathbf{C}_{33}, \mathbf{C}_{13}) \equiv (M_{ee}+M_{\mu\mu}=0, M_{e\mu}+M_{\mu\tau}=0)$ texture in the case of inverted hierarchy. The first and second rows represent the correlations between the mixing angles $(\theta_{12}, \theta_{23})$ and the CP-violating phases. The third and fourth rows show the correlations amidst the CP-violating phases and the correlations between the Dirac phase δ and each of J, m_{ee} and m_2 parameters, respectively. The last row shows the degree of mass hierarchy plus the (m_{ee}, m_2) correlation.

$$m_{23}^2 - m_{13}^2 = \frac{\mathrm{Num}(m_{23}^2 - m_{13}^2)}{\mathrm{Den}(m_{23}^2 - m_{13}^2)}:$$
$$\mathrm{Num}(m_{23}^2 - m_{13}^2) = 2c_z s_{2x} s_y c_\delta [c_z^4 c_y^2 (c_y^2 - 3) - 2c_z^3 s_z c_y s_y^2 + c_z^2 (6c_y^2 - 2c_y^4 - 1) + 4 s_z c_z c_y s_y^2 - c_{2y}]$$
$$+ 4c_z s_y^2 c_{2x} [c_z^3 c_{2y} - s_z c_z^2 c_y (c_y^2 - 2) - c_z c_{2y} - s_z c_y], \quad (66)$$

$$m_{23}^2 - m_{13}^2 = \frac{c_y s_{2x} s_{2y} s_y^2 c_\delta}{c_y^4 s_{2x}^2 c_\delta^2 - \frac{1}{2} c_y s_{2x} s_{2y} (1 + c_y^2) c_{2x} c_\delta + s_y^2 c_y^2 (-c_x^2 s_x^2 c_y^2 - 3 s_x^2 c_x^2 + 1)} + \mathcal{O}(s_z). \quad (67)$$

We understand now why δ around 270^o is singled out, as this would make $(m_{23}^2 - m_{13}^2)$ as small as possible [cf. Eq. (67)], and, moreover, substituting $(\delta \approx 270^0)$ in the truncated approximation we get

$$m_{23}^2 - m_{13}^2 \overset{\delta \to 270^o}{\approx} \frac{c_y s_{2x} s_{2y} s_y^2 c_\delta}{s_y^2 c_y^2 (-c_x^2 s_x^2 c_y^2 - 3 s_x^2 c_x^2 + 1)}.$$

As the coefficient in front of c_δ in the numerator is positive for allowed θ_x, θ_y, whereas the denominator is always positive, we deduce $(m_{23}^2 - m_{13}^2 \to 0^+) \Rightarrow (\delta \to 270^{o+})$. The higher order terms make $(\delta \to 270^{o-})$.

The zeros of $\mathrm{Num}(m_{23}^2 - m_{13}^2)$ give exact correlations in excellent agreement with the full correlations. However, we found that the zeros of the leading plus next-to-leading terms of the mass-squared difference numerator (i.e. the expansion of $m_{23}^2 - m_{13}^2$ in the form of a linear form $c_0 + c_1 s_z$) lead to approximate correlations which are not accurate, when compared to the full ones, and one needs to go to higher orders to match the full correlations.

Plugging the zeros of $(m_{23}^2 - m_{13}^2)$ in the expression of m_{13} leads to an exact correlation whose truncated approximation is given by

$$m_{13} = 1 + \frac{2 s_z^2}{s_y^2 c_y^2} + \mathcal{O}(s_z^3). \quad (68)$$

Scanning over the allowed values of $\theta_y . \theta_z$, we find that this truncated correlation leads to $(m_{13} \in [1.165, 1.205])$, whereas the exact range, coming from the zeros of $(m_{23}^2 - m_{13}^2)$, is [1.114, 1.143], which is very near the full correct range, so the ordering is of **IH** type. As to m_{ee}, and since we have $\rho \approx \sigma \approx 90^o$ in this pattern, we have $(m_{ee} \approx m_2)$. Actually, at leading order, $\delta \approx \frac{3\pi}{2}$ would lead to $(\rho \approx \sigma \approx \frac{\pi}{2})$.

For inverted ordering, the representative point is taken as follows:

$$(\theta_{12}, \theta_{23}, \theta_{13}) = (34.1770°, 49.4202°, 8.6885°),$$
$$(\delta, \rho, \sigma) = (264.9329°, 94.2458°, 80.6349°),$$
$$(m_1, m_2, m_3) = (0.1076\ \mathrm{eV}, 0.1080\ \mathrm{eV}, 0.0955\ \mathrm{eV}),$$
$$(m_{ee}, m_e) = (0.1005\ \mathrm{eV}, 0.1074\ \mathrm{eV}), \quad (69)$$

the corresponding neutrino mass matrix (in eV) is

$$M_\nu = \begin{pmatrix} -0.1005 + 0.0001i & 0.0076 - 0.0001i & 0.0372 + 0.0001i \\ 0.0076 - 0.0001i & 0.1005 - 0.0001i & -0.0076 + 0.0001i \\ 0.0372 + 0.0001i & -0.0076 + 0.0001i & 0.0957 - 0.0001i \end{pmatrix}. \quad (70)$$

F. Texture $(\mathbf{C_{11}}, \mathbf{C_{13}}) \equiv (M_{\mu\mu} + M_{\tau\tau} = 0, M_{e\mu} + M_{\mu\tau} = 0)$

The coefficients A and B are obtained from Eqs. (48) and (64). A and B are given by

$$A_1 = c_x^2 s_z^2 + s_x^2 e^{-2i\delta}, \qquad A_2 = s_x^2 s_z^2 + c_x^2 e^{-2i\delta} \qquad A_3 = c_z^2,$$
$$B_1 = c_x c_z (-c_x s_y s_z - s_x c_y e^{-i\delta}) + (-c_x s_y s_z - s_x c_y e^{-i\delta})(-c_x c_y s_z + s_x s_y e^{-i\delta}),$$
$$B_2 = s_x c_z (-s_x s_y s_z + c_x c_y e^{-i\delta}) + (-s_x s_y s_z + c_x c_y e^{-i\delta})(-s_x c_y s_z - c_x s_y e^{-i\delta}),$$
$$B_3 = s_z s_y c_z + s_y c_z^2 c_y. \quad (71)$$

The analytical approximate truncated expression for R_ν is

$$R_\nu = \frac{4(s_{2x}c_\delta - 2c_{2x}s_y)}{|s_y(2s_{2x}^2 - 4) + s_{4x}c_\delta|} + \mathcal{O}(s_z). \tag{72}$$

From Table V, we find that ($\mathbf{C}_{11}$, $\mathbf{C}_{13}$) is not viable at all σ levels for normal hierarchy. However, it can accommodate the experimental data at all σ levels in the case of inverted hierarchy. The mixing angles (θ_x, θ_y, θ_z) extend over their allowed experimental ranges at the all σ levels. We find that the allowed range for δ is very tight at all σ levels. It tends to be wider at the 3-σ level to be approximately $[292°, 322°]$. As for the Dirac phase δ, the Majorana phases $\rho(\sigma)$ are strongly restricted at all σ levels. They belong to the intervals $[165.23°, 167.75°]([46.81°, 52.37°])$ at the 1-σ level, $[163.81°, 169.35°]([43.84°, 56.57°])$ at the 2-σ level and $[162.53°, 170.80°]([39.98°, 60.41°])$ at the 3-σ level. One also notes that m_3 does not reach a vanishing value. Thus, the singular mass matrix is not expected.

We see from Fig. 8 the quasilinear correlations with negative slope between θ_x and CP-violating phases. We also see a strong linear relation for the correlation (σ, δ) together with quasilinear relations for (ρ, σ) and (ρ, δ) correlations. We also find a mild mass hierarchy where $1.68 \leq m_{13} \leq 1.79$ as well as a quasidegeneracy characterized by $m_1 \approx m_2$.

In order to explain the correlation plots, one computes the mass-squared-difference full and approximate expressions:

$$m_{23}^2 - m_{13}^2 = \frac{\mathrm{Num}(m_{23}^2 - m_{13}^2)}{\mathrm{Den}(m_{23}^2 - m_{13}^2)}:$$

$$\mathrm{Num}(m_{23}^2 - m_{13}^2) = 4c_z^3\left[\frac{1}{2}s_{2x}s_y c_\delta((1-3c_y^2)c_z^2 - c_y s_{2z} s_y^2 + c_{2y}) + c_y s_y^2 c_{2x}(c_y c_z + s_z)\right] \tag{73}$$

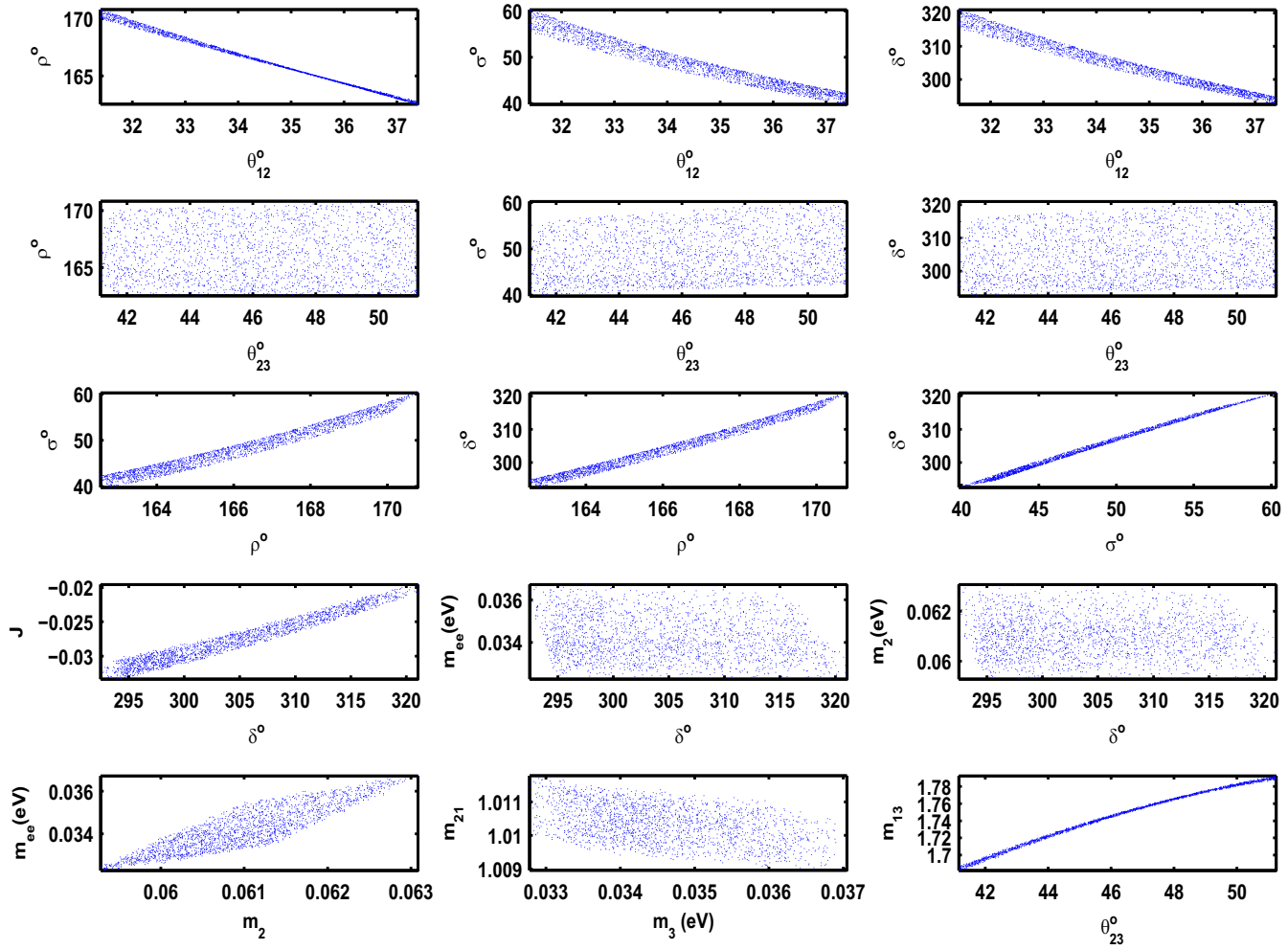

FIG. 8. The correlation plots for $(\mathbf{C}_{11}, \mathbf{C}_{13}) \equiv (M_{ee} + M_{\mu\mu} = 0, M_{e\mu} + M_{\mu\tau} = 0)$ texture in the case of inverted hierarchy. The first and second rows represent the correlations between the mixing angles $(\theta_{12}, \theta_{23})$ and the CP-violating phases. The third and fourth rows show the correlations amidst the CP-violating phases and the correlations between the Dirac phase δ and each of J, m_{ee} and m_2 parameters, respectively. The last row shows the degree of mass hierarchy plus the (m_{ee}, m_2) correlation.

$$m_{23}^2 - m_{13}^2 = \frac{2s_y(c_\delta s_{2x} - 2s_y c_{2x})}{c_x^2 s_x^2} + \mathcal{O}(s_z). \quad (74)$$

The zeros of Num$(m_{23}^2 - m_{13}^2)$ give exact correlations in excellent agreement with the full correlations. Likewise, we found that the zeros of the leading term of the mass-squared difference numerator [i.e. of $(c_\delta s_{2x} - 2s_y c_{2x})$ giving $(c_\delta = 2s_y \cot_{2x})$] lead to approximate correlations between the mixing and phase angles which are also good when compared to the full ones.

Plugging the zeros of $(m_{23}^2 - m_{13}^2)$ in the expression of m_{13} leads to an exact correlation whose truncated approximation is given by

$$m_{13} = \sqrt{1 + 4s_y^2}\left(1 + \frac{4s_y^2 c_{2y} s_z}{1 + 4s_y^2}\right) + \mathcal{O}(s_z^2). \quad (75)$$

Scanning over the allowed values of θ_y, θ_z, we find that this truncated correlation leads to $(m_{13} \in [1.68, 1.79])$, whereas the exact range, coming from the zeros of $(m_{23}^2 - m_{13}^2)$, is [1.7, 1.8], which is very near the full correct range, so the ordering is of **IH** type. As to m_{ee}, and since we have $\rho \approx 167^o, \sigma \approx 50^o$ in this pattern, we have, taking $\theta_x \approx 35^o$, $m_2 \approx 0.06$ eV, the value $(m_{ee} \approx 0.06|\cos^2(35^o)e^{2i167\pi/180} + \sin^2(35^o)e^{2i50\pi/180}| \approx 0.032$ eV).

For inverted ordering, the representative point is taken as follows:

$$\begin{aligned}(\theta_{12}, \theta_{23}, \theta_{13}) &= (34.2712°, 49.4721°, 8.6197°),\\ (\delta, \rho, \sigma) &= (306.3395°, 166.5813°, 49.8309°),\\ (m_1, m_2, m_3) &= (0.0601 \text{ eV}, 0.0607 \text{ eV}, 0.0338 \text{ eV}),\\ (m_{ee}, m_e) &= (0.0334 \text{ eV}, 0.0598 \text{ eV}). \end{aligned} \quad (76)$$

The corresponding neutrino mass matrix (in eV) is

$$M_\nu = \begin{pmatrix} 0.0334 + 0.0004i & -0.0322 - 0.0000i & 0.0378 - 0.0001i \\ -0.0322 - 0.0000i & 0.0127 - 0.0000i & 0.0322 + 0.0000i \\ 0.0378 - 0.0001i & 0.0322 + 0.0000i & -0.0127 + 0.0000i \end{pmatrix}. \quad (77)$$

G. Texture $(\mathbf{C_{13}}, \mathbf{C_{23}}) \equiv (M_{e\mu} + M_{\mu\tau} = 0, M_{ee} + M_{\mu\tau} = 0)$

A and B are given by

$$\begin{aligned} A_1 &= c_x c_z(-c_x s_y s_z - s_x c_y e^{-i\delta}) + (-c_x s_y s_z - s_x c_y e^{-i\delta})(-c_x c_y s_z + s_x s_y e^{-i\delta}),\\ A_2 &= s_x c_z(-s_x s_y s_z + c_x c_y e^{-i\delta}) + (-s_x s_y s_z + c_x c_y e^{-i\delta})(-s_x c_y s_z - c_x s_y e^{-i\delta}),\\ A_3 &= s_z s_y c_z + s_y c_z^2 c_y,\\ B_1 &= c_x^2 c_z^2 + (-c_x s_y s_z - s_x c_y e^{-i\delta})(-c_x c_y s_z + s_x s_y e^{-i\delta}),\\ B_2 &= s_x^2 c_z^2 + (-s_x s_y s_z + c_x c_y e^{-i\delta})(-s_x c_y s_z - c_x s_y e^{-i\delta}),\\ B_3 &= s_z^2 + s_y c_y c_z^2. \end{aligned} \quad (78)$$

The leading order expression for R_ν is given by

$$\begin{aligned} R_\nu &= \frac{2s_y^2(c_{2x} + s_{2x} c_y c_\delta)}{|s_{2y} s_{2x}^2 c_\delta^2 + s_{2x} c_{2x} s_y(2 - s_y c_y)c_\delta + (1 - 6s_x^2 c_x^2)c_y^2 - 2s_{2y} s_x^2 c_x^2 - c_{2x}^2|\text{sgn}(R_1)} + \mathcal{O}(s_z):\\ R_1 &= -2s_{2y} s_x^2 c_x^2 c_\delta^2 - s_{2x} c_{2x} s_y(1 - s_y c_y)c_\delta - s_x^2 c_x^2 c_y^4 + (5c_x^2 s_x^2 - 1)c_y^2 + s_{2y} s_x^2 c_x^2 + 1 - 3s_x^2 c_x^2. \end{aligned} \quad (79)$$

We see from Table V that $(\mathbf{C}_{13}, \mathbf{C}_{23})$ texture is viable at all σ levels for normal ordering. However, it cannot accommodate the experimental data for inverted ordering. The allowed experimental ranges for the mixing angles $(\theta_x, \theta_y, \theta_z)$ can be covered at all σ levels. The Dirac phase δ is bounded to the intervals: $[202.90°, 217.99°]$ at the 1-σ level, $[152.02°, 232.55°]$ at the 2-σ level and $[128.01°, 242.79°]$ at the 3-σ level. We find that ρ is tightly restricted at all σ levels, and its allowed range tends to be wider at the 3-σ levels to fall approximately in the interval $[73°, 108°]$. For the phase σ, one notes that there exists a strong restriction at the 1-σ level besides wide forbidden gaps at the 2-3-σ levels. The allowed values for the J parameter at the 1-σ level are negative, consistent with δ lying in the third quarter at this σ level. Table V also shows that m_1 cannot reach zero. Thus, a singular mass matrix is not predicted.

From Fig. 9, we see forbidden gaps in the correlations between the mixing angles (θ_x,θ_y) and CP-violating phases. We also see the quasilinear relations for the correlations between the CP-violating phases. Figure 9 also shows a mild mass hierarchy characterized by $0.68 \leq m_{13} \leq 0.79$ together with a quasidegeneracy characterized by $m_1 \approx m_2$.

In order to explain the correlation plots, one computes the mass-squared-difference full and approximate expressions:

$$
\begin{aligned}
m_{23}^2 - m_{13}^2 &= \frac{\mathrm{Num}(m_{23}^2 - m_{13}^2)}{\mathrm{Den}(m_{23}^2 - m_{13}^2)}: \\
\mathrm{Num}(m_{23}^2 - m_{13}^2) &= s_{2x}c_\delta[c_z^4 s_y(3c_y^2 - 1 - c_y s_y^3) + s_z s_y^2 c_z^3(s_{2y} - s_y^2) + c_z^2((2 - 5c_y^2)s_y - c_y s_y^2 c_{2y}) \\
&\quad - s_z c_z s_y^2(s_{2y} + c_{2y}) + s_y c_{2y}] + s_y^2 c_{2x}[c_z^3(s_{2y} + 1 - 3c_y^2) - 2c_y s_z c_z^2(2 + s_y c_y) \\
&\quad + c_z(c_{2y} - s_{2y}) + 2s_z c_y] \\
&= -c_y^2 s_y^2(c_\delta s_{2x} c_y + c_{2x}) + \mathcal{O}(s_z).
\end{aligned} \tag{80}
$$

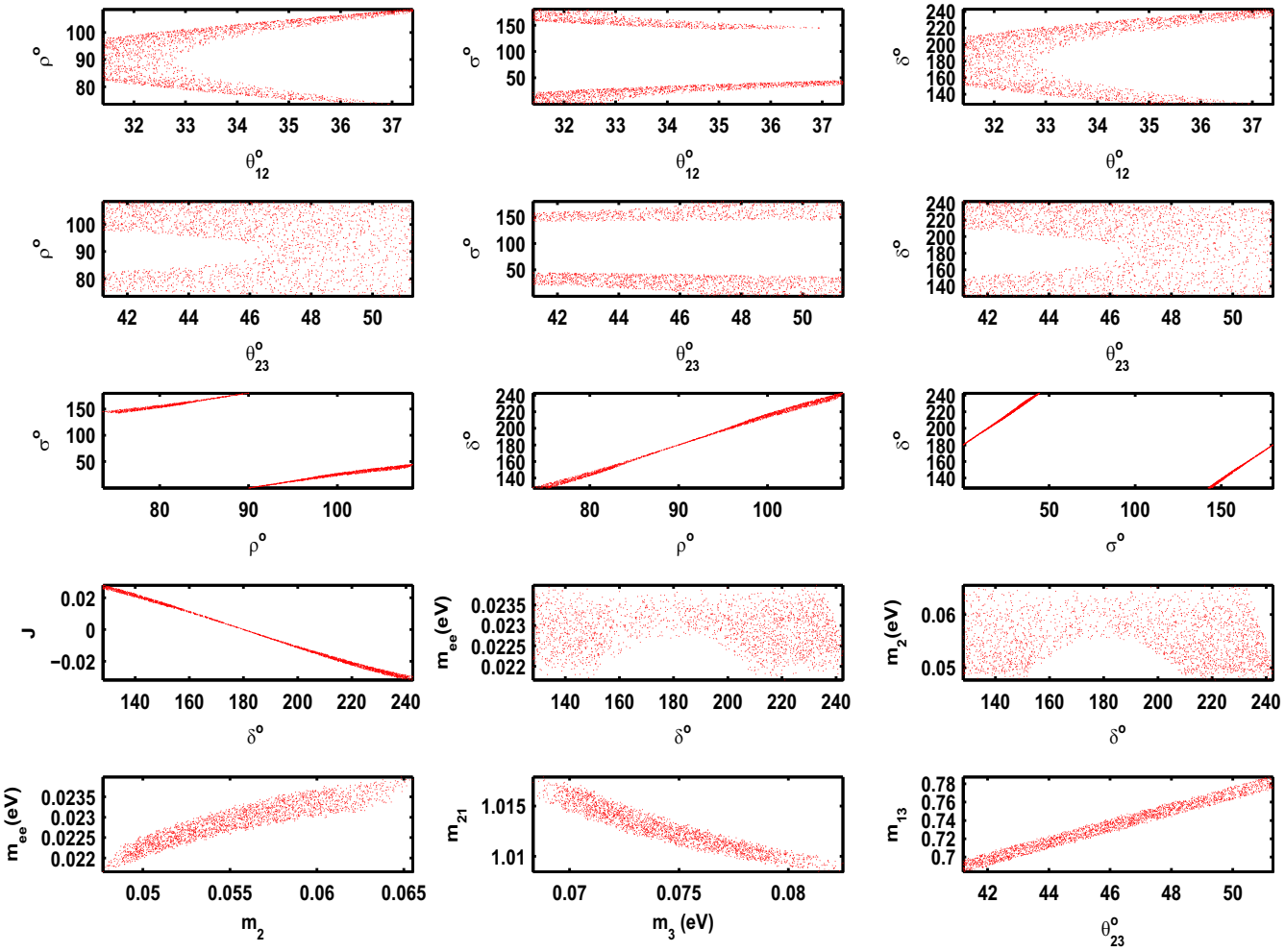

FIG. 9. The correlation plots for $(\mathbf{C}_{13}, \mathbf{C}_{23}) \equiv (M_{e\mu} + M_{\mu\tau} = 0, M_{ee} + M_{\mu\tau} = 0)$ texture in the case of normal hierarchy. The first and second rows represent the correlations between the mixing angles $(\theta_{12}, \theta_{23})$ and the CP-violating phases. The third and fourth rows show the correlations amidst the CP-violating phases and the correlations between the Dirac phase δ and each of J, m_{ee} and m_2 parameters, respectively. The last row shows the degree of mass hierarchy plus the (m_{ee}, m_2) correlation.

The zeros of $\mathrm{Num}(m_{23}^2 - m_{13}^2)$ give exact correlations in excellent agreement with the full correlations. Likewise, we found that the zeros of the leading term of the mass-squared difference numerator giving $(c_\delta = -\frac{1}{t_{2x}c_y})$ lead to approximate correlations between the mixing angles (θ_x, θ_y) and the Dirac phase angle δ which are also good when compared to the full ones. Moreover, we see that $c_\delta < 0$, which interprets the observation that δ lies in the second or third quadrant.

Plugging the zeros of $(m_{23}^2 - m_{13}^2)$ in the expression of m_{13} leads to an exact correlation whose truncated approximation is given by

$$m_{13} = \frac{s_y\sqrt{1+c_y^2}}{\sqrt{1+s_{2y}+c_y^2 s_y^2}}\left(1+\frac{3(s_y^3+c_y^3)s_z}{1+6c_y^6}\right)+\mathcal{O}(s_z^2). \quad (81)$$

One can see, for the allowed values of (θ_y), that the zeroth-order leading term $\frac{s_y\sqrt{1+c_y^2}}{\sqrt{1+s_{2y}+c_y^2 s_y^2}} < 1$, so the ordering is of **NH** type. Scanning over the allowed values of θ_y, θ_z, we find that the truncated correlation, up to order $\mathcal{O}(s_z^2)$, leads to $(m_{13} \in [0.69, 0.82])$, whereas the exact range, coming from the zeros of $(m_{23}^2 - m_{13}^2)$, is [0.69, 0.79], which is very near the full correct range [0.68, 0.79].

For normal ordering, the representative point is taken as follows:

$$\begin{aligned}(\theta_{12}, \theta_{23}, \theta_{13}) &= (34.1349°, 49.3654°, 8.5098°),\\ (\delta, \rho, \sigma) &= (214.0038°, 100.1902°, 23.9810°),\\ (m_1, m_2, m_3) &= (0.0594\ \text{eV}, 0.0600\ \text{eV}, 0.0777\ \text{eV}),\\ (m_{ee}, m_e) &= (0.0232\ \text{eV}, 0.0600\ \text{eV}).\end{aligned} \quad (82)$$

The corresponding neutrino mass matrix (in eV) is

$$M_\nu = \begin{pmatrix} -0.0232 - 0.0001i & -0.0232 - 0.0001i & 0.0503 + 0.0002i \\ -0.0232 - 0.0001i & 0.0624 - 0.0001i & 0.0232 + 0.0001i \\ 0.0503 + 0.0002i & 0.0232 + 0.0001i & 0.0391 - 0.0002i \end{pmatrix}. \quad (83)$$

VI. THEORETICAL REALIZATION

We present now some realizations of the texture under study characterized by two vanishing subtraces, irrespective of whether the corresponding texture is viable or not regarding phenomenological data. We present first a symmetry based on the non-Abelian group A_4 leading to a texture with the related subtraces consisted of the sum of diagonal elements. Second, we present a symmetry based on the non-Abelian group S_4 where one of the related subtraces corresponded to nondiagonal elements. In the realization, we introduce new scalars, but we have not discussed the question of the scalar potential and finding its general form under the imposed symmetry. Having these scalars may lead to rich phenomenology at colliders, and asking for just one SM-like Higgs at low scale requires a situation where fine-tuning of the many parameters in the scalar potential, to ensure new scalars are out of reach at current experiments, is heavily called upon.

Note that for each presented realizable pattern, there are automatically two other realizable patterns by transposition. Thus, by presenting an S_4 realization for the hitherto viable but now disallowed (C_{11}, C_{23}), then automatically we have, by the transposition $(1 \leftrightarrow 3)$, a realization for the viable pattern (C_{33}, C_{21}), and another realization, by doing now the transposition $(2 \leftrightarrow 3)$ on the latter, for the unviable pattern (C_{22}, C_{31}). Similarly, the A_4 realization of the viable pattern (C_{22}, C_{33}) can automatically be translated into a realization of the unviable patterns (C_{22}, C_{11}) and (C_{33}, C_{11}).

A. A_4-non-Abelian group realization

We present a realization based on the non-Abelian group A_4 leading to a texture of two vanishing subtraces where the related elements lie on the diagonal. We summarize the irreducible representations (irreps) of A_4 in Appendix C.

1. A_4 realization of two equalities: $(M_{\nu 11} = M_{\nu 22} = M_{\nu 33})$

We review briefly the setup given in [11] leading to a texture of two equalities $(M_{\nu 11} = M_{\nu 22} = M_{\nu 33})$. Taking the matter content shown in Table VI, one could form a "neutrino" singlet under $SU(2)_L$ gauge, A_4 flavor and Lorentz symmetries as

TABLE VI. Matter content and symmetry transformations, leading to texture with two equalities. $i = 1, \ldots, 3$ is a family index.

Fields	D_{L_i}	ℓ_{R_i}	ϕ_1	ϕ_2	ϕ_3	Δ_i	Δ_4
$SU(2)_L$	2	1	2	2	2	3	3
A_4	**3**	**3**	**1**	**1′**	**1″**	**3**	**1**

$$\begin{aligned}\mathcal{L} \ni Y[&(D_{L\mu}^T C^{-1} i\tau_2 \Delta_1 D_{L\tau} + D_{L\tau}^T C^{-1} i\tau_2 \Delta_1 D_{L\mu}) \\ &+ (D_{L\tau}^T C^{-1} i\tau_2 \Delta_2 D_{Le} + D_{Le}^T C^{-1} i\tau_2 \Delta_2 D_{L\tau}) \\ &+ (D_{Le}^T C^{-1} i\tau_2 \Delta_3 D_{L\mu} + D_{L\mu}^T C^{-1} i\tau_2 \Delta_3 D_{Le})] \\ &+ Y'[D_{Le}^T C^{-1} i\tau_2 \Delta_4 D_{Le} + D_{L\mu}^T C^{-1} i\tau_2 \Delta_4 D_{L\mu} \\ &+ D_{L\tau}^T C^{-1} i\tau_2 \Delta_4 D_{L\tau}], \end{aligned} \tag{84}$$

where τ_2 is the weak isospin matrix, and $\Delta_i = \begin{pmatrix} \Delta_i^+ & \sqrt{2}\Delta_i^{++} \\ \sqrt{2}\Delta_i^o & -\Delta_i^+ \end{pmatrix}$ is the Higgs triplet with $i = 1, \ldots, 4$ as a family index. When Δ_i acquires a small vacuum expectation value (VEV) along the neutral direction $\langle \Delta_i^0 \rangle_0$, then we get ($M_{\nu 11} = M_{\nu 22} = M_{\nu 33}$). As to the charged lepton mass matrix, we have

$$\begin{aligned}\mathcal{L} \ni\ & Y_1(\bar{D}_{Le} e_R + \bar{D}_{L\mu}\mu_R + \bar{D}_{L\tau}\tau_R)\phi_1 \\ &+ Y_2(\bar{D}_{Le} e_R + \omega \bar{D}_{L\mu}\mu_R + \omega^2 \bar{D}_{L\tau}\tau_R)\phi_2 \\ &+ Y_3(\bar{D}_{Le} e_R + \omega^2 \bar{D}_{L\mu}\mu_R + \omega \bar{D}_{L\tau}\tau_R)\phi_3. \end{aligned} \tag{85}$$

When ϕ_i acquire a VEV then we get a diagonal charged lepton mass:

$$\begin{aligned} M_\ell = \mathrm{diag}&(Y_1\langle\phi_1\rangle_0 + Y_2\langle\phi_2\rangle_0 + Y_3\langle\phi_3\rangle_0, \\ &Y_1\langle\phi_1\rangle_0 + Y_2\omega\langle\phi_2\rangle_0 + Y_3\omega^2\langle\phi_3\rangle_0, Y_1\langle\phi_1\rangle_0 \\ &+ Y_2\omega^2\langle\phi_2\rangle_0 + Y_3\omega\langle\phi_3\rangle_0). \end{aligned} \tag{86}$$

The charged lepton matrix has enough free parameters $\{Y_i, \langle\phi_i\rangle_0\}$ to produce the observed mass hierarchy.

2. A_4 realization of two antiequalities: ($-M_{\nu 11} = M_{\nu 22} = M_{\nu 33}$)

We show here how one can transform the past setup from two equalities into two antiequalities.

(1) *Strategy of basis choice.*—Actually, one can consider the two-equalities texture as arising from invariance under symmetry defined by the generators G such that

$$G^T M_\nu G = M_\nu \Rightarrow \text{equalities}. \tag{87}$$

If one performs a similarity transformation on the generators $G \to G' \equiv I^{-1} G I$ such that I is unitary ($I^{-1} = I^\dagger$), then we see that the form invariance of M_ν under G is equivalent to the invariance of $M'_\nu \equiv I^T M_\nu I$ under the generators (G'):

$$\begin{aligned} G^T M_\nu G = M_\nu &\Rightarrow I^T G^T I^{T^{-1}} I^T M_\nu I I^{-1} G I = I^T M_\nu I \\ &\Rightarrow G'^T M'_\nu G' = M'_\nu. \end{aligned} \tag{88}$$

The question is thus to find I such that equalities in M_ν translate as antiequalities in M'. Actually, in order to flip the sign of the element at the entry (1,1) while keeping the signs of the entries (2,2) and (3,3) intact, it suffices to take $I = \mathrm{diag}(-i, 1, 1)$, such that

$$M_{\nu 11} = M_{\nu 22} = M_{\nu 33} \Rightarrow -M'_{\nu 11} = M'_{\nu 22} = M'_{\nu 33}. \tag{89}$$

(2) *Basis* $\mathbf{B}' = (\mathbf{S}', \mathbf{T}')$.—For the irrep **3**, considering the expressions of $B = (S, T)$ in Appendix C, we have

$$\begin{aligned} (x'_1, x'_2, x'_3)^T &= I(x_1, x_2, x_3)^T = (-ix_1, x_2, x_3)^T, \\ S' &= I^\dagger S I = S = \mathrm{diag}(1, -1, -1), \\ T' &= I^\dagger T I = \begin{pmatrix} 0 & i & 0 \\ 0 & 0 & 1 \\ -i & 0 & 0 \end{pmatrix}. \end{aligned} \tag{90}$$

Note here that the combination $(x'_1 y'_1 + x'_2 y'_2 + x'_3 y'_3)$, whose "unprimed" version appears in the singlet decomposition of $\mathbf{3} \otimes \mathbf{3}$ in the basis (S, T), is not invariant under the basis (S', T'). Actually, from Eq. (90), we find the following:

$$\begin{aligned} &(x_1 y_1 + x_2 y_2 + x_3 y_3)_{\mathbf{1}} = (-x'_1 y'_1 + x'_2 y'_2 + x'_3 y'_3)_{\mathbf{1}} \\ &(x_1 y_1 + \omega^2 x_2 y_2 + \omega x_3 y_3)_{\mathbf{1}'} \\ &\quad = (-x'_1 y'_1 + \omega^2 x'_2 y'_2 + \omega x'_3 y'_3)_{\mathbf{1}'} \\ &(x_1 y_1 + \omega x_2 y_2 + \omega^2 x_3 y_3)_{\mathbf{1}''} \\ &\quad = (-x'_1 y'_1 + \omega x'_2 y'_2 + \omega^2 x'_3 y'_3)_{\mathbf{1}''}. \end{aligned} \tag{91}$$

One can check that when $(x'_1, x'_2, x'_3)^T$ transforms under T', i.e. under $(x'_1 \to i x'_2, x'_2 \to x'_3, x'_3 \to -i x'_1)$, idem for y', then $(\mathbf{3} \otimes \mathbf{3})_{\mathbf{3}_s} \equiv (x'_2 y'_3 + x'_3 y'_2, x'_3 y'_1 + x'_1 y'_3, x'_1 y'_2 + x'_2 y'_1)^T$ transforms under T'^*. The same applies for $(\mathbf{3} \otimes \mathbf{3})_{\mathbf{3}_a} \equiv (x'_2 y'_3 - x'_3 y'_2, x'_3 y'_1 - x'_1 y'_3, x'_1 y'_2 - x'_2 y'_1)^T$.

(3) *Basis* $\mathbf{B}'^* = (\mathbf{S}'^*, \mathbf{T}'^*)$.—For the irrep **3**, we have T as a complex matrix in the basis B'. This pushes us to consider the basis $B^* = (S'^*, T'^*)$.

$$\begin{aligned} S'^* = S', T'^* = \begin{pmatrix} 0 & -i & 0 \\ 0 & 0 & 1 \\ i & 0 & 0 \end{pmatrix} &= J^{-1} T' J : J \\ = \mathrm{diag}(-1, 1, 1) &\Rightarrow \\ (x'^*_1, x'^*_2, x'^*_3)^T = J(x'_1, x'_2, x'_3)^T &= (-x'_1, x'_2, x'_3)^T \\ = JI(x_1, x_2, x_3)^T & \\ = \mathrm{diag}(i, 1, 1)(x_1, x_2, x_3)^T & \\ = (i x_1, x_2, x_3)^T. & \end{aligned} \tag{92}$$

From Eqs. (90) and (92), we find the following:

$$\begin{aligned}
&(-x'_1y'_1 + x'_2y'_2 + x'_3y'_3)_{\mathbf{1}} = (x'^*_1y'_1 + x'^*_2y'_2 + x'^*_3y'_3)_{\mathbf{1}},\\
&(-x'_1y'_1 + \omega^2x'_2y'_2 + \omega x'_3y'_3)_{\mathbf{1}'}\\
&\quad = (x'^*_1y'_1 + \omega^2x'^*_2y'_2 + \omega x'^*_3y'_3)_{\mathbf{1}'},\\
&(-x'_1y'_1 + \omega x'_2y'_2 + \omega^2x'_3y'_3)_{\mathbf{1}''}\\
&\quad = (\,x'^*_1y'_1 + \omega x'^*_2y'_2 + \omega^2x'^*_3y'_3\,)_{\mathbf{1}''}. \qquad (93)
\end{aligned}$$

(4) *Matter content.*—It is the same content expressed in Table VI, but the generators of A_4 are taken to be expressed in the $(B' = \{S', T'\})$ basis. Note here that

$$\begin{aligned}
(D_L^T \otimes D_L)_{\mathbf{3}_s} = (&D^T_{L\mu}D_{L\tau} + D^T_{L\tau}D_{L\mu}, D^T_{L\tau}D_{Le}\\
&+ D^T_{Le}D_{L\tau}, D^T_{Le}D_{L\mu} + D^T_{L\mu}D_{Le})^T
\end{aligned} \qquad (94)$$

transforms as $\mathbf{3}^*$.

(5) *Neutrino mass matrix.*—With the Lagrangian

$$\begin{aligned}
\mathcal{L} \ni\ & Y[(D^T_{L\mu}C^{-1}i\tau_2\Delta_1D_{L\tau} + D^T_{L\tau}C^{-1}i\tau_2\Delta_1D_{L\mu})\\
&+ (D^T_{L\tau}C^{-1}i\tau_2\Delta_2D_{Le} + D^T_{Le}C^{-1}i\tau_2\Delta_2D_{L\tau})\\
&+ (D^T_{Le}C^{-1}i\tau_2\Delta_3D_{L\mu} + D^T_{L\mu}C^{-1}i\tau_2\Delta_3D_{Le})]\\
&+ Y'[-D^T_{Le}C^{-1}i\tau_2\Delta_4D_{Le} + D^T_{L\mu}C^{-1}i\tau_2\Delta_4D_{L\mu}\\
&+ D^T_{L\tau}C^{-1}i\tau_2\Delta_4D_{L\tau}]
\end{aligned} \qquad (95)$$

we get, upon acquiring small VEVs for $\Delta^o_i, i = 1, \ldots, 4$, the characteristic constraints $(-M_{\nu 11} = M_{\nu 22} = M_{\nu 33} =)$. Note that the Y term represents the trivial singlet expression in Eq. (93), using Eq. (94), whereas the Y' term represents the trivial singlet expression of Eq. (91).

By giving appropriate values to the four VEVs $(\Delta^o_i, i = 1, \ldots, 4)$ and to the two couplings (Y, Y'), one can reconstruct the mass matrix of normal type [Eq. (36)] leading to the spectrum of mixings of Eq. (35), or of inverted type [Eq. (38)] leading to the spectrum of mixings of Eq. (37). Thus, we have built an explicit A_4-flavor model which predicts the masses, mixing angles and CP phases. Moreover, one should mention that for type-II seesaw, the Yukawa couplings (Y, Y') are of order unity and the four VEVs $(\Delta^o_i, i = 1, \ldots, 4)$ are quite small compared to the electroweak scale due to the heavy triplet mass term.

(6) *Charged lepton sector.*—Note that if D_{Li} transforms under $(B' = (S', T'))$, then $\overline{D_{Li}}$ would transform under $B'^* = (S'^*, T'^*)$. Hence, with the expressions representing the singlets of Eq. (93) and the rule $\mathbf{1}' \otimes \mathbf{1}'' = \mathbf{1}$ (cf. Appendix C), the Lagrangian

$$\begin{aligned}
\mathcal{L} \ni\ & Y_1(\bar{D}_{Le}e_R + \bar{D}_{L\mu}\mu_R + \bar{D}_{L\tau}\tau_R)\phi_1\\
&+ Y_2(\bar{D}_{Le}e_R + \omega\bar{D}_{L\mu}\mu_R + \omega^2\bar{D}_{L\tau}\tau_R)\phi_2\\
&+ Y_3(\bar{D}_{Le}e_R + \omega^2\bar{D}_{L\mu}\mu_R + \omega\bar{D}_{L\tau}\tau_R)\phi_3
\end{aligned} \qquad (96)$$

leads, when ϕ_i acquire a VEV, to a diagonal charged lepton mass:

$$\begin{aligned}
M_\ell = \mathrm{diag}(&Y_1\langle\phi_1\rangle_0 + Y_2\langle\phi_2\rangle_0 + Y_3\langle\phi_3\rangle_0,\\
&Y_1\langle\phi_1\rangle_0 + Y_2\omega\langle\phi_2\rangle_0 + Y_3\omega^2\langle\phi_3\rangle_0, Y_1\langle\phi_1\rangle_0\\
&+ Y_2\omega^2\langle\phi_2\rangle_0 + Y_3\omega\langle\phi_3\rangle_0).
\end{aligned} \qquad (97)$$

The charged lepton matrix has enough free parameters $\{Y_i, \langle\phi_i\rangle_0\}$ to produce the observed mass hierarchy.

The method elaborated above allows us to move from any realization imposing a texture involving equalities, to another realization leading to the corresponding texture but with equalities replaced by antiequalities. Moreover, switching indices, say 1 and 2, allows to move from the texture under study, which is viable even when the strict lower bound of $\Sigma \geq 0.09$ eV is taken, to that characterized by $(M_{\nu 11} = -M_{\nu 22} = M_{\nu 33})$ which cannot accommodate data.

B. S_4-non-Abelian group realization of the texture ($M_{\nu 11} = -M_{\nu 23}$ and $M_{\nu 33} = -M_{\nu 22}$)

We proceed now with a realization based on the non-Abelian group S_4 leading to a texture with two vanishing subtraces, where the related elements do not lie all on the diagonal. For completeness, we summarize the irreps of $(S_n, n = 1, \ldots, 4)$ in Appendix D. Although the realized texture is unviable *vis-à-vis* data, however by switching the indices $(1 \leftrightarrow 3)$ one has a realization model for the viable texture ($M_{\nu 33} = -M_{\nu 21}$ and $M_{\nu 11} = -M_{\nu 22}$) which, as we saw, remains viable when the lower bound of Σ reaches 0.2 eV.

1. S_4 bases

The symmetric group of order 4 has two generators, and can be defined minimally as

$$\begin{aligned}
S_4 &= \langle d, b : d^4 = b^3 = 1, db^2d = b\rangle\\
&= \langle T, S : T^4 = S^2 = (ST)^3 = 1\rangle,
\end{aligned} \qquad (98)$$

leading to $dbd = bd^2b$ from the first minimal definition, and to $(TS)^3 = 1$ from the second one, and where one can take $(T = d, ST = b)$ linking the two sets of two generators. S_4 has five inequivalent irreps ($\mathbf{1}, \mathbf{1}', \mathbf{2}, \mathbf{3}$ and $\mathbf{3}'$). In Appendix D 3, we stated the expressions of the generators in a certain $\tilde{B}$ basis. As was done in the previous subsection, and in order to flip the sign in the texture, we carry out a similarity transformation to go from the $\tilde{B}$ basis to another

basis, call it the B basis, where the symmetry assignments for the matter fields will be given, and where the texture of the mass matrix is of the required form. We choose to do this only for the triplet irreps with similarity matrix given by $U = \mathrm{diag}(1, -1, 1)$, whereas the doublet, and evidently the singlets, will remain the same. Thus we have [$d^{(\prime,\prime\prime)}, b^{(\prime,\prime\prime)}$ refer to $\mathbf{3}(\mathbf{3}', \mathbf{2})$] [cf. Eq. (D25)]

$$d = U^\dagger \tilde{d}_4 U = \mathrm{diag}(-1, -i, i),$$
$$b = U^\dagger \tilde{b}_1 U = \begin{pmatrix} 0 & \frac{-i}{\sqrt{2}} & \frac{-i}{\sqrt{2}} \\ \frac{-1}{\sqrt{2}} & \frac{-i}{2} & \frac{i}{2} \\ \frac{1}{\sqrt{2}} & \frac{-i}{2} & \frac{i}{2} \end{pmatrix}, \tag{99}$$

$$d' = U^\dagger \tilde{d}'_4 U = \mathrm{diag}(1, i, -i),$$
$$b' = U^\dagger \tilde{b}'_1 U = \begin{pmatrix} 0 & \frac{-i}{\sqrt{2}} & \frac{-i}{\sqrt{2}} \\ \frac{-1}{\sqrt{2}} & \frac{-i}{2} & \frac{i}{2} \\ \frac{1}{\sqrt{2}} & \frac{-i}{2} & \frac{i}{2} \end{pmatrix}, \tag{100}$$

$$d'' = \tilde{d}''_4 = \mathrm{diag}(1, -1),$$
$$b'' = \tilde{b}''_1 = \frac{1}{2}\begin{pmatrix} -1 & -\sqrt{3} \\ \sqrt{3} & -1 \end{pmatrix}. \tag{101}$$

One can then check that the following "symmetry adapted linear combinations" (SALC) multiplication rules are valid in the adopted working B basis:

$$\begin{pmatrix} a_1 \\ a_2 \end{pmatrix}_{\mathbf{2}} \otimes \begin{pmatrix} b_1 \\ b_2 \end{pmatrix}_{\mathbf{2}} = (a_1 b_1 + a_2 b_2)_{\mathbf{1}} \oplus (a_1 b_2 - a_2 b_1)_{\mathbf{1}'} \oplus \begin{pmatrix} a_2 b_2 - a_1 b_1 \\ a_1 b_2 + a_2 b_1 \end{pmatrix}_{\mathbf{2}} \tag{102}$$

$$\begin{pmatrix} a_1 \\ a_2 \end{pmatrix}_{\mathbf{2}} \otimes \begin{pmatrix} b_1 \\ b_2 \\ b_3 \end{pmatrix}_{\mathbf{3}} = \begin{pmatrix} a_1 b_1 \\ -\frac{\sqrt{3}}{2} a_2 b_3 - \frac{1}{2} a_1 b_2 \\ -\frac{\sqrt{3}}{2} a_2 b_2 - a_1 b_3 \end{pmatrix}_{\mathbf{3}} \oplus \begin{pmatrix} -a_2 b_1 \\ -\frac{\sqrt{3}}{2} a_1 b_3 + \frac{1}{2} a_2 b_2 \\ -\frac{\sqrt{3}}{2} a_1 b_2 + \frac{1}{2} a_2 b_3 \end{pmatrix}_{\mathbf{3}'}, \tag{103}$$

$$\begin{pmatrix} a_1 \\ a_2 \end{pmatrix}_{\mathbf{2}} \otimes \begin{pmatrix} b_1 \\ b_2 \\ b_3 \end{pmatrix}_{\mathbf{3}'} = \begin{pmatrix} -a_2 b_1 \\ -\frac{\sqrt{3}}{2} a_1 b_3 + \frac{1}{2} a_2 b_2 \\ -\frac{\sqrt{3}}{2} a_1 b_2 + \frac{1}{2} a_2 b_3 \end{pmatrix}_{\mathbf{3}} \oplus \begin{pmatrix} a_1 b_1 \\ -\frac{\sqrt{3}}{2} a_2 b_3 - \frac{1}{2} a_1 b_2 \\ -\frac{\sqrt{3}}{2} a_2 b_2 - a_1 b_3 \end{pmatrix}_{\mathbf{3}'}, \tag{104}$$

$$\begin{pmatrix} a_1 \\ a_2 \\ a_3 \end{pmatrix}_{\mathbf{3}(\mathbf{3}')} \otimes \begin{pmatrix} b_1 \\ b_2 \\ b_3 \end{pmatrix}_{\mathbf{3}(\mathbf{3}')} = (a_1 b_1 - a_2 b_3 - a_3 b_2)_{\mathbf{1}} \oplus \begin{pmatrix} a_1 b_1 + \frac{1}{2}(a_2 b_3 + a_3 b_2) \\ \frac{\sqrt{3}}{2}(a_2 b_2 + a_3 b_3) \end{pmatrix}_{\mathbf{2}} \oplus \begin{pmatrix} a_3 b_3 - a_2 b_2 \\ -a_1 b_3 - a_3 b_1 \\ a_1 b_2 + a_2 b_1 \end{pmatrix}_{\mathbf{3}} \oplus \begin{pmatrix} -a_3 b_2 + a_2 b_3 \\ a_2 b_1 - a_1 b_2 \\ a_1 b_3 - a_3 b_1 \end{pmatrix}_{\mathbf{3}'}, \tag{105}$$

$$\begin{pmatrix} a_1 \\ a_2 \\ a_3 \end{pmatrix}_{\mathbf{3}} \otimes \begin{pmatrix} b_1 \\ b_2 \\ b_3 \end{pmatrix}_{\mathbf{3}'} = (a_1 b_1 - a_2 b_3 - a_3 b_2)_{\mathbf{1}'} \oplus \begin{pmatrix} \frac{\sqrt{3}}{2}(a_2 b_2 + a_3 b_3) \\ -a_1 b_1 - \frac{1}{2}(a_2 b_3 + a_3 b_2) \end{pmatrix}_{\mathbf{2}} \oplus \begin{pmatrix} -a_3 b_2 + a_2 b_3 \\ a_2 b_1 - a_1 b_2 \\ a_1 b_3 - a_3 b_1 \end{pmatrix}_{\mathbf{3}} \oplus \begin{pmatrix} a_3 b_3 - a_2 b_2 \\ -a_1 b_3 - a_3 b_1 \\ a_1 b_2 + a_2 b_1 \end{pmatrix}_{\mathbf{3}'}. \tag{106}$$

Noting that $\mathbf{v}^*$ transforms according to the irrep $\mathcal{D}^*$ provided $\mathbf{v} \sim \mathcal{D}$ (i.e. $\mathbf{v} \to \mathcal{D}\mathbf{v}$), which gives $\mathbf{v}^\dagger \to \mathbf{v}^\dagger \mathcal{D}^\dagger$, and observing that taking trace and taking conjugate commute, which leads to $\mathcal{D}$ being equivalent to $\mathcal{D}^*$ for S_4 where the corresponding character table is real (cf. Table X), we state for completeness the rules involving conjugate irreps, stressing the fact that the singlet in, say ($\mathbf{3} \otimes \mathbf{3}$), changes upon conjugation

from $(a_1b_1 - a_2b_3 - a_3b_2)$ to $(a_1^*b_1 + a_2^*b_2 + a_3^*b_3)$ in $(\mathbf{3}^* \otimes \mathbf{3})$:

$$\begin{pmatrix} a_1^* \\ a_2^* \end{pmatrix}_{\mathbf{2}^*} \otimes \begin{pmatrix} b_1 \\ b_2 \end{pmatrix}_{\mathbf{2}} = (a_1^*b_1 + a_2^*b_2)_{\mathbf{1}} \oplus (a_1^*b_2 - a_2^*b_1)_{\mathbf{1}'} \oplus \begin{pmatrix} a_2^*b_2 - a_1^*b_1 \\ a_1^*b_2 + a_2^*b_1 \end{pmatrix}_{\mathbf{2}} \tag{107}$$

$$\begin{pmatrix} a_1^* \\ a_2^* \end{pmatrix}_{\mathbf{2}^*} \otimes \begin{pmatrix} b_1 \\ b_2 \\ b_3 \end{pmatrix}_{\mathbf{3}} = \begin{pmatrix} a_1^*b_1 \\ -\frac{\sqrt{3}}{2}a_2^*b_3 - \frac{1}{2}a_1^*b_2 \\ -\frac{\sqrt{3}}{2}a_2^*b_2 - \frac{1}{2}a_1^*b_3 \end{pmatrix}_{\mathbf{3}} \oplus \begin{pmatrix} -a_2^*b_1 \\ -\frac{\sqrt{3}}{2}a_1^*b_3 + \frac{1}{2}a_2^*b_2 \\ -\frac{\sqrt{3}}{2}a_1^*b_2 + \frac{1}{2}a_2^*b_3 \end{pmatrix}_{\mathbf{3}'}, \tag{108}$$

$$\begin{pmatrix} a_1^* \\ a_2^* \end{pmatrix}_{\mathbf{2}^*} \otimes \begin{pmatrix} b_1 \\ b_2 \\ b_3 \end{pmatrix}_{\mathbf{3}'} = \begin{pmatrix} -a_2^*b_1 \\ -\frac{\sqrt{3}}{2}a_1^*b_3 + \frac{1}{2}a_2^*b_2 \\ -\frac{\sqrt{3}}{2}a_1^*b_2 + \frac{1}{2}a_2^*b_3 \end{pmatrix}_{\mathbf{3}} \oplus \begin{pmatrix} a_1^*b_1 \\ -\frac{\sqrt{3}}{2}a_2^*b_3 - \frac{1}{2}a_1^*b_2 \\ -\frac{\sqrt{3}}{2}a_2^*b_2 - \frac{1}{2}a_1^*b_3 \end{pmatrix}_{\mathbf{3}'}, \tag{109}$$

$$\begin{pmatrix} a_1^* \\ a_2^* \\ a_3^* \end{pmatrix}_{\mathbf{3}^*(\mathbf{3}'^*)} \otimes \begin{pmatrix} b_1 \\ b_2 \\ b_3 \end{pmatrix}_{\mathbf{3}(\mathbf{3}')} = (a_1^*b_1 + a_2^*b_2 + a_3^*b_3)_{\mathbf{1}} \oplus \begin{pmatrix} a_1^*b_1 - \frac{1}{2}(a_2^*b_2 + a_3^*b_3) \\ \frac{-\sqrt{3}}{2}(a_2^*b_3 + a_3^*b_2) \end{pmatrix}_{\mathbf{2}} \oplus \begin{pmatrix} -a_3^*b_2 + a_2^*b_3 \\ a_1^*b_2 - a_3^*b_1 \\ -a_1^*b_3 + a_2^*b_1 \end{pmatrix}_{\mathbf{3}^*} \oplus \begin{pmatrix} a_3^*b_3 - a_2^*b_2 \\ a_1^*b_3 + a_2^*b_1 \\ -a_1^*b_2 - a_3^*b_1 \end{pmatrix}_{\mathbf{3}'^*}, \tag{110}$$

$$\begin{pmatrix} a_1^* \\ a_2^* \\ a_3^* \end{pmatrix}_{\mathbf{3}^*} \otimes \begin{pmatrix} b_1 \\ b_2 \\ b_3 \end{pmatrix}_{\mathbf{3}'} = (a_1^*b_1 + a_2^*b_2 + a_3^*b_3)_{\mathbf{1}'} \oplus \begin{pmatrix} -\frac{\sqrt{3}}{2}(a_2^*b_3 + a_3^*b_2) \\ -a_1^*b_1 + \frac{1}{2}(a_2^*b_2 + a_3^*b_3) \end{pmatrix}_{\mathbf{2}} \oplus \begin{pmatrix} a_3^*b_3 - a_2^*b_2 \\ a_2^*b_1 + a_1^*b_3 \\ -a_1^*b_2 - a_3^*b_1 \end{pmatrix}_{\mathbf{3}^*} \oplus \begin{pmatrix} -a_3^*b_2 + a_2^*b_3 \\ a_1^*b_2 - a_3^*b_1 \\ -a_1^*b_3 + a_2^*b_1 \end{pmatrix}_{\mathbf{3}'^*}, \tag{111}$$

$$\begin{pmatrix} a_1^* \\ a_2^* \end{pmatrix}_{\mathbf{2}^*} \otimes \begin{pmatrix} b_1^* \\ b_2^* \end{pmatrix}_{\mathbf{2}^*} = (a_1^*b_1^* + a_2^*b_2^*)_{\mathbf{1}^*} \oplus (a_1^*b_2^* - a_2^*b_1^*)_{\mathbf{1}'^*} \oplus \begin{pmatrix} a_2^*b_2^* - a_1^*b_1^* \\ a_1^*b_2^* + a_2^*b_1^* \end{pmatrix}_{\mathbf{2}^*} \tag{112}$$

$$\begin{pmatrix} a_1^* \\ a_2^* \end{pmatrix}_{\mathbf{2}^*} \otimes \begin{pmatrix} b_1^* \\ b_2^* \\ b_3^* \end{pmatrix}_{\mathbf{3}^*} = \begin{pmatrix} a_1^*b_1^* \\ -\frac{\sqrt{3}}{2}a_2^*b_3^* - \frac{1}{2}a_1^*b_2^* \\ -\frac{\sqrt{3}}{2}a_2^*b_2^* - \frac{1}{2}a_1^*b_3^* \end{pmatrix}_{\mathbf{3}^*} \oplus \begin{pmatrix} -a_2^*b_1^* \\ -\frac{\sqrt{3}}{2}a_1^*b_3^* + \frac{1}{2}a_2^*b_2^* \\ -\frac{\sqrt{3}}{2}a_1^*b_2^* + \frac{1}{2}a_2^*b_3^* \end{pmatrix}_{\mathbf{3}'^*}, \tag{113}$$

$$\begin{pmatrix} a_1^* \\ a_2^* \end{pmatrix}_{\mathbf{2}^*} \otimes \begin{pmatrix} b_1^* \\ b_2^* \\ b_3^* \end{pmatrix}_{\mathbf{3}'^*} = \begin{pmatrix} -a_2^*b_1^* \\ -\frac{\sqrt{3}}{2}a_1^*b_3^* + \frac{1}{2}a_2^*b_2^* \\ -\frac{\sqrt{3}}{2}a_1^*b_2^* + \frac{1}{2}a_2^*b_3^* \end{pmatrix}_{\mathbf{3}^*} \oplus \begin{pmatrix} a_1^*b_1^* \\ -\frac{\sqrt{3}}{2}a_2^*b_3^* - \frac{1}{2}a_1^*b_2^* \\ -\frac{\sqrt{3}}{2}a_2^*b_2 - \frac{1}{2}a_1^*b_3^* \end{pmatrix}_{\mathbf{3}'^*}, \tag{114}$$

$$\begin{pmatrix} a_1^* \\ a_2^* \\ a_3^* \end{pmatrix}_{\mathbf{3}^*(\mathbf{3}'^*)} \otimes \begin{pmatrix} b_1^* \\ b_2^* \\ b_3^* \end{pmatrix}_{\mathbf{3}^*(\mathbf{3}'^*)} = (a_1^* b_1^* - a_2^* b_3^* - a_3^* b_2^*)_{\mathbf{1}^*} \oplus \begin{pmatrix} a_1^* b_1^* + \frac{1}{2}(a_2^* b_3^* + a_3^* b_2^*) \\ \frac{\sqrt{3}}{2}(a_2^* b_2^* + a_3^* b_3^*) \end{pmatrix}_{\mathbf{2}^*} \oplus \begin{pmatrix} a_3^* b_3^* - a_2^* b_2^* \\ -a_1^* b_3^* - a_3^* b_1^* \\ a_1^* b_2^* + a_2^* b_1^* \end{pmatrix}_{\mathbf{3}^*} \oplus \begin{pmatrix} -a_3^* b_2^* + a_2^* b_3^* \\ a_2^* b_1^* - a_1^* b_2^* \\ a_1^* b_3^* - a_3^* b_1^* \end{pmatrix}_{\mathbf{3}'^*}, \quad (115)$$

$$\begin{pmatrix} a_1^* \\ a_2^* \\ a_3^* \end{pmatrix}_{\mathbf{3}^*} \otimes \begin{pmatrix} b_1^* \\ b_2^* \\ b_3^* \end{pmatrix}_{\mathbf{3}'^*} = (a_1^* b_1^* - a_2^* b_3^* - a_3^* b_2^*)_{\mathbf{1}'^*} \oplus \begin{pmatrix} \frac{\sqrt{3}}{2}(a_2^* b_2^* + a_3^* b_3^*) \\ -a_1^* b_1^* - \frac{1}{2}(a_2^* b_3^* + a_3^* b_2^*) \end{pmatrix}_{\mathbf{2}^*} \oplus \begin{pmatrix} -a_3^* b_2^* + a_2^* b_3^* \\ a_2^* b_1^* - a_1^* b_2^* \\ a_1^* b_3^* - a_3^* b_1^* \end{pmatrix}_{\mathbf{3}^*} \oplus \begin{pmatrix} a_3^* b_3^* - a_2^* b_2^* \\ -a_1^* b_3^* - a_3^* b_1^* \\ a_1^* b_2^* + a_2^* b_1^* \end{pmatrix}_{\mathbf{3}'^*}. \quad (116)$$

2. Type-II seesaw matter content

We present now a type-II seesaw scenario leading to a neutrino mass matrix of the required form. The matter content is summarized in Table VII.

The Lorentz-, gauge- and S_4-invariant terms relevant for the neutrino mass matrix are

TABLE VII. Matter content and symmetry transformations, leading to texture with two antiequalities. $i = 1, \ldots, 3$ is a family index.

Fields	D_{L_i}	Δ_i	Δ_4	ℓ_{R_i}	ϕ_I	ϕ_{II}	ϕ_{III}	ϕ'_{III}
$SU(2)_L$	2	3	3	1	2	2	2	2
S_4	**3**	**3**	**1**	**3**	**1**	**2**	**3**	**3′**

$$\mathcal{L} \ni Y(D_{L1}^T C^{-1} i\tau_2 D_{L1} - D_{L2}^T C^{-1} i\tau_2 D_{L3} - D_{L3}^T C^{-1} i\tau_2 D_{L2})\Delta_4 + Y'[(D_{L3}^T C^{-1} i\tau_2 D_{L3} - D_{L2}^T C^{-1} i\tau_2 D_{L2})\Delta_1 + (D_{L1}^T C^{-1} i\tau_2 D_{L3} + D_{L3}^T C^{-1} i\tau_2 D_{L1})\Delta_3 - (D_{L1}^T C^{-1} i\tau_2 D_{L2} + D_{L2}^T C^{-1} i\tau_2 D_{L1})\Delta_2]. \quad (117)$$

The $Y(Y')$ term picks up the singlet (triplet) combination from the product of the two triplets ($D_{L_i}^T$ and D_{L_i}) [Eq. (105)], before multiplying it with the Higgs flavor singlet Δ_4 (triplet Δ_i). We get, upon acquiring small VEVs for $\Delta_i^o, i = 1, \ldots, 4$, the characteristic constraints ($M_{\nu 33} = -M_{\nu 22} = Y'\langle\Delta_1^0\rangle$) and ($M_{\nu 11} = -M_{\nu 23} = Y\langle\Delta_4^0\rangle$).

3. Charged lepton sector

In constructing the charged lepton mass matrix M_ℓ, we did not find a way to construct a nondegenerate diagonal mass matrix. However, we can build a generic mass matrix and impose suitable hierarchy conditions in order to diagonalize M_ℓ by rotating infinitesimally the left-handed charged lepton fields. This means that, up to approximations of the order of the charged lepton mass-ratios hierarchies, we are in the flavor basis, and the aforementioned phenomenological study is valid, especially that, after all, these corrections due to rotating the fields are not larger than other, hitherto discarded, corrections coming, say, from a radiative renormalization group running from the seesaw high scale to the observed data low scale.

Noting that D_{Li} transforming under ($\mathcal{D}$) implies that $\overline{D}_{Li}$ would transform under $\mathcal{D}^*$, one can use Eq. (110) of the product ($\mathbf{3}^* \otimes \mathbf{3}$) and get output irreps of ($\mathbf{1}$), to be multiplied by a Higgs flavor singlet ϕ_I, and of ($\mathbf{2}$), to be multiplied by a Higgs flavor doublet ϕ_{II} [cf. Eq. (102)], and of ($\mathbf{3}^*$), to be multiplied by a Higgs flavor triplet ϕ_{III} [cf. Eq. (110)], and finally of ($\mathbf{3}'^*$), to be multiplied by another Higgs flavor triplet $\phi_{III'}$ [cf. Eq. (110)]. The relevant Lagrangian is

$$\begin{aligned}\mathcal{L} \ni\ & \lambda_1(\bar{D}_{L1}\ell_{R1} + \bar{D}_{L2}\ell_{R2} + \bar{D}_{L3}\ell_{R3})\phi_I \\ & + \lambda_2\left[\bar{D}_{L1}\ell_{R1}\phi_{II_1} - \frac{1}{2}(\bar{D}_{L2}\ell_{R2} + \bar{D}_{L3}\ell_{R3})\phi_{II_1} - \frac{\sqrt{3}}{2}(\bar{D}_{L2}\ell_{R3} + \bar{D}_{L3}\ell_{R2})\phi_{II_2}\right] \\ & + \lambda_3[(-\bar{D}_{L3}\ell_{R2} + \bar{D}_{L2}\ell_{R3})\phi_{III_1} + (\bar{D}_{L1}\ell_{R2} - \bar{D}_{L3}\ell_{R1})\phi_{III_2} + (-\bar{D}_{L1}\ell_{R3} + \bar{D}_{L2}\ell_{R1})\phi_{III_3}] \\ & + \lambda'_3[(\bar{D}_{L3}\ell_{R3} - \bar{D}_{L2}\ell_{R2})\phi_{III'_1} + (\bar{D}_{L1}\ell_{R3} + \bar{D}_{L2}\ell_{R1})\phi_{III'_2} - (\bar{D}_{L1}\ell_{R2} + \bar{D}_{L3}\ell_{R1})\phi_{III'_3}], \end{aligned} \quad (118)$$

which leads, when $\phi_i, i \in \{I, II, III, III'\}$ acquire a VEV, to a charged lepton mass:

$$M_\ell = \lambda_1 \begin{pmatrix} \langle\phi_I\rangle_0 & 0 & 0 \\ 0 & \langle\phi_I\rangle_0 & 0 \\ 0 & 0 & \langle\phi_I\rangle_0 \end{pmatrix} + \lambda_2 \begin{pmatrix} \langle\phi_{II_1}\rangle_0 & 0 & 0 \\ 0 & -\frac{1}{2}\langle\phi_{II_1}\rangle_0 & -\frac{\sqrt{3}}{2}\langle\phi_{II_2}\rangle_0 \\ 0 & -\frac{\sqrt{3}}{2}\langle\phi_{II_2}\rangle_0 & -\frac{1}{2}\langle\phi_{II_1}\rangle_0 \end{pmatrix} + \lambda_3 \begin{pmatrix} 0 & \langle\phi_{III_2}\rangle_0 & -\langle\phi_{III_3}\rangle_0 \\ \langle\phi_{III_3}\rangle_0 & 0 & \langle\phi_{III_1}\rangle_0 \\ -\langle\phi_{III_2}\rangle_0 & -\langle\phi_{III_1}\rangle_0 & 0 \end{pmatrix} + \lambda'_3 \begin{pmatrix} 0 & -\langle\phi_{III'_3}\rangle_0 & \langle\phi_{III'_2}\rangle_0 \\ \langle\phi_{III'_2}\rangle_0 & -\langle\phi_{III'_1}\rangle_0 & 0 \\ -\langle\phi_{III'_3}\rangle_0 & 0 & \langle\phi_{III'_1}\rangle_0 \end{pmatrix}. \quad (119)$$

We state now two ways to get a generic M_ℓ.

(i) We assume a VEV hierarchy such that the first components are dominant and comparable ($\langle\phi_I\rangle_0 \approx \langle\phi_{II_1}\rangle_0 \approx \langle\phi_{III_1}\rangle_0 \approx \langle\phi_{III'_1}\rangle_0 \approx v$, whereas other VEVs can be neglected). We do not study the Higgs scalar potential, but assume that its various free parameters can be adjusted to lead naturally to this assumption. This leads to a diagonal M_ℓ:

$$M_\ell \approx v\,\mathrm{diag}\left(\lambda_1+\lambda_2, \lambda_1-\frac{1}{2}\lambda_2-\lambda'_3, \lambda_1-\frac{1}{2}\lambda_2+\lambda'_3\right). \quad (120)$$

The mass matrix is approximately diagonal with enough parameters to produce the observed charged lepton mass hierarchies by taking

$$m_e \approx (\lambda_1+\lambda_2)v, \qquad m_\mu \approx \left(\lambda_1-\frac{1}{2}\lambda_2-\lambda'_3\right)v, \qquad m_\tau \approx \left(\lambda_1-\frac{1}{2}\lambda_2+\lambda'_3\right)v. \quad (121)$$

Thus, we are, up to a good approximation which can be adjusted to be of the order of the mass ratio $\leq 10^{-2}$, in the flavor basis. The effect of the "small" neglected nondiagonal terms is to require rotating infinitesimally the left-handed charged lepton fields, leading thus to corrections on the observed V_{PMNS} of the same small order 10^{-2}.

(ii) Looking at Eq. (119), we see that we have nine free VEVs and four free perturbative coupling constants, appearing in nine linear combinations, *a priori* enough to construct the generic 3×3 complex matrix. Thus, M_ℓ can be cast in the form

$$M_\ell = \begin{pmatrix} \mathbf{a}^T \\ \mathbf{b}^T \\ \mathbf{c}^T \end{pmatrix} \Rightarrow M_\ell M_\ell^\dagger = \begin{pmatrix} \mathbf{a}.\mathbf{a} & \mathbf{a}.\mathbf{b} & \mathbf{a}.\mathbf{c} \\ \mathbf{b}.\mathbf{a} & \mathbf{b}.\mathbf{b} & \mathbf{b}.\mathbf{c} \\ \mathbf{c}.\mathbf{a} & \mathbf{c}.\mathbf{b} & \mathbf{c}.\mathbf{c} \end{pmatrix}, \quad (122)$$

where $\mathbf{a}$, $\mathbf{b}$ and $\mathbf{c}$ are three linearly independent vectors, so taking only the following natural assumption on the norms of the vectors,

$$\|\mathbf{a}\|/\|\mathbf{c}\| = m_e/m_\tau \sim 3\times 10^{-4}, \qquad \|\mathbf{b}\|/\|\mathbf{c}\| = m_\mu/m_\tau \sim 6\times 10^{-2}, \quad (123)$$

one can diagonalize $M_\ell M_\ell^\dagger$ by an infinitesimal rotation as was done in [8], which proves that we are to a good approximation in the flavor basis.

VII. SUMMARY AND CONCLUSION

In this study, we carry out a systematic study of the Majorana neutrino mass matrix characterized by two 2×2 vanishing subtraces. In light of the recent experimental data for oscillation and nonoscillation parameters, we update the results of the past study [17]. We introduce the analytical expressions for A and B coefficients as given by Eq. (15), and the leading order term in s_z for the neutrino physical parameter R_ν. Moreover, all full correlations, resulting from the full numerical analysis taking all experimental constraints into consideration, are very well approximated by exact correlations assuming "zero" solar-to-atmospheric ratio R_ν, and in many cases they even do not deviate much from correlations resulting from roots of the leading order of R_ν. This helps in studying analytically the 15 textures and justifies their viability to accommodate data. Actually, the two vanishing trace conditions put four real constraints on M_ν, thus we have only five free parameters corresponding to the three mixing angles ($\theta_x \equiv \theta_{12}, \theta_y \equiv \theta_{23}$, $\theta_z \equiv \theta_{13}$), Dirac phase δ and the solar neutrino mass difference δm^2. In contrast to [17], we vary the five parameters in their allowed experimental range and check whether or not the texture satisfies the bounds of $|\Delta m^2|$ besides those in Eq. (9). We find that only seven textures out of the 15 can accommodate the experimental data with only one case viable at both hierarchy types. We notice that neither m_1 for normal ordering nor m_3 for inverted ordering does reach a vanishing value. Therefore, there are no signatures for the singular textures for all cases at all σ levels with either hierarchy type. We find the phases δ, ρ and σ are strongly restricted at all σ levels with either hierarchy types. We present 15 correlation plots for each viable texture for both hierarchy types (red and blue plots correspond to normal and inverted orderings respectively)

generated from the accepted points of the neutrino physical parameters at the 3-σ level. Moreover, we introduce M_ν for each viable texture for both orderings at one representative point at the 3-σ level. The point is chosen to be as close as possible to the best fit values of the mixing and Dirac phase angles.

Finally, we present the symmetry realization for the two-vanishing traces texture, irrespective of whether or not it was accommodating data. We present two examples based on non-Abelian groups. The first one uses the alternating group A_4 within the type-II seesaw scenario to realize a texture where the defining elements lie on the diagonal. The second example uses the symmetry group S_4 to find a realization, within type-II seesaw scenario, of a two-vanishing-subtraces texture where the elements defining the texture do not lie all on the diagonal.

We have not discussed the question of the scalar potential and finding its general form under the imposed symmetry. Nor did we deal with the radiative corrections effect on the phenomenology and whether or not it can spoil the form of the texture while running from the ultraviolet scale where the seesaw scale imposes the texture form to the low scale where phenomenology was analyzed.

ACKNOWLEDGMENTS

E. I. L. and N. C. acknowledge support from International Center for Theoretical Physics (ICTP, Republic of Italy) through the Senior Associate programs where a significant part of this work was carried out. N. C. acknowledges support also from the Chinese Academy of Sciences-President's International Fellowship Initiative (CAS-PIFI, People's Republic of China) and from the Alexander von Humboldt Foundation (Federal Republic of Germany). E. I. L.'s work was partially supported by the Science and Technology Development Fund (STDF, Arab Republic of Egypt) Project No. 37272.

APPENDIX A: FAILING TEXTURES

We list now all the unviable eight textures, where, for each texture, studying the roots of $(m_{23}^2 - m_{13}^2)$ gives a justification for the failure to accommodate data.

1. Texture $(\mathbf{C_{33}},\mathbf{C_{23}}) \equiv (M_{ee}+M_{\mu\mu}=0, M_{ee}+M_{\tau\mu}=0)$

A and B are given by

$$\begin{aligned}
A_1 &= c_x^2 c_z^2 + (-c_x s_y s_z - s_x c_y e^{-i\delta})^2,\\
A_2 &= s_x^2 c_z^2 + (-s_x s_y s_z + c_x c_y e^{-i\delta})^2, \qquad A_3 = s_z^2 + s_y^2 c_z^2,\\
B_1 &= c_x^2 c_z^2 + (-c_x s_y s_z - s_x c_y e^{-i\delta})(-c_x c_y s_z + s_x s_y e^{-i\delta}),\\
B_2 &= s_x^2 c_z^2 + (-s_x s_y s_z + c_x c_y e^{-i\delta})(-s_x c_y s_z - c_x s_y e^{-i\delta}),\\
B_3 &= s_z^2 + s_y c_y c_z^2. \qquad \text{(A1)}
\end{aligned}$$

We find

$$m_{23}^2 - m_{13}^2 = \frac{s_y^4(1-2/t_y)}{c_y^2(1+s_{2y})} + \mathcal{O}(s_z).$$

We find that $\frac{2}{t_y} > 1$, $\forall\, \theta_y \in [41^o, 51, 3^o]$ implying $m_2 < m_1$, and this result will not be changed by including higher order terms, or by taking the exact result. Actually the exact result gives always $(m_{23}^2 - m_{13}^2)$ as negative and of order unity. Thus, we deduce that this texture is excluded experimentally.

2. Texture $(\mathbf{C_{11}},\mathbf{C_{23}}) \equiv (M_{\mu\mu}+M_{\tau\tau}=0, M_{ee}+M_{\tau\mu}=0)$

A and B are given by

$$\begin{aligned}
A_1 &= c_x^2 s_z^2 + s_x^2 e^{-2i\delta}, \qquad A_2 = s_x^2 s_z^2 + c_x^2 e^{-2i\delta}, \qquad A_3 = c_z^2,\\
B_1 &= c_x^2 c_z^2 + (-c_x s_y s_z - s_x c_y e^{-i\delta})(-c_x c_y s_z + s_x s_y e^{-i\delta}),\\
B_2 &= s_x^2 c_z^2 + (-s_x s_y s_z + c_x c_y e^{-i\delta})(-s_x c_y s_z - c_x s_y e^{-i\delta}),\\
B_3 &= s_z^2 + s_y c_y c_z^2. \qquad \text{(A2)}
\end{aligned}$$

We find

$$m_{23}^2 - m_{13}^2 = \frac{c_{2y}^2}{c_{2x}} + \frac{s_{2x} s_{2y} c_{2y} c_\delta (-1+s_{2y}) s_z}{c_{2x}^2} + \mathcal{O}(s_z^2). \qquad \text{(A3)}$$

We find that at order $\mathcal{O}(s_z)$, we have $(m_{23}^2 - m_{13}^2 \geq 0)$. However, we checked that by including the order $\mathcal{O}(s_z^2)$, the sign would be inverted $(m_{23}^2 - m_{13}^2 \leq 0)$, such that higher orders, indeed the exact result, will no longer change this sign. So, the texture is excluded experimentally.

3. Texture $(\mathbf{C_{22}},\mathbf{C_{23}}) \equiv (M_{ee}+M_{\tau\tau}=0, M_{ee}+M_{\tau\mu}=0)$

A and B are given by

$$\begin{aligned}
A_1 &= c_x^2 c_z^2 + (-c_x c_y s_z + s_x s_y e^{-i\delta})^2,\\
A_2 &= s_x^2 c_z^2 + (-s_x c_y s_z - c_x s_y e^{-i\delta})^2, \qquad A_3 = s_z^2 + c_y^2 c_z^2,\\
B_1 &= c_x^2 c_z^2 + (-c_x s_y s_z - s_x c_y e^{-i\delta})(-c_x c_y s_z + s_x s_y e^{-i\delta}),\\
B_2 &= s_x^2 c_z^2 + (-s_x s_y s_z + c_x c_y e^{-i\delta})(-s_x c_y s_z - c_x s_y e^{-i\delta}),\\
B_3 &= s_z^2 + s_y c_y c_z^2. \qquad \text{(A4)}
\end{aligned}$$

We find

$$m_{23}^2 - m_{13}^2 = \frac{c_y^4(1-2t_y)}{s_y^2 c_{2x}(1+s_{2x})} + \mathcal{O}(s_z). \qquad \text{(A5)}$$

We find that $2t_y > 1$, $\forall\, \theta_y \in [41^o, 51, 3^o]$ implying $m_2 < m_1$, and this result will not be changed by including higher order terms, or by taking the exact result which shows that δm^2 is negative and of order unity. No zeros were found for the $(m_{23}^2 - m_{13}^2)$ expression. Thus, we deduce that this texture is excluded experimentally.

4. Texture $(\mathbf{C_{33}},\mathbf{C_{11}}) \equiv (M_{ee}+M_{\mu\mu}=0, M_{\mu\mu}+M_{\tau\tau}=0)$

A and B are given by

$$\begin{aligned}
&A_1 = c_x^2c_z^2 + (-c_xs_ys_z - s_xc_ye^{-i\delta})^2,\\
&A_2 = s_x^2c_z^2 + (-s_xs_ys_z + c_xc_ye^{-i\delta})^2, \quad A_3 = s_z^2 + s_y^2c_z^2,\\
&B_1 = c_x^2s_z^2 + s_x^2e^{-2i\delta}, \quad B_2 = s_x^2s_z^2 + c_x^2e^{-2i\delta}, \quad B_3 = c_z^2. \qquad \text{(A6)}
\end{aligned}$$

We find

$$m_{23}^2 - m_{13}^2 = \frac{c_{2y}^4}{c_{2x}} + \mathcal{O}(s_z). \qquad \text{(A7)}$$

We find that the $(m_{23}^2 - m_{13}^2)$-leading term is positive but of order unity, for all the allowed values of (θ_x, θ_y). This fact remains intact in the case of the exact result for the $(m_{23}^2 - m_{13}^2)$ expression, such that there are no zeros for this expression for all allowed $(\theta_x, \theta_y, \theta_z, \delta)$; whence, the texture is excluded.

5. Texture $(\mathbf{C_{22}},\mathbf{C_{11}}) \equiv (M_{ee}+M_{\tau\tau}=0, M_{\mu\mu}+M_{\tau\tau}=0)$

A and B are given by

$$\begin{aligned}
&A_1 = c_x^2c_z^2 + (-c_xc_ys_z + s_xs_ye^{-i\delta})^2,\\
&A_2 = s_x^2c_z^2 + (-s_xc_ys_z - c_xs_ye^{-i\delta})^2, \quad A_3 = s_z^2 + c_y^2c_z^2,\\
&B_1 = c_x^2s_z^2 + s_x^2e^{-2i\delta}, \quad B_2 = s_x^2s_z^2 + c_x^2e^{-2i\delta}, \quad B_3 = c_z^2. \qquad \text{(A8)}
\end{aligned}$$

We find

$$m_{23}^2 - m_{13}^2 = \frac{s_{2y}^2}{c_{2x}} + \mathcal{O}(s_z). \qquad \text{(A9)}$$

We find that the $m_{23}^2 - m_{13}^2$-leading term is positive but of order unity, for all the allowed values of $(\theta_x, \theta_y, \theta_z, \delta)$. This fact remains intact in the case of the exact result for the $(m_{23}^2 - m_{13}^2)$ expression, such that there are no zeros for this expression. Actually, for the exact result we have

$$\begin{aligned}
m_{23}^2 - m_{13}^2 &= \frac{\mathrm{Num}(m_{23}^2 - m_{13}^2)}{\mathrm{Den}(m_{23}^2 - m_{13}^2)}:\\
\mathrm{Num}(m_{23}^2 - m_{13}^2) &= -4c_z^2c_y(c_y^2c_z^2 - c_{2z})\\
&\quad \times (-c_yc_{2x} + s_{2x}s_zs_yc_\delta). \qquad \text{(A10)}
\end{aligned}$$

The zeros of $(\mathrm{Num}(m_{23}^2 - m_{13}^2))$ give $c_\delta = \frac{1}{t_yt_{2x}s_z} > 1$ for all acceptable values of $(\theta_x, \theta_y, \theta_z)$. Thus, the texture is excluded phenomenologically.

6. Texture $(\mathbf{C_{13}},\mathbf{C_{12}}) \equiv (M_{\mu e}+M_{\tau\mu}=0, M_{\mu e}+M_{\tau\tau}=0)$

A and B are given by

$$\begin{aligned}
A_1 &= c_xc_z(-c_xs_ys_z - s_xc_ye^{-i\delta})\\
&\quad + (-c_xs_ys_z - s_xc_ye^{-i\delta})(-c_xc_ys_z + s_xs_ye^{-i\delta}),\\
A_2 &= s_xc_z(-s_xs_ys_z + c_xc_ye^{-i\delta})\\
&\quad + (-s_xs_ys_z + c_xc_ye^{-i\delta})(-s_xc_ys_z - c_xs_ye^{-i\delta}),\\
A_3 &= s_zs_yc_z + s_yc_z^2c_y,\\
B_1 &= c_xc_z(-c_xs_ys_z - s_xc_ye^{-i\delta}) + (-c_xc_ys_z + s_xs_ye^{-i\delta})^2,\\
B_2 &= s_xc_z(-s_xs_ys_z + c_xc_ye^{-i\delta}) + (-s_xc_ys_z - c_xs_ye^{-i\delta})^2,\\
B_3 &= s_yc_zs_z + c_y^2c_z^2. \qquad \text{(A11)}
\end{aligned}$$

We find

$$m_{23}^2 - m_{13}^2 = \frac{c_y^4s_{2x}s_y(1-t_y)c_\delta - c_y^2s_y^2c_{2x}}{s_x^2c_x^2s_y^2c_y^2(1+s_{2y})} + \mathcal{O}(s_z). \qquad \text{(A12)}$$

We find that the zeros of the $m_{23}^2 - m_{13}^2$-leading term should satisfy $(c_\delta = \frac{t_y^2}{t_{2x}s_y(1-t_y)} \notin [-1,+1])$ for acceptable (θ_x, θ_y), and so there are no zeros at $\mathcal{O}(s_z)$. Actually, we could find by scanning over allowed values of $(\theta_x, \theta_y, \theta_z, \delta)$ that $(m_{23}^2 - m_{13}^2 < 0)$. Thus texture is rejected.

7. Texture $(\mathbf{C_{13}},\mathbf{C_{22}}) \equiv (M_{\mu e}+M_{\tau\mu}=0, M_{ee}+M_{\tau\tau}=0)$

A and B are given by

$$\begin{aligned}
A_1 &= c_xc_z(-c_xs_ys_z - s_xc_ye^{-i\delta})\\
&\quad + (-c_xs_ys_z - s_xc_ye^{-i\delta})(-c_xc_ys_z + s_xs_ye^{-i\delta}),\\
A_2 &= s_xc_z(-s_xs_ys_z + c_xc_ye^{-i\delta})\\
&\quad + (-s_xs_ys_z + c_xc_ye^{-i\delta})(-s_xc_ys_z - c_xs_ye^{-i\delta}),\\
A_3 &= s_zs_yc_z + s_yc_z^2c_y,\\
B_1 &= c_x^2c_z^2 + (-c_xc_ys_z + s_xs_ye^{-i\delta})^2,\\
B_2 &= s_x^2c_z^2 + (-s_xc_ys_z - c_xs_ye^{-i\delta})^2,\\
B_3 &= s_z^2 + c_y^2c_z^2. \qquad \text{(A13)}
\end{aligned}$$

We find

$$\begin{aligned}
m_{23}^2 - m_{13}^2 &= \frac{\mathrm{Num}(m_{23}^2 - m_{13}^2)}{\mathrm{Den}(m_{23}^2 - m_{13}^2)}:\\
\mathrm{Num}(m_{23}^2 - m_{13}^2) &= -2c_z(c_y^2c_z^2 - s_z^2)[s_{2x}s_y(c_z^2s_y^2 + c_{2y})c_\delta\\
&\quad + s_zs_ys_{2y}c_{2x}]. \qquad \text{(A14)}
\end{aligned}$$

The zeros of $(\mathrm{Num}(m_{23}^2 - m_{13}^2))$ give, when plugged in m_{13}, m_{23}, the approximation $(m_{13} = m_{23} = 1)$. As mentioned before, this leads to rejection of the texture. This comes because we have at these zeros a degenerate

spectrum ($m_1 \approx m_2 \approx m_3$), and so $m_3^2 - m_1^2 \approx m_2^2 - m_1^2$, thus forming ($R_\nu \approx \frac{m_2^2-m_1^2}{m_3^2-m_1^2} \approx 1$), which is rejected.

8. Texture $(\mathbf{C_{23}},\mathbf{C_{12}}) \equiv (\boldsymbol{M_{ee}+M_{\mu\tau}=0}, \boldsymbol{M_{\mu e}+M_{\tau\tau}=0})$

A and B are given by

$$\begin{aligned}
A_1 &= c_x^2 c_z^2 + (-c_x s_y s_z - s_x c_y e^{-i\delta})(-c_x c_y s_z + s_x s_y e^{-i\delta}),\\
A_2 &= s_x^2 c_z^2 + (-s_x s_y s_z + c_x c_y e^{-i\delta})(-s_x c_y s_z - c_x s_y e^{-i\delta}),\\
A_3 &= s_z^2 + s_y c_y c_z^2,\\
B_1 &= c_x c_z(-c_x s_y s_z - s_x c_y e^{-i\delta}) + (-c_x c_y s_z + s_x s_y e^{-i\delta})^2,\\
B_2 &= s_x c_z(-s_x s_y s_z + c_x c_y e^{-i\delta}) + (-s_x c_y s_z - c_x s_y e^{-i\delta})^2,\\
B_3 &= s_y c_z s_z + c_y^2 c_z^2.
\end{aligned} \tag{A15}$$

We find

$$\begin{aligned}
m_{23}^2 - m_{13}^2 &= \frac{\mathrm{Num}(m_{23}^2 - m_{13}^2)}{\mathrm{Den}(m_{23}^2 - m_{13}^2)}:\\
\mathrm{Num}(m_{23}^2 - m_{13}^2) &= (s_z^2 - c_z^2 c_y^2)\{s_{2x}[c_z^3(c_y^3 - s_y^3)\\
&\quad - s_z c_z^2(1 - 3 s_y c_y) - c_{2y}(c_y + s_y)c_z\\
&\quad - s_z s_{2y}]c_\delta - c_{2x}[c_z^2(4c_y^2 - 2)\\
&\quad + s_z s_{2y}(s_y + c_y)c_z - c_{2y}]\}.
\end{aligned} \tag{A16}$$

The zeros of ($\mathrm{Num}(m_{23}^2 - m_{13}^2)$) give, when plugged in m_{13}, m_{23}, the approximation ($m_1 \approx m_2 \approx m_3$), which—like the previous pattern—is rejected phenomenologically, as it cannot accommodate a "small" value for R_ν.

APPENDIX B: MAJORANA PHASES

We state here for each of the viable patterns the leading orders, in powers of s_z, of the Majorana phases, up to multiples of $\pi/2$. Any constraint on (θ_x, θ_y and δ) stemming from meeting the acceptable value of ($R_\nu \sim 10^{-2}$) would be reflected as a constraint on ρ and σ.

(i) Texture $(\mathbf{C}_{22}, \mathbf{C}_{33})$

$$\begin{aligned}
\rho &= \frac{1}{2}\tan^{-1}\left(\frac{s_{2\delta} s_x^2}{1 - 2 s_x^2 s_\delta^2}\right) + \mathcal{O}(s_z),\\
\sigma &= \frac{1}{2}\tan^{-1}\left(\frac{s_{2\delta} c_x^2}{1 - 2 c_x^2 s_\delta^2}\right) + \mathcal{O}(s_z).
\end{aligned} \tag{B1}$$

(ii) Texture $(\mathbf{C}_{22}, \mathbf{C}_{12})$

$$\begin{aligned}
\rho &= \frac{1}{2}\tan^{-1}\left(\frac{\rho_{N3}}{\rho_{D3}}\right) + \mathcal{O}(s_z),\\
\sigma &= \frac{1}{2}\tan^{-1}\left(\frac{\sigma_{N3}}{\sigma_{D3}}\right) + \mathcal{O}(s_z),
\end{aligned} \tag{B2}$$

where

$$\begin{aligned}
\rho_{N3} &= 4 s_x s_\delta \left[\left(\left(c_\delta + \frac{1}{4}\right)c_y^2 - c_\delta^2 - \frac{1}{2}\right)c_y c_x^3\right.\\
&\quad - \frac{1}{2} s_x s_y^2 (c_y^2 - 2) c_\delta c_x^2 + \left(c_y s_y^2 c_\delta^2 + \frac{1}{4} c_y\right) c_x\\
&\quad \left. - \frac{1}{2} s_x s_y^2 c_\delta\right],\\
\sigma_{N3} &= 2 s_\delta \left[(c_y^4 - 3 c_y^2 + 2) c_\delta c_x^3\right.\\
&\quad - \left(\left(2 c_\delta^2 + \frac{1}{2}\right)c_y^2 - 2 c_\delta^2 - 1\right) s_x c_y c_x^2\\
&\quad \left. - s_y^4 c_\delta c_x - \frac{1}{2} s_x c_y s_y^2\right],\\
\rho_{D3} &= [c_{2\delta} c_y^4 + 2(1 - 3 c_\delta^2) c_y^2 + 2 c_{2\delta}] c_x^4\\
&\quad - 4 s_x c_y c_\delta \left[\left(c_\delta^2 - \frac{1}{4}\right)c_y^2 - c_\delta^2\right] c_x^3\\
&\quad - [c_{2\delta} c_y^4 + (3 - 8 c_\delta^2) c_y^2 + 3 c_{2\delta}] c_x^2\\
&\quad + 2 s_x c_y c_\delta \left[c_{2\delta} c_y^2 - 2 c_\delta^2 + \frac{1}{2}\right] c_x + c_{2\delta} s_y^2,\\
\sigma_{D3} &= [c_{2\delta} c_y^4 + 2(1 - 3 c_\delta^2) c_y^2 + 2 c_{2\delta}] c_x^3\\
&\quad - 4 s_x c_y c_\delta \left[\left(c_\delta^2 - \frac{1}{4}\right)c_y^2 - c_\delta^2\right] c_x^2\\
&\quad - [c_{2\delta} c_y^4 + (1 - 4 c_\delta^2) c_y^2 + c_{2\delta}] c_x\\
&\quad - s_x s_y^2 c_y c_\delta.
\end{aligned} \tag{B3}$$

(iii) Texture $(\mathbf{C}_{11}, \mathbf{C}_{12})$

$$\begin{aligned}
\rho &= \frac{1}{2}\tan^{-1}\left[\frac{(c_x c_{2y} - 2 s_x c_y c_\delta) s_\delta}{c_x c_{2y} c_\delta - s_x c_y c_{2\delta}}\right] + \mathcal{O}(s_z),\\
\sigma &= \frac{1}{2}\tan^{-1}\left[\frac{(s_x c_{2y} + 2 c_x c_y c_\delta) s_\delta}{s_x c_{2y} c_\delta + c_x c_y c_{2\delta}}\right] + \mathcal{O}(s_z).
\end{aligned} \tag{B4}$$

(iv) Texture $(\mathbf{C}_{33}, \mathbf{C}_{12})$

$$\begin{aligned}
\rho &= \frac{1}{2}\tan^{-1}\left(\frac{\rho_{N2}}{\rho_{D2}}\right) + \mathcal{O}(s_z),\\
\sigma &= \frac{1}{2}\tan^{-1}\left(\frac{\sigma_{N2}}{\sigma_{D2}}\right) + \mathcal{O}(s_z),
\end{aligned} \tag{B5}$$

where

$$\begin{aligned}
\rho_{N2} &= -s_x c_y c_\delta [2 s_x c_x^2 c_y^5 c_\delta + (c_x^3 + 4 c_x s_x^2 c_\delta^2) c_y^4 \\
&\quad - 2 s_x (c_{2x} + c_x^2) c_y^3 c_\delta + c_x (s_x^2 - c_y^2) + 2 s_x c_{2x} c_y c_\delta], \\
\sigma_{N2} &= 2 c_x c_y s_\delta \Big[(c_y^5 - 3 c_y^3 + 2 c_y) c_x^3 c_\delta \\
&\quad + 2 s_x \left(c_y^4 c_\delta^2 - \frac{1}{4} c_y^4 + \frac{1}{4} \right) c_x^2 - c_y s_y^4 c_\delta c_x - \frac{1}{8} s_x s_{2y}^2 \Big], \\
\rho_{D2} &= -\frac{1}{4} s_{2x}^2 c_{2\delta} c_y^6 + s_{2x} c_\delta \left[\left(2 c_\delta^2 - \frac{3}{2} \right) c_x^2 - c_{2\delta} \right] c_y^5 \\
&\quad + [(-6 c_\delta^2 + 8) c_x^4 + (8 c_\delta^2 - 7) c_x^2 - c_{2\delta}] c_y^4 \\
&\quad + \frac{1}{2} s_{2x} c_\delta (1 - 4 c_x^2) c_y^3 [(4 c_\delta^2 - 9) c_x^4 \\
&\quad + (-6 c_\delta^2 + 7) c_x^2 + c_{2\delta}] c_y^2 + \frac{1}{2} s_{2x} (c_{2x} + c_x^2) c_\delta c_y \\
&\quad + c_x^2 c_{2x}, \\
\sigma_{D2} &= [(2 c_y^6 - 6 c_y^4 + 4 c_y^2) c_\delta^2 - c_y^6 + 8 c_y^4 - 9 c_y^2 + 2] c_x^4 \\
&\quad + 4 s_x c_y c_\delta \left[c_y^4 c_\delta^2 - \frac{3}{4} c_y^4 - c_y^2 + \frac{3}{4} \right] c_x^3 \\
&\quad + [(-2 c_y^6 + 4 c_y^4 - 2 c_y^2) c_\delta^2 + c_y^6 - 9 c_y^4 \\
&\quad + 11 c_y^2 - 3] c_x^2 + c_y s_x c_\delta (c_y^4 + 3 c_y^2 - 2) c_x \\
&\quad + 2 c_y^4 - 3 c_y^2 + 1.
\end{aligned} \tag{B6}$$

(v) Texture ($\mathbf{C}_{33}$, $\mathbf{C}_{13}$)

$$\begin{aligned}
\rho &= \frac{1}{2} \tan^{-1} \left(\frac{\rho_{N1}}{\rho_{D1}} \right) + \mathcal{O}(s_z), \\
\sigma &= \frac{1}{2} \tan^{-1} \left(\frac{\sigma_{N1}}{\sigma_{D1}} \right) + \mathcal{O}(s_z),
\end{aligned} \tag{B7}$$

where

$$\begin{aligned}
\rho_{N1} &= s_y s_x^2 s_{2\delta} [s_y (-1 + c_x^2 (c_y^2 + 2)) - s_{2x} c_y^2 c_\delta], \\
\rho_{D1} &= (c_{2\delta} c_y^4 - 2 c_y^2 s_\delta^2 - 4 c_\delta^2 + 3) c_x^4 \\
&\quad - s_{2x} c_x^2 s_y c_\delta (1 - c_y^2 c_{2\delta}) \\
&\quad + c_x^2 s_y^2 (c_y^2 + 3) c_{2\delta} - c_{2\delta} s_y (s_y + s_{2x} c_y^2 c_\delta), \\
\sigma_{N1} &= s_{2\delta} c_x^2 [c_x^2 c_y^2 (1 - t_x^2 c_y^2) - c_{2x} + s_{2x} s_y c_y^2 c_\delta], \\
\sigma_{D1} &= (c_{2\delta} c_y^4 - 2 c_y^2 s_\delta^2 - 4 c_\delta^2 + 3) c_x^4 \\
&\quad - s_{2x} c_x^2 s_y c_\delta (1 - c_y^2 c_{2\delta}) \\
&\quad - (c_{2\delta} c_y^4 - 2 c_y^2 - 2 c_\delta^2 + 3) c_x^2 \\
&\quad + s_y (s_y + s_{2x} c_\delta).
\end{aligned} \tag{B8}$$

(vi) Texture ($\mathbf{C}_{11}$, $\mathbf{C}_{13}$)

$$\begin{aligned}
\rho &= \frac{1}{2} \tan^{-1} \left[\frac{s_{2x} s_\delta (s_y - t_x c_\delta)}{s_{2x} s_y c_\delta - s_x^2 c_{2\delta}} \right] + \mathcal{O}(s_z), \\
\sigma &= \frac{1}{2} \tan^{-1} \left[\frac{2 c_x s_\delta (c_\delta + t_x s_y)}{2 s_x s_y c_\delta + c_x c_{2\delta}} \right] + \mathcal{O}(s_z).
\end{aligned} \tag{B9}$$

(vii) Texture ($\mathbf{C}_{13}$, $\mathbf{C}_{23}$)

$$\begin{aligned}
\rho &= \frac{1}{2} \tan^{-1} \left(\frac{\rho_{N4}}{\rho_{D4}} \right) + \mathcal{O}(s_z), \\
\sigma &= \frac{1}{2} \tan^{-1} \left(\frac{\sigma_{N4}}{\sigma_{D4}} \right) + \mathcal{O}(s_z),
\end{aligned} \tag{B10}$$

where

$$\begin{aligned}
\rho_{N4} &= 4 s_x s_y s_\delta \Big[-s_y c_x c_y s_x^2 c_\delta^2 + \frac{1}{2} s_x s_y (c_x^2 c_y^2 - c_{2x}) c_\delta \\
&\quad + \frac{1}{4} c_x (s_y c_x^2 c_y + s_x^2) \Big], \\
\sigma_{N4} &= 2 s_y s_\delta \Big[\left(c_x^3 (c_y^2 - 2) c_\delta - 2 s_x c_x^2 c_y \left(c_\delta^2 + \frac{1}{4} \right) \right. \\
&\quad \left. + c_x s_y^2 c_\delta + \frac{1}{2} s_x c_y \right) s_y + \frac{1}{2} s_x c_x^2 \Big], \\
\rho_{D4} &= -4 s_x c_x c_y s_y^2 s_x^2 c_\delta^3 + 2 s_y^2 s_x^2 (c_x^2 c_y^2 - c_{2x}) c_\delta^2 \\
&\quad + s_x c_x [s_x^2 s_y - c_y s_y^2 (c_x^2 - 2)] c_\delta \\
&\quad + s_x^2 [c_x^2 c_y^4 + (1 - 3 c_x^2) c_y^2 - s_y c_x^2 c_y + c_{2x}], \\
\sigma_{D4} &= [s_y c_y + (c_y^4 - 3 c_y^2 + 2) c_{2\delta}] c_x^3 \\
&\quad - s_x c_\delta [s_y - c_y s_y^2 (4 c_\delta^2 - 1)] c_x^2 \\
&\quad - [s_y c_y + (c_y^4 - 2 c_y^2 + 2) c_{2\delta}] c_x \\
&\quad - s_x c_y s_y^2 c_\delta.
\end{aligned} \tag{B11}$$

APPENDIX C: A_4-IRREPS

A_4 is the group of even permutations of four objects. It is defined in terms of two generators (S, T) such that

$$S^2 = T^3 = (ST)^3 = 1, \tag{C1}$$

leading also to $(TS)^3 = 1$. It has four irreps ($\mathbf{1}$, $\mathbf{1}'$, $\mathbf{1}''$, $\mathbf{3}$)

(i) $\mathbf{1}$: $S = 1$, $T = 1$
(ii) $\mathbf{1}'$: $S = 1$, $T = \omega : \omega^3 = 1$
(iii) $\mathbf{1}''$: $S = 1$, $T = \omega^2$
(iv) $\mathbf{3}$: $S = \begin{pmatrix} 1 & 0 & 0 \\ 0 & -1 & 0 \\ 0 & 0 & -1 \end{pmatrix}$, $T = \begin{pmatrix} 0 & 1 & 0 \\ 0 & 0 & 1 \\ 1 & 0 & 0 \end{pmatrix} \equiv (123)$.

We have

$$\mathbf{1}' \otimes \mathbf{1}' = \mathbf{1}'', \mathbf{1}'' \otimes \mathbf{1}' = \mathbf{1}, \quad \mathbf{1}'' \otimes \mathbf{1}'' = \mathbf{1}', \mathbf{1} \otimes \mathbf{1} = \mathbf{1}, \tag{C2}$$

$$\mathbf{3}\otimes\mathbf{3}=\mathbf{1}\oplus\mathbf{1}'\oplus\mathbf{1}''\oplus\mathbf{3_s}\oplus\mathbf{3_a}: \tag{C3}$$

$$\begin{aligned}&(x_1,\ x_2,\ x_3)^T\otimes(y_1,\ y_2,\ y_3)^T\\&=(x_1y_1+x_2y_2+x_3y_3)_{\mathbf{1}}\\&\oplus(x_1y_1+\omega^2x_2y_2+\omega x_3y_3)_{\mathbf{1}'}\\&\oplus(x_1y_1+\omega x_2y_2+\omega^2x_3y_3)_{\mathbf{1}''}\\&\oplus(x_2y_3+x_3y_2,\ x_3y_1+x_1y_3,\ x_1y_2+x_2y_1)^T_{\mathbf{3_s}}\\&\oplus(x_2y_3-x_3y_2,\ x_3y_1-x_1y_3,\ x_1y_2-x_2y_1)^T_{\mathbf{3_a}}.\end{aligned} \tag{C4}$$

APPENDIX D: S_n-IRREPS

The symmetric group of order n, S_n is the group of permutations of $N_n=\{1,\ldots n\}$. It is of order $n!$, and for $n\geq 3$, it is non-Abelian. Any permutation can be decomposed as a product of cycles with disjoint supports, which in turn can be decomposed as a product of transpositions. S_1 is the trivial group consisting of just one element. Any group G is divided into conjugacy classes according to the equivalence relation $(a\sim b\Leftrightarrow\exists\, c\in G: b=c^{-1}ac)$. The number of equivalence classes is equal to the number of inequivalent unitary irreps, which is depicted by the corresponding character table showing, for each irrep $\mathcal{D}$, listed in upper line of the table, and each equivalence class C, listed in the leftmost column of the table, the trace $(\chi_{\mathcal{D}}(g))$ of the irrep $\mathcal{D}$ evaluated at one representative member g of the class C.

In order to construct, for a group G of order n_G, the character table, for n_c classes (the class $sC_h=[g]$ includes s elements g all of order h[4]) and n_r inequivalent unitary irreps (the number of inequivalent unitary n-dimenional irrep $\mathcal{D}_n$ is m_n), one usually uses the following rules:

$$n_c=n_r,\qquad \sum_{n\in N}m_n n^2=n_G, \tag{D1}$$

$$\sum_{a\in G}\chi_\alpha(a)\chi^*_\beta(a)=n_G\delta_{\alpha\beta}, \tag{D2}$$

$$\sum_{\alpha\in\text{irreps}}\chi_\alpha(a)\chi^*_\alpha(b)=\frac{n_G}{\text{card}[a]}\delta_{[a][b]}, \tag{D3}$$

$$\chi_{\alpha\otimes\beta}(g)=\chi_\alpha(g)\chi_\beta(g),\qquad \forall\, g\in G, \tag{D4}$$

$$\mathcal{D}=\bigoplus_{\alpha\in\text{irreps}}m_\alpha\alpha\Rightarrow m_\alpha=\frac{1}{n_G}\sum_{g\in G}\chi^*_\alpha(g)\chi_{\mathcal{D}}(g), \tag{D5}$$

$$P_\alpha\phi=\sum_{g\in G}\chi^*_\alpha(g)g.\phi. \tag{D6}$$

The "orthogonality" relations [Eq. (D2)] means that the columns of the character table are orthogonal and that the inner product of each column with itself is the cardinality of the group. Since the product of the character table matrix with its conjugate is a scalar matrix, then the rows of the character table are as well orthogonal with squared-norm equal to n_G [Eq. (D3)]. The "direct product" rule [Eq. (D4)] gives the character for a direct product of irreps, whereas Eq. (D5) gives the number m_α the irrep α appears in the decomposition of the reducible representation $\mathcal{D}$. In order to find the linear combination corresponding to a given symmetry characterized by an irrep, or what the chemists call the symmetry adapted linear combination (SALC), one uses Eq. (D6) which gives the projection of the "basis function" ϕ onto the subspace transforming under the irrep α.

1. S_2

It has two elements: the identity E, and the transposition $A=(12)$, with $A^2=1$. We have two classes: $(1C_1=\{E\}$, $1C_2=\{A\})$. There are two singlet irreps $(\mathbf{1},\mathbf{1}')$, with character Table VIII.

Taking $(x_1,x_2)^T$ as the defining (fundamental) representation transforming under $(E=\text{diag}(1,1)$, $A\equiv(12)=\left(\begin{smallmatrix}0&1\\1&0\end{smallmatrix}\right))$, then applying Eq. (D6), we find

$$\begin{aligned}x_1+x_2&\sim\mathbf{1}\\x_1-x_2&\sim\mathbf{1}'.\end{aligned} \tag{D7}$$

2. S_3

In terms of cycles' notation, we have the six-elements symmetry group of order 3: $S_3=\{E,A=(23),B=(13),C=(12),D=(132),F=(123)\}$ which can be divided into three classes $(1C_1=\{E\},3C_2=\{A,B,C\}$, $2C_3=\{D,F\})$, so we have three unitary inequivalent irreps, and by applying Eq. (D1),

$$\sum_{n\in N}m_n=3,\quad \sum_{n\in N}m_nn^2=6\Rightarrow m_1=2,\quad m_2=1. \tag{D8}$$

Applying Eqs. (D2) and (D3), we have the character table of S_3 (Table IX).

TABLE VIII. Character table of S_2.

Classes/irreps	$\chi_{\mathbf{1}}$	$\chi_{\mathbf{1}'}$
$1C_1$	1	1
$1C_2$	1	−1

[4]The order of an element g is the order of the subgroup generated by this element and is equal to $(\min\{n\in N\backslash\{0\}: g^n=1\})$. For a permutation written as a product of disjoint cycles, the order is the least common multiplier of the cardinalities of these cycles' supports.

TABLE IX. Character table of S_3.

Classes/irreps	$\chi_{\mathbf{1}}$	$\chi_{\mathbf{1}'}$	$\chi_{\mathbf{2}}$
$1C_1$	1	1	2
$2C_3$	1	1	−1
$3C_2$	1	−1	0

One can apply Eq. (D6) in order to find the SALC, but, sometimes, it turns out to be more illuminating to investigate directly the irreps. Concretely, if one takes the defining 3-dim representation of the permutations acting on (x_1, x_2, x_3), then one can check that its character values for the three classes $(1C_1, 2C_3, 3C_2)$ are respectively (3,0,1) which, by applying Eq. (D5), gives $(\mathbf{3} = \mathbf{1} \oplus \mathbf{2})$. Now, one can see directly that the combination $W \equiv (x_1 + x_2 + x_3)/\sqrt{3}$ is invariant under all permutations expressing, thus, the irrep $\mathbf{1}$. The corresponding orthogonal subspace, spanned by, say, $(V \equiv (x_3 - x_2)/\sqrt{2}$, and $W \equiv (x_2 + x_3 - 2x_1)/\sqrt{3})$ is also invariant under the action of the permutations representation, which gives the SALC for the irrep $\mathbf{2}$. The symmetry group S_3 is generated by two elements, like (A, C) or (B, F). In the space $\langle V, W\rangle$ spanned by the basis (V, W), we have

$$A = \begin{pmatrix} -1 & 0 \\ 0 & 1 \end{pmatrix}, \qquad C = \frac{1}{2}\begin{pmatrix} 1 & \sqrt{3} \\ \sqrt{3} & -1 \end{pmatrix}. \tag{D9}$$

We see here the advantage of taking (A, C) as generators since both belong to the same conjugacy class, having thus common character, and that A is diagonal in the basis (V, W), which makes its action evident. For example, if we take two defining irreps on $\langle V, W\rangle$ with four linear combinations,

$$\begin{aligned} &(x_1, x_2)^T \sim \mathbf{2}, \quad (y_1, y_2)^T \sim \mathbf{2}: \\ &\quad L_1 = (x_1 y_1 + x_2 y_2), \quad L_2 = (x_1 y_1 - x_2 y_2), \\ &\quad L_3 = (x_1 y_2 + x_2 y_1), \quad L_4 = (x_1 y_2 - x_2 y_1), \end{aligned} \tag{D10}$$

then we have

$$\begin{aligned} (L_1 \overset{A,C}{\to} L_1) &\Rightarrow L_1 \sim \mathbf{1}, \\ (L_4 \overset{A,C}{\to} -L_4) &\Rightarrow L_4 \sim \mathbf{1}', \\ (L_3, L_2)^T \overset{A(C)}{\to} A(C)(L_3, L_2)^T &\Rightarrow (L_3, L_2)^T \sim \mathbf{2}. \end{aligned} \tag{D11}$$

Moreover, if we assume $y' \sim \mathbf{1}'$ then it is immediate to check that $(y' x_2, -y' x_1)^T \sim \mathbf{2}$ so we get $(\mathbf{1}' \otimes \mathbf{2} = \mathbf{2})$. Similarly, one checks that $(\mathbf{1} \otimes \mathbf{1} \sim \mathbf{1}, \mathbf{1}' \otimes \mathbf{1}' \sim \mathbf{1}, \mathbf{1}' \otimes \mathbf{1} \sim \mathbf{1}', \mathbf{1} \otimes \mathbf{2} \sim \mathbf{2})$.

One could look at the basis (X, Y, Z) as resulting from applying onto the canonical basis a similarity transformation defined by the unitary matrix U:

$$U = \begin{pmatrix} \frac{1}{\sqrt{3}} & 0 & \frac{\sqrt{2}}{\sqrt{3}} \\ \frac{1}{\sqrt{3}} & \frac{1}{\sqrt{2}} & \frac{-1}{\sqrt{6}} \\ \frac{1}{\sqrt{3}} & \frac{-1}{\sqrt{2}} & \frac{-1}{\sqrt{6}} \end{pmatrix},$$

$$A^{\text{can}} = (23) = \begin{pmatrix} 1 & 0 & 0 \\ 0 & 0 & 1 \\ 0 & 1 & 0 \end{pmatrix}$$

$$\Rightarrow A = U^\dagger \times A^{\text{can}} \times U = \begin{pmatrix} 1 & 0 & 0 \\ 0 & -1 & 0 \\ 0 & 0 & 1 \end{pmatrix},$$

$$C^{\text{can}} = (12) = \begin{pmatrix} 0 & 1 & 0 \\ 1 & 0 & 0 \\ 0 & 0 & 1 \end{pmatrix}$$

$$\Rightarrow C = U^\dagger \times C^{\text{can}} \times U = \begin{pmatrix} 1 & 0 & 0 \\ 0 & \frac{1}{2} & \frac{\sqrt{3}}{2} \\ 0 & \frac{\sqrt{3}}{2} & \frac{-1}{2} \end{pmatrix}, \tag{D12}$$

which shows explicitly that $\mathbf{3} = \mathbf{1} \oplus \mathbf{2}$. Actually, one can look at $(U^\dagger g U)_{ij}$ as the inner product of the ith and jth columns of the matrix U using g as metric. Another common similarity transformation, when the generators are taken as (B, F), is given by U_ω:

$$U_\omega = \frac{1}{\sqrt{3}}\begin{pmatrix} 1 & 1 & 1 \\ 1 & \omega & \omega^2 \\ 1 & \omega^2 & \omega \end{pmatrix} : \omega = e^{2i\pi/3},$$

$$B^{\text{can}} = (13) = \begin{pmatrix} 0 & 0 & 1 \\ 0 & 1 & 0 \\ 1 & 0 & 0 \end{pmatrix}$$

$$\Rightarrow B = U_\omega^\dagger \times B^{\text{can}} \times U_\omega = \begin{pmatrix} 1 & 0 & 0 \\ 0 & 0 & \omega \\ 0 & \omega^2 & 0 \end{pmatrix},$$

$$F^{\text{can}} = (123) = \begin{pmatrix} 0 & 1 & 0 \\ 0 & 0 & 1 \\ 1 & 0 & 0 \end{pmatrix}$$

$$\Rightarrow F = U_\omega^\dagger \times F^{\text{can}} \times U_\omega = \begin{pmatrix} 1 & 0 & 0 \\ 0 & \omega & 0 \\ 0 & 0 & \omega^2 \end{pmatrix}. \tag{D13}$$

One notes again that, in this basis, the decomposition $\mathbf{3} = \mathbf{1} \oplus \mathbf{2}$ is explicit. Moreover, since F is diagonal then its

action on any defining representation is easy to compute. Concretely, we have

$$\begin{aligned}
&(t_1,t_2)^T \sim \mathbf{2}, t = x, y \Rightarrow \\
&(x_1y_2 + x_2y_1 \overset{B,F}{\to} x_1y_2 + x_2y_1) \Rightarrow x_1y_2 + x_2y_1 \sim \mathbf{1}, \\
&(x_1y_2 - x_2y_1 \overset{B(F)}{\to} -(+)(x_1y_2 - x_2y_1)) \Rightarrow x_1y_2 - x_2y_1 \sim \mathbf{1}', \\
&(x_2y_2, x_1y_1)^T \overset{B(F)}{\to} B(F)(x_2y_2, x_1y_1)^T \Rightarrow (x_2y_2, x_1y_1)^T \sim \mathbf{2},
\end{aligned} \tag{D14}$$

showing $\mathbf{2} \otimes \mathbf{2} = \mathbf{1} \oplus \mathbf{1}' \oplus \mathbf{2}$.

It is easier in this "complex" basis to find rules involving conjugate irreps. For example,

$$\begin{aligned}
&(x_1^*, x_2^*)^T \sim \mathbf{2}^*, (y_1, y_2)^T \sim \mathbf{2} \Rightarrow \\
&(x_1^*y_1 + x_2^*y_2 \overset{B,F}{\to} x_1^*y_1 + x_2^*y_2) \Rightarrow x_1^*y_1 + x_2^*y_2 \sim \mathbf{1}, \\
&(x_1^*y_1 - x_2^*y_2 \overset{B(F)}{\to} -(+)(x_1^*y_1 - x_2^*y_2)) \Rightarrow x_1^*y_1 - x_2^*y_2 \sim \mathbf{1}', \\
&(x_1^*y_2, x_2^*y_1)^T \overset{B(F)}{\Rightarrow} B(F)(x_1^*y_2, x_2^*y_1)^T \Rightarrow (x_1^*y_2, x_2^*y_1)^T \sim \mathbf{2},
\end{aligned} \tag{D15}$$

showing $\mathbf{2}^* \otimes \mathbf{2} = \mathbf{1} \oplus \mathbf{1}' \oplus \mathbf{2}$.

3. S_4

In terms of cycles' notation, we have the 24-elements symmetry group of order 4: $S_4 = \{a_1 = e, a_2 = (12)(34), a_3 = (13)(24), a_4 = (14)(23), b_1 = (243), b_2 = (142), b_3 = (123), b_4 = (134), c_1 = (234), c_2 = (132), c_3 = (143), c_4 = (124), d_1 = (34), d_2 = (12), d_3 = (1423), d_4 = (1324), e_1 = (23), e_2 = (1342), e_3 = (1243), e_4 = (14), f_1 = (24), f_2 = (1432), f_3 = (13), f_4 = (1234)\}$ which can be divided into five classes[5]

$$\begin{aligned}
&1C_1 = \{e\}, \\
&3C_2 = \{a_2, a_3, a_4\}, \\
&6C_2 = \{d_1, d_2, e_1, e_4, f_1, f_3\}, \\
&8C_3 = \{b_1, b_2, b_3, b_4, c_1, c_2, c_3, c_4\}, \\
&6C_4 = \{d_3, d_4, e_2, e_3, f_2, f_4\},
\end{aligned} \tag{D16}$$

so we have five unitary inequivalent irreps, and by applying Eq. (D1),

[5]One can find the order of a product of disjoint cycles as being equal to the least common multiplier of the cardinalities of cycles' supports.

TABLE X. Character table of S_4.

Classes/irreps	$\chi_{\mathbf{1}}$	$\chi_{\mathbf{1}'}$	$\chi_{\mathbf{2}}$	$\chi_{\mathbf{3}}$	$\chi_{\mathbf{3}'}$
$1C_1$	1	1	2	3	3
$3C_2$	1	1	2	−1	−1
$6C_2$	1	−1	0	1	−1
$6C_4$	1	−1	0	−1	1
$8C_3$	1	1	−1	0	0

$$\begin{aligned}
&\sum_{n\in N} m_n = 5, \qquad \sum_{n\in N} m_n n^2 = 24 \Rightarrow m_1 = 2, \\
&m_2 = 1, \qquad m_3 = 2.
\end{aligned} \tag{D17}$$

Applying Eqs. (D2) and (D3), we have the character table of S_4 (Table X). It has two generators, and actually it can be defined as

$$\begin{aligned}
S_4 &= \langle D, B : D^4 = B^3 = 1, DB^2D = B \rangle, \\
&= \langle T, S : T^4 = S^2 = (ST)^3 = 1 \rangle,
\end{aligned} \tag{D18}$$

with the first (second) definition leading to $DBD = BD^2B$ ($(TS)^3 = 1$). One can take $(D = d_4, B = b_1)$ for the first set of generators, or $(T = D, S = BD^{-1})$ for the second set. In the canonical basis (x_1, x_2, x_3, x_4), the linear combination $(x_1 + x_2 + x_3 + x_4)$ is invariant under the action of the permutations representation. Thus, the orthogonal subspace spanned by

$$\begin{pmatrix} A_x \\ A_y \\ A_z \end{pmatrix} = \begin{pmatrix} x_1 + x_2 - x_3 - x_4 \\ x_1 - x_2 + x_3 - x_4 \\ x_1 - x_2 - x_3 + x_4 \end{pmatrix} \tag{D19}$$

is also invariant. The restriction of the permutations representation onto the 3-dim A-space is the $\mathbf{3}$ irrep given, in this A-basis, by

$$b_1^{\text{can}} = \begin{pmatrix} 1 & 0 & 0 & 0 \\ 0 & 0 & 0 & 1 \\ 0 & 1 & 0 & 1 \\ 0 & 0 & 1 & 0 \end{pmatrix} \Rightarrow b_1^{\text{A}} = \begin{pmatrix} 0 & 0 & 1 \\ 1 & 0 & 0 \\ 0 & 1 & 0 \end{pmatrix} \tag{D20}$$

$$d_4^{\text{can}} = \begin{pmatrix} 0 & 0 & 1 & 0 \\ 0 & 0 & 0 & 1 \\ 0 & 1 & 0 & 0 \\ 1 & 0 & 0 & 0 \end{pmatrix} \Rightarrow d_4^{\text{A}} = \begin{pmatrix} -1 & 0 & 0 \\ 0 & 0 & -1 \\ 0 & 1 & 0 \end{pmatrix}, \tag{D21}$$

whereas the $\mathbf{3}'$ irrep is given, in an A-like basis, by

$$b'^{\mathrm{A}}_1 = \begin{pmatrix} 0 & 0 & 1 \\ 1 & 0 & 0 \\ 0 & 1 & 0 \end{pmatrix}, \qquad d'^{\mathrm{A}}_4 = \begin{pmatrix} 1 & 0 & 0 \\ 0 & 0 & 1 \\ 0 & -1 & 0 \end{pmatrix}, \tag{D22}$$

and the **2** irrep is

$$b''^{\mathrm{A}}_1 = \begin{pmatrix} \omega & 0 \\ 0 & \omega^2 \end{pmatrix}, \qquad d''^{\mathrm{A}}_4 = \begin{pmatrix} 0 & 1 \\ 1 & 0 \end{pmatrix}, \tag{D23}$$

where $\omega = e^{i2\pi/3}$, and one can compute the corresponding $T^{(',")\mathrm{A}} = d_4^{(',")\mathrm{A}}, S^{(',")\mathrm{A}}: S^{(',")\mathrm{A}} T^{(',")\mathrm{A}} = b_1^{(',")\mathrm{A}}$ in these irreps.

Another common basis is the $\tilde{B}$-basis given by the unitary similarity matrices $U_{\mathrm{doublet}}, U_{\mathrm{triplet}}$:

$$U_{\mathrm{doublet}} = \frac{1}{\sqrt{2}} \begin{pmatrix} 1 & i \\ 1 & -i \end{pmatrix},$$
$$U_{\mathrm{triplet}} = \frac{1}{\sqrt{2}} \begin{pmatrix} \sqrt{2} & 0 & 0 \\ 0 & 1 & 1 \\ 0 & i & -i \end{pmatrix}, \tag{D24}$$

so we have

$$\tilde{b}_1 = U^\dagger_{\mathrm{triplet}} b^{\mathrm{A}}_1 U_{\mathrm{triplet}} = \begin{pmatrix} 0 & \frac{i}{\sqrt{2}} & \frac{-i}{\sqrt{2}} \\ \frac{1}{\sqrt{2}} & \frac{-i}{2} & \frac{-i}{2} \\ \frac{1}{\sqrt{2}} & \frac{i}{2} & \frac{i}{2} \end{pmatrix},$$
$$\tilde{d}_4 = U^\dagger_{\mathrm{triplet}} d^{\mathrm{A}}_4 U_{\mathrm{triplet}} = \mathrm{diag}(-1, -i, i),$$
$$\tilde{b}'_1 = U^\dagger_{\mathrm{triplet}} b'^{\mathrm{A}}_1 U_{\mathrm{triplet}} = \begin{pmatrix} 0 & \frac{i}{\sqrt{2}} & \frac{-i}{\sqrt{2}} \\ \frac{1}{\sqrt{2}} & \frac{-i}{2} & \frac{-i}{2} \\ \frac{1}{\sqrt{2}} & \frac{i}{2} & \frac{i}{2} \end{pmatrix},$$
$$\tilde{d}'_4 = U^\dagger_{\mathrm{triplet}} d'^{\mathrm{A}}_4 U_{\mathrm{triplet}} = \mathrm{diag}(1, i, -i),$$
$$\tilde{b}''_1 = U^\dagger_{\mathrm{doublet}} b''^{\mathrm{A}}_1 U_{\mathrm{doublet}} = \frac{1}{2} \begin{pmatrix} -1 & -\sqrt{3} \\ \sqrt{3} & -1 \end{pmatrix},$$
$$\tilde{d}''_4 = U^\dagger_{\mathrm{doublet}} d''^{\mathrm{A}}_4 U_{\mathrm{doublet}} = \mathrm{diag}(1, -1), \tag{D25}$$

and one can compute $\tilde{T}, \tilde{T}', \tilde{T}'', \tilde{S}, \tilde{S}', \tilde{S}''$.

One can find the multiplication rules, as was done in the previous subsection in any basis. However, we refer the reader to [20] for the $\tilde{B}$-basis rules, whereas we state explicitly in Sec. VI B 1 the corresponding rules in the B-basis adopted to define the texture and the matter field symmetry assignments.

[1] Paul H. Frampton, Sheldon L. Glashow, and Danny Marfatia, Zeroes of the neutrino mass matrix, Phys. Lett. B 2002) 79 ,**536**).

[2] Zhi-Zhong Xing, Texture zeros and Majorana phases of the neutrino mass matrix, Phys. Lett. B **530**, 159 (2002).

[3] Harald Fritzsch, Zhi-Zhong Xing, and Shun Zhou, Two-zero textures of the Majorana neutrino mass matrix and current experimental tests, J. High Energy Phys. 09 (2011) 83.

[4] A. Merle and W. Rodejohann, Elements of the neutrino mass matrix: Allowed ranges and implications of texture zeros, Phys. Rev. D **73**, 073012 (2006).

[5] L. Lavoura, Zeros of the inverted neutrino mass matrix, Phys. Lett. B **609**, 317 (2005).

[6] E. I. Lashin and N. Chamoun, Zero minors of the neutrino mass matrix, Phys. Rev. D **78**, 073002 (2008).

[7] E. I. Lashin, N. Chamoun, C. Hamzaoui, and S. Nasri, Neutrino mass textures and partialsymmetry, Phys. Rev. D **89**, 093004 (2014).

[8] E. I. Lashin and N. Chamoun, One-zero textures of Majorana neutrino mass matrix and current experimental tests, Phys. Rev. D **85**, 113011 (2012).

[9] E. I. Lashin and N. Chamoun, One vanishing minor in the neutrino mass matrix, Phys. Rev. D **80**, 093004 (2009).

[10] A. Ismael, M. AlKhateeb, N. Chamoun, and E. I. Lashin, Texture of single vanishing subtrace in neutrino mass matrix, Phys. Rev. D **103**, 035020 (2021).

[11] S. Dev, Radha Raman Gautam, and Lal Singh, Neutrino mass matrices with two equalities between the elements or cofactors, Phys. Rev. D **87**, 073011 (2013).

[12] Ji-Yuan Liu and Shun Zhou, Hybrid textures of Majorana neutrino mass matrix and current experimental tests, Phys. Rev. D **87**, 093010 (2013).

[13] S. Dev and Desh Raj, New hybrid textures for neutrino mass matrices, Nucl. Phys. **B957**, 115081 (2020).

[14] Davide Meloni, Aurora Meroni, and Eduardo Peinado, Two-zero Majorana textures in the light of the Planck results, Phys. Rev. D **89**, 053009 (2014).

[15] Julien Alcaide, Jordi Salvado, and Arcadi Santamaria, Fitting flavour symmetries: The case of two-zero neutrino mass textures, J. High Energy Phys. 07 (2018) 164.

[16] A. Ismael, E. I. Lashin, M. AlKhateeb, and N. Chamoun, Texture of one equality in neutrino mass matrix, Nucl. Phys. **B971**, 115541 (2021).

[17] H. A. Alhendi, E. I. Lashin, and A. A. Mudlej, Textures with two traceless submatrices of the neutrino mass matrix, Phys. Rev. D **77**, 013009 (2008).
[18] Daya Bay Collaboration, Observation of Electron-Antineutrino Disappearance at Daya Bay, Phys. Rev. Lett. **108**, 171803 (2012).
[19] Guido Altarelli and Ferruccio Feruglio, Discrete flavor symmetries and models of neutrino mixing, Rev. Mod. Phys. **82**, 2701 (2010).
[20] Hajime Ishimori, Tatsuo Kobayashi, Hiroshi Ohki, Hiroshi Okada, Yusuke Shimizu, and Morimitsu Tanimoto, Non-Abelian discrete symmetries in particle physics, Prog. Theor. Phys. Suppl. **183**, 1 (2010).
[21] C. Jarlskog, Commutator of the Quark Mass Matrices in the Standard Electroweak Model and a Measure of Maximal *CP* Nonconservation, Phys. Rev. Lett. **55**, 1039 (1985).
[22] P. F. de Salas, D. V. Forero, S. Gariazzo, P. Martnez-Mirav, O. Mena, C. A. Ternes, M. Trtola, and J. W. F. Valle, 2020 global reassessment of the neutrino oscillation picture, J. High Energy Phys. 02 (**2021**) 071.
[23] KATRIN Collaboration, Improved Upper Limit on the Neutrino Mass from a Direct Kinematic Method by KATRIN, Phys. Rev. Lett. **123**, 221802 (2019).
[24] GERDA Collaboration, Probing Majorana neutrinos with double-β decay, Science **365**, 1445 (2019).
[25] Diana S. Parno and Kathrin Valerius, Probing the neutrino mass scale with the KATRIN experiment, Europhysics News **53**, 24 (2022).
[26] Planck Collaboration, Planck 2018 results, Astron. Astrophys. **641**, A6 (2020).
[27] Eleonora Di Valentino, Stefano Gariazzo, and Olga Mena, On the most constraining cosmological neutrino mass bounds, Phys. Rev. D **104**, 083504 (2021).
[28] Zackaria Chacko, Abhish Dev, Peizhi Du, Vivian Poulinb, and Yuhsin Tsaia, Cosmological limits on the neutrino mass and lifetime, J. High Energy Phys. 04 (2020) 020.